

The effects of seagrass edges on hydrodynamic conditions, sediment transport, and
bivalve recruitment

Elise Turrietta
Norfolk, Virginia

B.S. Biology & Environmental Science, William & Mary, 2020

A Thesis presented to the Graduate Faculty
of the University of Virginia in Candidacy for the Degree of
Master of Science

Department of Environmental Sciences

University of Virginia
August, 2022

Abstract

Coastal seagrass environments provide an extensive array of ecosystem services to the areas they occupy including carbon sequestration, shoreline protection, economic support of fishery industries, and enhanced quality of water and habitat. An increasingly warming climate and anthropogenic development have directly threatened these valuable environments and spurred accelerated decline of seagrass ecosystems, leading to overall loss and fragmentation. This advancing degradation has prompted new and expanded efforts in protection and restoration, and one of the world's largest seagrass restoration endeavors exists at the Virginia Coast Reserve Long Term Ecological Research site. As this project and others like it aim to restore seagrass in new locations while combatting concurrent degradation, questions arise regarding the impact of vegetation on its surrounding environment. Considering the presence or absence of vegetation, seagrass has well-studied and significant influences on hydrodynamic conditions, wave activity, sediment transport, and faunal communities. As loss and fragmentation accelerate while restoration generates new frontiers of growth, considerations of spatial ecology have driven work asking how these well-established effects change over heterogenous landscapes, with implications for the value and consequences of a changing seagrass ecosystem. These factors have motivated the work presented here which asks how hydrodynamic and wave activity change across various edges of seagrass vegetation, and whether there are resulting effects on sediment transport and bivalve recruitment.

A combination of hydrodynamic instrumentation, novel physical sampling techniques, meteorological data, and manipulated seagrass landscapes were used at the VCR LTER during 2021 and 2022 to answer these questions and quantify the response of

flow, sediment movement, and bivalve recruitment across variable seagrass vegetation and its edges. Mean flow velocities were consistently and significantly reduced in seagrass vegetation regardless of proximity to edges, with reductions compared to unvegetated areas ranging from 30% to over 75% and corresponding to seasonal increases in shoot density. Recruitment of juvenile bivalves was also significantly elevated in the same locations. Bare and vegetated sampling locations across edges yielded no significant differences in wave activity or sediment resuspension, but significant correlations between these factors revealed the sensitivity of edge-adjacent, low-density areas to sediment transport driven by weather events and changes in flow. This was demonstrated by a tenfold increase in sediment collection within benthic traps following severe storms and indicated that wave heights were a major predictor for sediment transport in this study. These results found across various edge configurations and a heterogeneous vegetation landscape reveal direct hydrodynamic responses to meteorological conditions (e. g., winds, storms) and shoot density that alter both sediment transport and bivalve recruitment dynamics. This has implications for the success and influence of restoration attempting to combat ecosystem degradation caused by a changing climate and human development.

| <u>Table of Contents</u> | Page |
|---|-------------|
| <u>Chapter 1: Introduction</u> | |
| 1.1 Background | 1 |
| 1.2 Research questions | 10 |
| 1.3 Site setting and study areas | 11 |
| 1.4 Figures | 15 |
| <u>Chapter 2: Hydrodynamic conditions and wave activity</u> | |
| 2.1 Objectives | 18 |
| 2.2 Methods | 18 |
| 2.3 Results | 24 |
| 2.4 Discussion | 36 |
| 2.5 Photos, figures, and tables | 40 |
| <u>Chapter 3: Effects of flow conditions on sediment transport and bivalve recruitment</u> | |
| 3.1 Objectives | 50 |
| 3.2 Background | 50 |
| 3.3 Methods | 54 |
| 3.4 Results | 57 |
| 3.5 Discussion | 64 |
| 3.6 Photos, figures, and tables | 70 |
| <u>Chapter 4: Conclusions</u> | |
| 4.1 Conclusions | 79 |
| 4.2 Future work and implications for restoration | 83 |
| <u>Appendices</u> | 85 |
| <u>References</u> | 92 |
| <u>Acknowledgements</u> | 101 |

Chapter 1: Introduction

1.1 Background

Seagrass ecosystems

Seagrass meadows, expanses of submerged aquatic vegetation with an underlying root rhizome structure and flowering leaves in the water column, provide an extensive range of ecosystem services to the marine environments they occupy. These include coastal protection, faunal habitats, greenhouse gas sequestration, enhanced water quality, and economic support of fisheries (Oreska et al., 2016; 2020). However, as human development and use of coastal landscapes increases along with a warming climate, seagrass ecosystems have been degraded leading to a global loss estimated at roughly 7% per year or 19% overall (Dunic et al., 2021; Waycott et al., 2009). This accelerating degradation has spurred recovery efforts (Orth et al., 2006) and has simultaneously generated questions regarding how alterations of these vegetated environments lead to ecological and physical consequences and state changes (Orth & McGlathery, 2012). The work of this thesis addresses the influence of seagrass on the hydrodynamic, sedimentary, and faunal components of their ecosystems, specifically along meadow edges and in bare patch settings, with implications for restoration and seagrass expansion projects that combat ecosystem loss and fragmentation.

Hydrodynamic conditions and wave activity

Seagrasses have extensive influence on the hydrodynamic patterns of their local flow environments at several scales. Seagrass induces drag on the surrounding flow

leading to velocity gradients encompassing the canopy and resulting in the formation of boundary layers (Denny, 1988). This drag force manifests itself at multiple spatial scales of the canopy structure, and leads to hydrodynamic changes ranging from turbulence generation around individual grass blades to enhanced velocity gradients and reduced flow across an entire meadow (Nepf, 1999; Reidenbach & Thomas, 2018). The array of hydrodynamic shifts stemming from seagrass presence has been documented in the literature in a variety of coastal settings.

At the largest scale, encompassing the entire vegetated canopy, seagrass reduces ambient flow (Ackerman & Okubo, 1993) as drag occurs when flow encounters the grasses. Hansen & Reidenbach (2012) found seagrass presence to reduce near-bottom mean velocities by up to 90% compared to unvegetated regions. The induced drag also alters velocity profiles above the canopy, as a shear layer forms at the interface of the canopy and overlying water (Gambi et al., 1990). The vertical velocity profiles surrounding this interface are characterized by an inflection point separating regions of increased velocity above the top of the canopy relative to flow below it (Ghisalberti & Nepf, 2002). At high seagrass densities, ‘skimming flow’ can occur, where increased velocity above the canopy arises as the amount of bulk water flow through the canopy is substantially reduced (Koch & Gust, 1999). The result of this inflection point is instability in the velocity profile which locally enhances turbulence in the shear layer above the canopy (Widdows et al., 2008).

The density and morphology of the vegetation has a direct influence on these boundary layer dynamics, with higher blade density resulting in a thicker shear layer above the canopy and reduced mixing below it (Carr et al., 2010; Chen et al., 2007).

Similar relationships have been found between blade height and canopy friction, with taller blades resulting in reduced flow velocity throughout the vegetation (Fonseca & Fisher, 1986; Gacia et al., 1999). Seagrass density and patch morphology also influence resulting turbulence regimes. The decreased tangential shear stress associated with near-bed velocity reduction simultaneously results in lower turbulent energy near the seafloor (Widdows et al., 2008; Worcester, 1995). High density beds result in decreased turbulence with progression into the canopy (Hansen & Reidenbach, 2012). However, at low densities, flow can penetrate within the canopy and corresponds to increased turbulence caused by stem-wake interactions (Fonseca & Koehl, 2006; Granata et al., 2001; Hansen & Reidenbach, 2013).

Not only do seagrasses cause hydrodynamic changes in the region they occupy in the water column, but they also have a strong impact on wave motion. It has been well established that seagrass presence results in wave attenuation (Fonseca & Cahalan, 1992). However, the degree of attenuation depends on whether the prevailing flow conditions are driven by winds or tides (Koch & Gust, 1999) and the characteristics of the waves themselves influence the extent of seagrass response (Bradley & Houser, 2009). Results from both modeling and experimental studies have shown that higher seagrass density and biomass leads to greater attenuation and a larger decrease in wave height, respectively (Chen et al., 2007; Reidenbach & Thomas, 2018).

Clearly the morphology of a vegetated seagrass area has direct effects on its hydrodynamic consequences. These varied outcomes become particularly important when considering fragmentation of seagrass beds. A study by Allaoui et al. (2016) sought to quantify the variability in hydrodynamic response from fragmented seagrass canopies

caused by climate change. They found that more fragmented canopies resulted in less attenuation of waves and increased mean flow velocities, concluding that fragmented seagrass environments are less efficient at providing a sheltering habitat. However, little work has been done to explicitly quantify wave and hydrodynamic changes or near-bed turbulence structure within a fragmented seagrass meadow, or along the edges of vegetation that characterize these environments following disturbance events.

Sediment suspension and transport

The interaction of wind- and tide-dominated flows becomes particularly relevant when examining the influence of seagrass on shallow water flow as it relates to sediment resuspension. The combination of these forces and their effect on flow conditions is nonlinear, but generally oscillatory wave motions (which penetrate deeper into the seagrass canopy than tidally driven flow) lead to initial sediment resuspension and tidal currents lead to net sediment transport through a system at large (Jing & Ridd, 1996). Over unvegetated seafloor, wave presence results in a separate, smaller wave-specific boundary layer which, when combined with current flow, enhances bottom shear stresses that can exceed the critical stress threshold necessary for sediment resuspension (Reidebach & Timmerman, 2019). This combined wave-current boundary layer dictates the amount of shear stress affecting the seafloor (Grant & Madsen, 1979) and resulting tangential shearing force just above the sediment-water interface mediates the amount of sediment resuspended past its critical threshold of movement depending on grain size.

This type of wave action largely determines suspended sediment concentrations (SSCs) particularly in shallow coastal bay settings (Lawson et al., 2007), but the presence of seagrass alters these interactions with varied outcomes for sediment transport. The

associated reduction in energy within the seagrass canopy corresponding to lower velocities and wave motions has been linked to a simultaneous reduction in bottom shear stress and sediment resuspension (Koch et al., 2006; Ward et al., 1984). Hansen & Reidenbach (2012) found that in a combined wave-current flow, bed shear stress in bare areas often exceeded the critical stress threshold to initiate sediment movement, but at vegetated sites the bed shear stress was lower than this critical value 80% of the time. Additionally, the correlation between bed shear stress and increased SSCs was high in bare areas and lower in vegetation, showing that areas with seagrass had “decreased tendency for periods of high SSCs to correspond with periods of high bottom shear stress.” The reduction in particle flux shown in seagrass ecosystems can be attributed to the reduction in canopy flow velocity as well as root stabilization (Gacia et al., 1999; Hansen & Reidenbach, 2013).

Because of this limited resuspension, seagrass meadows are considered depositional environments for sediment, and quantifying SSCs and transport in seagrass beds is particularly relevant as light availability in the water column influences meadow growth and productivity. Using seagrass to enhance these depositional environments may create a positive feedback loop where more light availability encourages more seagrass growth, further reducing SSCs (Reidenbach & Thomas, 2018). Recent work by Zhu et al. (2021) modeled the “synergistic effects of flow-wave-vegetation-sediment interaction at a meadow scale” and concluded that vegetation density mediated the response of SSCs and transport to variable hydrodynamic and wave conditions. High-density vegetation in the summer significantly attenuated flow, waves, and SSCs, but low-density vegetation (< 160 shoots/m²) in the winter resulted in much smaller reductions (Zhu et al., 2021).

Meadow edges were the most sensitive to changes in erosional or depositional conditions and controlled the amount of suspended sediment advected throughout the system at large (Zhu et al., 2022).

Other recent work conducted with flume experiments showed a similar density-dependent relationship between flow regime and distance of sediment advection past a seagrass edge (Zhang et al., 2020). This laboratory work addressed distance scales of centimeters, and modeling studies have addressed kilometers of meadow vegetation (Zhu et al., 2021 & 2022), but no work has explored these relationships at an intermediate scale of meters with field-based research. By further quantifying short-term fluctuations in SSCs in response to flow dynamics along edges of vegetation *in situ*, it is possible to understand how meadow fragmentation or regrowth may contribute to a positive feedback loop of light availability with implications for seagrass restoration efforts.

Bivalve settlement, recruitment, and abundance

In addition to their pronounced effect on surrounding flow regime, seagrass presence has been linked to increased species richness, diversity, density, and abundance of associated macrofauna (Bologna & Heck, 2002; Orth, 1973; Orth et al., 1984; Orth & Heck, 1980). Studies have also shown significant positive correlations between bivalve abundance and seagrass density and biomass (Glaspie & Seitz, 2017; Homziak et al., 1982; Peterson et al., 1984; Peterson, 1986). Based on these results, there has been effort to show that the positive relationship between seagrasses and bivalves depends on the surrounding hydrodynamic conditions (Eckman, 1983; Harvey & Bourget, 1995; Irlandi, 1996; Irlandi & Peterson, 1991).

Underlying this theory is the mechanism by which bivalve larvae disperse and settle. Many benthic invertebrates have planktonic larvae that passively settle in turbulent flow environments (Butman, 1989; Eckman & Duggins, 1998). This applies to bivalve larvae which, due to their limited swimming abilities, move under the influence of the near-bottom shear layer (Eckman, 1990; Jonsson et al., 1991). Drawing from established conclusions about how seagrasses influence their surrounding flow, experimental research has shown that seagrasses may trap these passive larvae just as they trap sediment and that bivalve settlement patterns may be associated with seagrass presence and structural canopy differences which alter flow (Eckman, 1983; Bologna & Heck, 2000, 2002).

Bay scallops, *Argopecten irradians*, for example, have an extremely close association to seagrass beds by nature of their settlement method (Thayer & Stuart, 1974). *A. irradians* larvae cling to individual seagrass blades with byssal threads as they move through the canopy, lending stability upon attachment (Ambrose et al., 1992). Eckman (1987) studied the influence of hydrodynamic forces on recruitment, growth, and survival of bay scallops, concluding that the altered hydrodynamics of eelgrass (*Z. marina*) beds significantly affected larval recruitment to a higher degree than predation or inter-blade abrasion. Hydrodynamics also influence the settlement and recruitment of hard clams, *Mercenaria mercenaria*. Regardless of seagrass presence, tidal currents significantly influence hard clam growth rates (Grizzle & Morin, 1989). Early studies traced increased clam population density and individual growth rates to seagrass presence, citing reductions in velocity and changes in sediment movement at the seafloor within the canopy as explanations for enhanced growth (Peterson et al., 1984). In this

work, the seagrass-induced impact of local hydrodynamics on passively settling larvae sufficiently explained differences in clam densities between bare and vegetated sites, even when accounting for altered post-settlement survival (Peterson, 1986).

However, not all studies considering the effect of seagrasses on bivalve settlement and recruitment have produced consistent results, particularly concerning edge environments. Wilson (1990) studied differential mollusk settlement along seagrass edges and noted patterns of increased bivalve settlement density in vegetation, but no significant differences in abundance across the edge between bare and vegetated locations. Similar patterns have been shown for bay scallops in edge environments. Carroll et al. (2012) sought to determine the magnitude and direction of edge effects on bay scallop settlement and recruitment but found counteracting evidence for a simultaneous positive effect of enhanced larval settlement along edges but a negative effect of diminished recruitment in these locations most likely due to enhanced predation.

Based on these and other studies, landscape ecology has become an increasingly important approach in examining the effects of seagrass on bivalve distribution. Differences in the spatial patterning of a seagrass meadow (in terms of percent cover) can influence the distribution and abundance of faunal inhabitants and alter trophic interactions at several levels (Irlandi et al., 1995; 1999). The influence of fragmented seagrass habitats on its associated fauna is extremely variable but not always negative as traditionally thought (Bostrom et al., 2006; Carroll et al., 2012), and previous work suggests that fauna along seagrass edges may experience tradeoffs to balance counteracting influences of simultaneously enhanced settlement and predation (Bologna & Heck, 1999).

A considerable amount of work has established that seagrass edges have significant influences on associated fauna (Bell et al., 2001; Bologna & Heck, 2002; Moore & Hovel, 2010; Smith et al., 2011). Investigations into the effect of seagrass edges on differential particle settlement mainly began with the seminal research of Robert Orth (1973) who described the phenomena of a “settlement shadow” in which, due to the decrease in current speed through a seagrass canopy, particle settlement should be greatest at a canopy edge and decrease into the meadow (Orth, 1992; Roughgarden et al., 1988). This trend was experimentally observed in bivalve larvae by Bologna & Heck (2000) who found significantly greater larval densities at seagrass patch edges. Flume experiments have also been used to confirm that seagrass-induced mean flow reduction directly influences larval settlement at edges of vegetation (Peterson et al., 2004), but further detailed hydrodynamic analysis relating to bivalve larval settlement and recruitment in seagrass edge environments has been limited.

Seagrass ecosystem fragmentation and landscape ecology

Anthropogenic influence from coastal development and a simultaneously warming climate have accelerated the rate of seagrass ecosystem loss to upwards of 7% per year (Waycott et al., 2009) and 19% overall (Dunic et al., 2021), creating a “global crisis” for these environments (Orth et al., 2006) and threatening the variety of services they offer. This extensive degradation manifests not only in ecosystem loss, but also fragmentation, leading to a higher proportion of edges over a more discontinuous habitat (Yarnall et al., 2021). While the natural edges of seagrass meadows have previously posed interesting questions regarding a ‘presence vs absence’ binary of vegetation and its

ecotonal zones, the increased prevalence of edges across fragmented seagrass ecosystems adds new considerations to these well-studied topics (Colomer & Serra, 2021).

Perspectives of spatial ecology help address change in seagrass landscapes with the goal of elucidating the effects of ecosystem heterogeneity. Heterogeneity arises in seagrass beds from fragmentation, patch presence, bed expansion, and the resulting shifts in hydrodynamic conditions (Robbins & Bell, 1994). However, research addressing varied seagrass landscape structure at a wide range of scales using a spatial ecological framework has yielded inconsistent results regarding the relationships between flow regime, sediment transport, and faunal distribution (Allaoui et al., 2016; Bostrom et al., 2006; Hovel et al., 2002), particularly at edges and patches (Carroll et al., 2012; Irlandi et al., 1995; Murphy et al., 2010). Remaining ambiguity surrounding the consequences of edge effects, variable landscape structure, and fragmentation on hydrodynamic conditions and its associated influences motivate the questions of this thesis.

1.2 Research questions

Despite previous work investigating the relationships between seagrass presence, hydrodynamic conditions, sediment transport, and bivalve recruitment, there remains to be a thorough investigation into how these dynamics persist over a variety of edge settings including that of a meadow in entirety, or those which characterize fragmented or heterogeneous landscapes. Further, despite ongoing and newly proposed restoration efforts, little work has been done to quantify these phenomena as they relate to a restored, expanding seagrass meadow and its self-perpetuating feedback loops. To address these knowledge gaps, the research outlined here will answer the following questions: (1) How do hydrodynamic conditions and wave activity change across various edges of seagrass

vegetation? (2) How do these altered flow conditions influence sediment resuspension and transport? And (3) Does bivalve settlement and recruitment vary in response to these flow changes? The purpose of answering these questions is to contribute high resolution, robust hydrodynamic analysis of seagrass edge settings to the literature and help inform the growing body of work regarding seagrass restoration and the positive feedback loops it generates for sediment resuspension, primary productivity, and further resilience. By also linking changes in flow to differential bivalve recruitment, these results will elucidate how restored seagrass settings and new edges of vegetation mediate faunal response via hydrodynamic changes.

1.3 Site setting and study areas

Field studies for this research occurred in South Bay, Virginia, a coastal lagoon set behind the barrier islands bordering the east side of the Delmarva Peninsula. This shallow bay is part of the National Science Foundation's Virginia Coast Reserve Long Term Ecological (VCR LTER) site which consists of several coastal bays and their interconnected salt marshes, ocean inlets, and barrier islands. Nestled between these islands and the peninsula's coast, this network of bays and marshes experiences exchange with the ocean through narrow channels and tidal flushing. South Bay has an approximate area of 31.5 km² with an average depth of roughly 1.0 m and a tidal range between 0.5 and 1.5 m (Reidenbach & Thomas, 2018).

Due to the shallow depth, low freshwater inputs, and low nutrient inputs into South Bay, turbidity is primarily caused by sediment resuspension induced by wind-driven waves and transport driven by tidal currents (Fagherazzi & Wiberg, 2009; Lawson et al., 2007). In this system, since non-algal particulate matter mainly controls light

attenuation, high concentrations of resuspended sediment may limit light penetration through the water column with resulting decreases in primary productivity (McGlathery et al., 2001). Seagrass presence in South Bay has been shown to limit resuspension and promote deposition of suspended sediment, generating a positive feedback loop where continued seagrass expansion further decreases turbidity, enhances light penetration in the water column, and encourages more primary production (Carr et al., 2012; Hansen & Reidenbach, 2012).

Previous seagrass research in South Bay has been extensive. A combination of disease and extreme weather in the early 1930s led to vast destruction of *Zostera marina*, the eelgrass species that once dominated the bay's seafloors. However, when natural occurrences of *Z. marina* were discovered in the 1990s, systematic restoration efforts began in several coastal bays including South Bay and this work has been largely successful with continued meadow reseeding and growth (Oreska, 2020; Orth, 2006; Orth & McGlathery, 2012). Meadow expansion in South Bay continues to change the fluid dynamics of this system, further limiting sediment resuspension and promoting seagrass growth (Hansen & Reidenbach, 2013; Orth et al., 2012) by increasing light availability in the water column and contributing to the positive feedback loop of primary productivity.

For these reasons, the expanding eelgrass meadow in South Bay provides an ideal location to answer questions concerning how new edges of vegetation contribute to alteration of local flow environments and the resulting consequences for sediment transport and bivalve recruitment. In May 2021 a study area, Site 1, was selected on the northern edge of the South Bay eelgrass meadow to conduct field work (Figure 1.1). This northern boundary sits just south of the oceanic inlet between Wreck and Cobb Islands

and therefore experiences a greater magnitude of tidal flushing resulting in larger temperature variations and more varied flow dynamics than the more static center of the meadow. Differences in these temperature and flow regimes became apparent in the marine heat wave of 2015 that caused a significant die-off event in the meadow's center but during which northern sites experienced greater resiliency (Berger et al., 2020).

A 500 m² study area was delineated at Site 1, starting in naturally unvegetated seafloor, spanning the meadow's edge of vegetation, and covering over 400 m² of eelgrass adjacent to this edge (Figure 1.2, Photo 1.1). Three parallel, replicative transects were delineated along a 130° trajectory, roughly perpendicular to the dominant North-South flow direction of South Bay. Each transect (1-3) had four locations (A-D) for sediment, bivalve, and hydrodynamic sampling with A in naturally unvegetated seafloor, B closest to the meadow's edge, and D furthest into the meadow 25 m past the edge of vegetation. All sampling locations labeled C were within a manmade patch of bare seafloor. During study area formation in May 2021, these patches were created by manually removing seagrass from a circular area of a 3 m diameter. These sampling locations were used to simulate fragmentation and address how bare patches and edges of discontinuous seagrass cover contribute to alterations of local flow conditions.

This study area is roughly 250 m to the northwest of the adjacent, concurrent Seagrass Resilience Experiment (SRE) overseen by researchers at the VCR LTER (Figure 1.1, Tassone et al., in prep). The goal of this larger removal project is to understand patterns of seagrass resilience and regrowth following disturbance events. With sites in both the central and northern sections of the meadow, the SRE uses a paired design where each sampling plot is a 6 m diameter circle of seafloor with natural

vegetation as a control and manually removed bare plots as a treatment. This work was largely motivated by the marine heat wave which occurred in 2015 and led to significant die-off and subsequent natural regrowth of the South Bay seagrass meadow.

In April 2022 a new study area, Site 2, was chosen to conduct a second round of sampling in a similar location and configuration to that of Site 1, approximately 100 m to its northeast and still positioned along the northern edge of the South Bay seagrass meadow (Figure 1.1). Site 2 was selected in response to changes in edge morphometrics following a year of seasonal senescence and growth, and to minimize bathymetric changes between unvegetated and vegetated regions across the meadow's natural edge. Site 2 was also chosen to increase proximity of the innermost vegetated location to the northern site of the SRE to enhance potential for comparison and generalization.

One transect was delineated at Site 2 with three designated sampling locations (A-C) each with 3 replicates used for sediment and bivalve sampling (Figure 1.3). Location A was in naturally bare seafloor and C furthest into seagrass vegetation, approximately 110 m past the meadow's edge. This transect ran along a 150° trajectory, roughly perpendicular to the meadow's edge in this location and to South Bay's dominant flow direction. Hydrodynamic instrumentation was deployed in designated locations along this transect to evenly span the seagrass edge in areas with ideal physical settings for data collection. No manmade bare patches were created at Site 2, but repeated sampling was performed in these locations at Site 1 in 2022 to assess consistency of results following the disturbance of manual vegetation removal in 2021.

Understanding how seagrass systems respond to disturbance events like these can inform restoration decisions following future disruptions, but questions remain regarding

the mechanisms of this natural resilience process. The work presented in this thesis began in conjunction with the SRE to understand the effect of hydrodynamic conditions on these regrowth processes, particularly in areas of discontinuous vegetation, as changes in flow in these settings are less understood. The new, adjacent study areas in this thesis were formed to avoid disrupting the SRE and to answer additional research questions regarding sediment transport and bivalve recruitment.

1.4 Figures

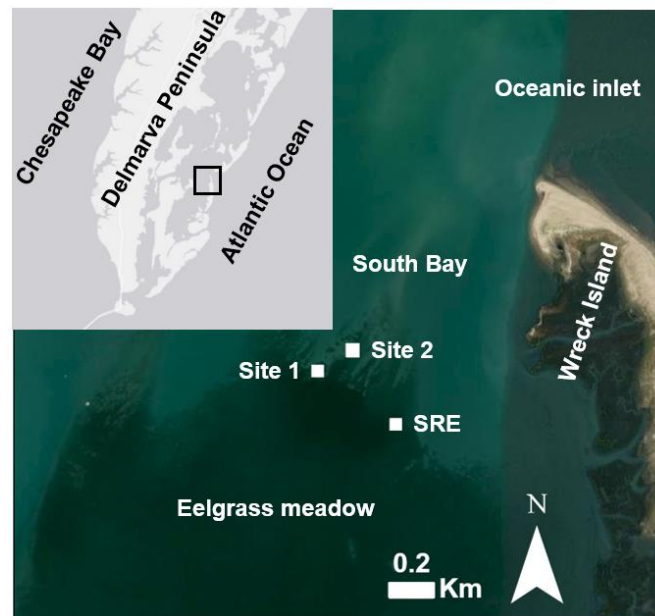


Figure 1.1. Map of thesis study locations Site 1 (37.278611 N, -75.811389 W) and Site 2 (37.279167 N, -75.810833 W) along northern edge of South Bay eelgrass meadow between the Delmarva Peninsula and Wreck Island. Northern site of Seagrass Resilience Experiment (SRE) also pictured.

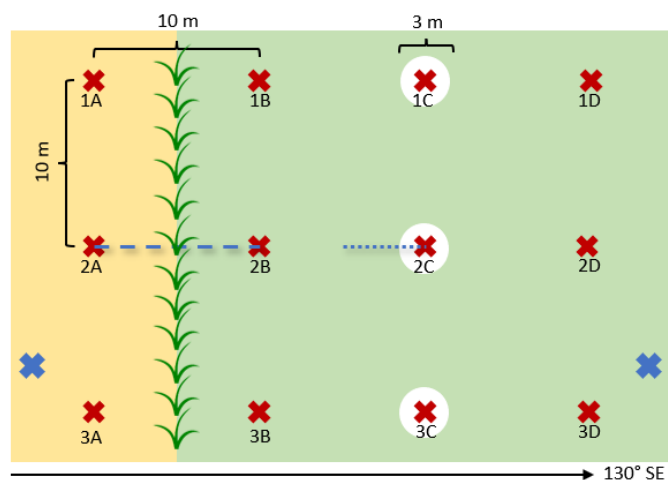


Figure 1.2. Site 1 sampling array with three parallel transects (1-3) heading 130° SE from naturally unvegetated seafloor (yellow) past the meadow's edge into vegetation (green), each with four replicative, designated locations (A-D) for bivalve and sediment sampling (red Xs). C locations occur in manmade bare patches of 3 m diameter (white). Hydrodynamic sampling occurred along smaller transects and at site perimeters (blue dashes, blue Xs).

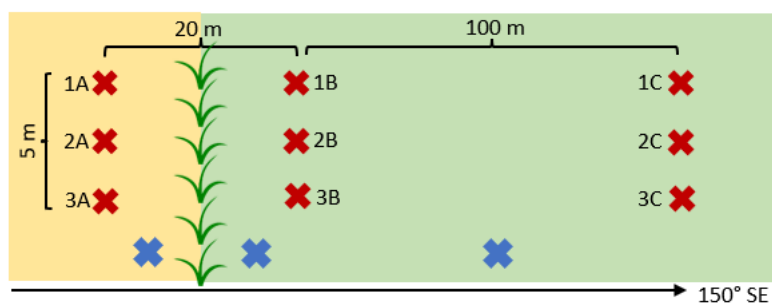


Figure 1.3. Site 2 sampling array with three sampling locations (A-C) each with three replicates roughly 1 m apart. Sampling locations aligned on a transect heading 150° SE from naturally unvegetated seafloor (yellow) past the meadow's edge into vegetation (green) for bivalve and sediment sampling (red Xs). Long-term hydrodynamic instrumentation was deployed further into seagrass vegetation and short-term deployments occurred simultaneously spanning the meadow's edge of vegetation (blue Xs).



Photo 1.1. Drone photo of Site 1 taken by Spencer Tassone where naturally bare seafloor (left), the meadow's natural edge of vegetation, bare patches, and innermost vegetated sites (right) are visualized.

Chapter 2: Hydrodynamic conditions and wave activity

2.1 Objectives

Research question #1 asks: How do hydrodynamic conditions and wave activity change across various edges of seagrass vegetation? The objective of this question is to quantify how the presence of seagrass changes hydrodynamic conditions across natural meadow edges of vegetation and in discontinuous patch areas by studying flow patterns ranging from small-scale turbulence regimes to larger-scale fluctuations in mean flow and wave dynamics. Based on previous research I hypothesize that areas with any vegetation will experience lower mean flows and wave attenuation compared to bare areas. However, I expect that changes to turbulence regimes may vary depending on seagrass density and may locally increase directly along edges of vegetation.

2.2 Methods

Instrumentation

To assess differences in wave characteristics across the meadow's edge of seagrass vegetation, wave gauges (Richard Branker Research© RBRduo³) were concurrently deployed near-continually from May through August 2021 at Site 1. These instruments were fastened to weighted metal frames which remained on the seafloor for 2-5 weeks at a time in their respective locations, one in naturally bare seafloor near A transect sites and one in full vegetation near D transect sites (blue Xs, Figure 1.2). These instruments were programmed to record wave height measurements every 10 minutes at 4 Hz for bursts of 1024 samples which were averaged to produce a mean value for that time frame. Critical metrics measured by this instrumentation include water depth, tidal slope,

and significant wave height. These instruments were used again in summer 2022 to collect the same data concurrently with other instrumentation for several days at a time. To measure similar wave characteristics over 2-5 weeks, in summer 2022 a RBR TWR 2050 wave gauge was deployed from May through June on a weighted instrument frame in seagrass vegetation (blue X, Figure 1.3). This wave gauge was similarly programmed to collect data every 10 minutes to produce a mean representative data point for that time.

Two high resolution Nortek Aquadopp© acoustic Doppler current profilers (ADCPs) were used to quantify and compare general flow conditions at Site 1 in summer 2021 in bare and vegetated sampling locations (blue Xs, Figure 1.2). Instruments were fastened to the same frames as the RBRduo³ instruments and deployed for the same time periods, collecting data for two to three weeks with extended battery and internal storage capabilities (Photo 2.1). The ADCPs were programmed to collect velocity data every 10 minutes at 2 Hz for a burst of 60 samples in 0.03 m bins starting roughly 0.1 m above the seafloor. Using the internal instrument compass and tilt sensors, velocity measurements were recorded in the east-north-up (ENU) coordinate system to produce both directional and horizontally averaged velocity profiles in 0.03 m bin elevations from $z = 0.1$ m to roughly $z = 1.5$ m (upper boundary due to instrument limit). Due to signal interactions with the water surface, velocities within 0.2 m of the water surface were not recorded. In summer 2022, one Aquadopp was deployed at Site 2 (blue X, Figure 1.3) to measure velocities in seagrass vegetation for background information.

A Teledyne RD Instruments© Streampro ADCP was used to produce instantaneous velocity and depth profiles along two transects at Site 1 during summer 2021. The Streampro has a small transmitter probe attached to internal machinery housed

by a floatation device. The instrument was moved by pulley system along a 10 m towline between two stationary but movable PVC poles. Velocity data in the x, y, z directions were collected in ~0.05 m vertical bins roughly every 0.5 m along the transect depending on tow speed. This generates a continuous profile of flow speeds in 0.05 m depth increments across the entire transect, with corresponding depth information. The Streampro collected data in two locations at Site 1: 1) edge transects starting near A sites moving into vegetated B sites with the natural seagrass edge as the midpoint, and 2) patch transects covering the edge of the manmade bare patch. Due to the length of the towline, transects covering these sites were set up so that the end marker poles were both in full vegetation on either side with the patch center as the midpoint. Care was taken to align these transects roughly perpendicular to dominant flow direction and at least 20 transect pulls were conducted during each round of sampling.

During summer 2021, a Nortek© Vectrino II acoustic Doppler profiler was used to quantify high resolution velocity and turbulence statistics (Photo 2.2). Like the Streampro, the Vectrino was deployed along two transects at Site 1 to address changes in flow and turbulence conditions across various edges of vegetation (blue dashed lines, Figure 1.2). The edge transect covered 10 meters, beginning 5 m away from the seagrass edge over a naturally bare seafloor, with the edge of vegetation as the transect midpoint, and continuing 5 more meters into full vegetation past the edge (Photo 2.4A). Data was collected across 10 sampling locations with the Vectrino in 1-meter increments along this transect. The patch transect spanned 3 meters beginning in the center of the manmade bare patch (C), crossing the edge of vegetation, and continuing 1.5 more meters into the seagrass (Photo 2.4B). Data was collected across 7 sampling locations in 0.5-meter

increments along this transect. At each transect sampling location, the Vectrino was situated 0.15 m above the seafloor and emitted doppler pulses from a center transmitter received by four passive transducers angled 30° towards the center with recorded velocity data corresponding to a sampling volume of $z = 0.1$ m. Data was collected at 25 Hz for 5 minutes resulting in 7500 samples at each location on the transect which were averaged into a representative value for that location. When sampling over vegetation, seagrass blades below the transducer which could interrupt data collection were removed if necessary. The transducer was aligned along a uniform 220° trajectory.

To provide concurrent quantifications of velocities and turbulence statistics across a seagrass edge and to expand on previous data collection, in summer 2022 two Nortek© Vector acoustic Doppler profiler instruments were deployed (Photo 2.3). These were placed 10 m apart at Site 2 (blue Xs, Figure 1.3; Photo 2.5), each 5 m from the natural edge of seagrass vegetation. This distance was chosen to mimic the scale of Vectrino data collection. The Vectors were placed on weighted metal frames and positioned 0.35 m above the seafloor to collect data .15 m below the instrument's sensor for a sampling volume at $z = 0.2$ m, which is within the canopy of vegetated locations. The instruments recorded data for at least 72 hours per deployment during which they were programmed to collect data every 20 minutes for a burst of 10-minute duration at a sampling rate of 32 Hz. The data collected during these bursts were averaged into a mean representative value for that time. The Vector instrument frames each housed an RBRDuo³ to simultaneously quantify wave activity, and these were fastened with the sensor tips facing towards the Vector sensor at a 0.30 m height above the seafloor.

Data analysis

Data from the Vectrino instrument was collected and averaged in 5-minute bursts to produce a representative value of each metric for that sampling period at each transect location. Relevant data points analyzed from this instrument include mean dominant (\bar{u}), transverse (\bar{v}), and vertical velocities (\bar{w}) in cm/s and turbulent Reynolds stresses in cm^2/s^2 . The Vectrino was positioned so that the instrument recorded dominant mean velocities (\bar{u}) in the same direction during every deployment, a 220° trajectory roughly parallel to dominant mean flow direction in South Bay. Equation 1 was used to generate a horizontally averaged velocity magnitude (U) for each sampling burst.

$$U = \sqrt{\bar{u}^2 + \bar{v}^2} \quad (1)$$

Turbulent Reynolds stress quantifies magnitude of turbulent velocity fluctuations in a flow regime and may be expressed as $\overline{u'w'}$, where u' and w' represent the horizontal and vertical components respectively.

Data from the Vector was collected and averaged in 10-minute bursts to produce representative values of similar metrics where U was quantified as previously described. The Vector records directional mean velocities in the east-north-up (ENU) reference frame using internal compass and tilt sensors, and then rotates the velocities to dominant flow direction (u) to produce mean velocity and turbulence statistics along the u , v , and w trajectories. Turbulent kinetic energy (TKE) was also quantified with Equation 2 using the burst-averaged outputs of $\langle u'u' \rangle$, $\langle v'v' \rangle$, and $\langle w'w' \rangle$ estimates from the Vector.

$$TKE = 0.5(u'^2 + v'^2 + w'^2) \quad (2)$$

Vector data was also used to produce Power Spectral Densities (PSDs) and directional wave orbital velocities. To generate PSDs, raw velocity and turbulence data was analyzed using the methodology of wave-turbulence decomposition outlined by

Hansen & Reidenbach (2012) following the phase method of spectral decomposition (Bricker & Monismith, 2007). Underlying this methodology is the separation of directional velocity components in a flow experiencing both waves and tides. For example, the horizontal component of instantaneous flow (u) can be expressed as Equation 3, where u' is the turbulent velocity, \tilde{u} is wave induced orbital velocity and \bar{u} is the mean velocity.

$$u = u' + \tilde{u} + \bar{u} \quad (3)$$

This same distinction exists for the transverse (v) and vertical (w) velocity directions, and the components must be separated to determine which motions arise from turbulent stress, wave activity, and mean flow. This method of decomposition allows quantification of turbulent Reynolds stress with Equation 4.

$$\overline{u'w'} = \overline{uw} - \overline{\tilde{u}\tilde{w}} \quad (4)$$

This separation also allows quantification of the spectral densities of directional velocity components, and their visualization with PSDs. Adapted from Hansen & Reidenbach (2012), Figure 2.1 is a representative example of a PSD showing both wave and turbulence activity in the vertical velocity direction. Following the decomposition methodology, the spectral densities from waves are visible in the notable peak distinguished from the underlying turbulent energy. The green line shows the least squares fit to mean flow and turbulent energy regardless of wave peak, where a line with slope of $-5/3$ indicates the characteristic inertial subrange in these combined flow regimes. PSD plots like these show the spectral density of a directional component (S_{ww} , cm^2/s) on the y axis and energy frequency on the x axis, further visualizing the separation of flow components. Larger values of spectral density correspond to a higher magnitude

of energy in the flow for a given frequency, and integrating the area under the plotted curve would quantify that magnitude.

Considering the frequencies plotted in PSDs like Figure 2.1, $f < 0.3$ Hz generally reflect mean current flow and $0.3 < f < 1$ Hz encompass motions from the wave band. However, linear wave theory allows predictions for which frequencies may be influenced by attenuation throughout the entire wave domain, including for $f > 1$ Hz. Adapted from Wiberg & Sherwood (2008), Equation 5 predicts the frequencies at or above which wave attenuation may occur at elevation z above the seafloor and in water depth h .

$$f > \sqrt{g/[4\pi(h - z)]} \quad (5)$$

Wave theory also allows quantification of orbital motion velocities from data collected by the Vector's pressure sensor. Methodology and computations adapted from Dean & Dalrymple (1991) were used to quantify significant wave height (H_s) and average period (T) from the spectral densities of surface elevation and pressure. The horizontal orbital velocity may also be calculated from spectral decomposition of horizontal velocity components and isolation of wave orbital particle motion, which may be quantified regardless of vertical orbital velocity as these decay to zero at the seafloor according to linear wave theory.

2.3 Results

Physical conditions

Meteorological data for this study were taken from the nearby NOAA Station WAHV2 – 8631044 in Wachapreague, VA where weather metrics such as wind speed (m/s) and direction were measured every six minutes and the resulting quality-controlled

monthly datasets are publicly published. Depth and wave data were measured by RBR instrumentation in both seasons of sampling to quantify significant wave height (H_s). During summer 2021, average water depth of the unvegetated location was 1.5 m with minimum and maximum depths of 0.38 m and 2.98 m. Average depth at the vegetated location was 1.13 m with fluctuations between 0.06 m and 2.65 m (Table 2.1). During summer 2022, long-term depth fluctuations were only measured in seagrass vegetation at Site 2 and were 1.2 m on average during May and June with minimum depths close to zero during extreme low tides and maximum depths exceeding 2 m in June (Table 2.2).

Average monthly wind speeds from May through October 2021 during periods of data collection ranged from 2.5 ± 0.02 to 4.2 ± 0.05 m/s (Figure 2.2A). Wind direction was highly variable over each month and dominant direction changed throughout the study period with implications for wave patterns. From May through August 2021, monthly-averaged H_s at the bare location ranged from 0.05 to 0.1 m, and at the seagrass location also ranged from 0.05 to 0.1 m (Figure 2.2B). H_s did not differ significantly between the two locations over the entire study period or during any month (one-way ANOVA, $p > 0.05$). Maximum H_s during the study period occurred during a storm in late May and reached 0.6 m at both locations, leading to significantly higher H_s averages for the month of May overall (one-way ANOVA, $p < 0.001$).

Average wind speed during summer 2022 was 4.7 m/s in May and 3.4 m/s in June (Table 2.2). Wind direction was variable over this time, except for a notable period of consistently northern winds in late May with wind speeds reaching over 10 m/s. Average H_s in seagrass vegetation at Site 2 was 0.07 m in May and 0.068 m in June (Table 2.2), potentially reflecting elevated wave heights in May due to increased wind speeds. H_s also

reached a monthly maximum during the late May storm with heights exceeding 0.3 m and concurrently elevated wind speed.

Monthly figures from 2021 (Appendix I) include aligned time series data of wind speed and wind direction (trimmed to match time periods of wave data collection) and their combined, summarized data in wind rose plots, as well as depth fluctuations and H_s at the unvegetated and vegetated sampling locations. The difference in wave heights between the two locations are depicted in blue where positive differences indicate higher H_s at the bare location and negative differences reflect higher H_s in seagrass. Visualizing the lack of wave attenuation between the two locations, these differences oscillated around zero and for May through August the average differences were -0.005, -0.002, -0.006, and 0.0005 respectively. During mid-June, data was only collected from the seagrass location and these data were not included in statistical calculations as they had no corresponding values of comparison from the bare site. Monthly figures from 2022 (Appendix I) show fluctuations in H_s , wind speed, wind direction, and depth from the vegetated sampling location.

In summer 2022, seagrass biomass characteristics of blade length, width, and shoot density were measured at Site 2 with field samples and density quadrats, which were randomly placed around the site and within which the contained seagrass shoots were counted. Resulting averages for May and June were 152 and 245 shoots/m² respectively (Table 2.3). This data collection was not performed at Site 1 during 2021, but for hydrodynamic comparison in future sections, comparable density counts from the adjacent northern site of the SRE were collected and shared by Spencer Tassone and subsequently analyzed.

Mean flow conditions

Mean velocities throughout the water column were quantified concurrently across Site 1 in seagrass vegetation and in bare seafloor from June through August 2021. To control for large sample sizes, the velocity magnitudes calculated from directional components (East, North, and up) produced at each bin location in the water column were averaged into one value for that depth for each round of data collection. Two bin heights in the water column were identified as areas of interest: 29 cm (presumed to be approximately canopy height in this system) and 59 cm. Over the study period, mean velocities at 29 cm ranged from 2.5 to 5.1 cm/s in seagrass vegetation and from 6.8 to 9.1 cm/s over unvegetated seafloor (Figure 2.3A).

One-way ANOVAs were performed to assess differences in these mean velocities between the two sampling locations and the two depths of interest. Mean velocities were significantly different between unvegetated and vegetated locations at both 29 cm ($p < 0.001$) and 59 cm ($p < 0.01$). Mean velocities in seagrass vegetation were consistently lower than in adjacent bare areas, with reductions between the two sites at $z = 29$ cm ranging from 40% to over 60% in midsummer. Considering how the presence of seagrass creates greater attenuation of mean flow through the water column, there were also significant reductions in velocity at each sampling site comparing elevations of 59 cm to 29 cm ($p < 0.05$), but the seagrass site had up to 35% reductions throughout the water column where the bare site only experienced up to a 20% decrease (Figure 2.3B). Figure 2.4 includes time series velocity magnitude data and depth fluctuations at the bare (A) and seagrass (B) sites from 7/29/21 – 8/9/21 when mean flow velocities reached their minimum for the study period: 6.8 cm/s in the unvegetated location and 2.5 cm/s in

vegetation, resulting in a 63% decrease which was the largest observed over the summer. Velocity magnitude was greatest during the transition between high and low tides.

In summer 2021, seagrass shoot density was measured monthly at the northern control sites of the SRE by Spencer Tassone who collected and shared these density counts, and which are comparable to those at Site 1. These shoot densities show a negative correlation with mean flow velocities collected from May through September 2021 at the vegetated measurement location of Site 1 (Figure 2.5). Seagrass density peaked in July with an average of 476 shoots/m² and corresponded with season's lowest measured mean velocities, with a monthly-averaged rate of 3.5 cm/s during July at the vegetated site at $z = 29$ cm. Flow velocities were also measured in May and June 2022 at Site 2 in seagrass vegetation at $z = 29$ cm with an average of 4.8 cm/s during May and early June and 4.5 cm/s during late June (Figure 2.6, Table 2.2). These values are consistent with average values from summer 2021 in seagrass vegetation and show a gradual decrease in mean flow with increased shoot density (Table 2.3).

Hydrodynamic conditions across edges

Summer 2021

In summer 2021, a Streampro was used to produce instantaneous velocity profiles throughout the water column along the two hydrodynamic transects at Site 1: one crossing the natural edge of vegetation and one covering the manmade bare patch (Photo 2.4). Over 100 profiles per transect were collected during summer 2021 to assess changes in bathymetry along these transects and to quantify continuous current flow in the two edge settings. Representative profiles from both transects taken on the same day in June

and July are shown in Figures 2.7. Gaps of data in the figures occur where the instrument failed to receive a proper signal often due to interference surrounding vegetation edges.

On June 28, mean flow over the bare patch was approximately 20 cm/s with a depth of nearly 1 m which decreased to 0.75 m over adjacent vegetation (Figure 2.7A). Mean flow on this day over naturally bare seafloor reached up to 30 cm/s over 1.25 m depth, both of which decreased to 15 cm/s and 1 m respectively over seagrass vegetation past its natural edge (Figure 2.7C). On July 29, mean flow over the bare patch was around 20 cm/s over 0.85 m water depth which decreased to 0.7 m over adjacent vegetation (Figure 2.7B). Across the natural edge transect on this day, mean flow over unvegetated areas reached 30 cm/s and 1 m deep, and past the edge over vegetation was 20 cm/s on average in depths slightly greater than 0.5 m (Figure 2.7D).

Profiles from both days of data collection show depth gradients across the transects that were consistent over the study period: depth increased in areas without vegetation due to absence of the seagrass itself or topographic changes in the seafloor that typically accompany seagrass meadows. At the bare patch, flow was consistently measured as approximately 0.25 m deeper over the patch area than over vegetation. This change likely results from the canopy removal and not actual bathymetric changes, as canopy height in this system is around 0.25 m. However, across the natural edge, flow depth increased up to 0.5 m from vegetation into naturally bare seafloor likely reflecting a true bathymetric response due to changes in sediment accumulation in vegetated areas. Site 2 was selected in summer 2022 to minimize these bathymetric changes across the meadow's natural edge of vegetation.

High resolution data quantifying mean flow and turbulence regimes were collected along the same two transects at Site 1 in summer 2021 with the Vectrino instrument. Data were collected in 1 m increments along the edge transect and in 0.5 m increments over the patch transect for 5 minutes in each sampling location at an elevation of $z = 0.1$ m. Values quantified during this five-minute burst were averaged into a representative mean for each sampling increment and notable metric of interest, including mean velocity magnitude, turbulent Reynolds stress (TRS), and power spectra showing magnitude of energy in the flow at different frequencies. Two complete, representative profiles of velocity and TRS from the patch transect on two separate sampling dates are shown here for further analysis along with corresponding PSDs from unvegetated and vegetated sampling locations along that transect (Figure 2.8). Two complete velocity profiles from the edge transect are also depicted (Figure 2.9). Wind and/or wave conditions during times of data collection are included in Table 2.4.

All profiles show higher mean velocity magnitudes in unvegetated areas compared to vegetated locations (Table 2.5). Along the patch transect, mean velocities were reduced in seagrass by over 75% on July 15 (Figure 2.8A) and by over 50% on August 18 (Figure 2.8C). Along the edge transect, reductions of mean flow in vegetated areas exceeded 80% on both July 26 and August 10 (Figure 2.9). These magnitudes and reductions were similar to those quantified by the ADCPs deployed at Site 1 to address changes over longer timescales. Mean velocities within the constructed bare patch were lower than those over naturally bare seafloor during the same period of data collection with similar flow conditions. The fastest velocities across all profiles, over 20 cm/s,

occurred over naturally bare seafloor of the edge transect and the lowest flow speeds, under 1 cm/s, occurred in vegetated locations of both transects.

Mean turbulent Reynolds stress was quantified along the same transect locations and normalized by flow direction to address turbulent kinetic energy (TKE) magnitude. These trends followed similar expected patterns to mean velocities where TRS was greater in unvegetated areas, reflecting higher energy flows which decrease within the seagrass vegetation (Figure 2.8A, C). However, these values were variable and included extreme outliers in many rounds of data collection, likely due to low mean flow velocities (< 3 cm/s) surrounding low or slack tide during times of data collection when quantification of turbulence statistics becomes unreliable (due to autocorrelation of velocity fluctuations). Because of this and excessive bathymetric changes along the edge transect, only Reynolds stresses (cross-corrected velocity fluctuations) from patch transects are shown here and more detailed data collection and analysis of turbulent energy regimes was conducted in 2022 (see next subsection).

Flow energy and associated reductions in vegetation at different frequencies are visualized with PSDs in Figure 2.8B and D which depicts energy magnitude at corresponding frequencies from sampling at the patch transect on July 15 and August 18. Data plotted in blue are from the vegetated sampling location furthest from the patch edge (Transect Site 7) and data in yellow are from the unvegetated location at the center of the bare patch (Transect Site 1). At almost all frequencies, flow energy in bare areas exceeds that of flows within the vegetation as expected based on trends in velocity and Reynolds stress. However, energy from frequencies in the wave band (~ 1 Hz) are similar in both sampling locations suggesting that low frequency oscillatory wave energy may

penetrate the seagrass canopy and reach similar magnitude close to the seafloor in both bare and vegetated areas. This agrees with previous findings from the same South Bay seagrass system measured by Hansen & Reidenbach (2012) and has implications for sediment resuspension (see Chapter 3).

Summer 2022

To expand on previous data collection while minimizing bathymetric changes, enhancing quantification of turbulent energy regimes, and generating a concurrent high-resolution dataset across a seagrass edge, Nortek Vector ADVs were concurrently deployed three times during the summer of 2022, each for a minimum of 72 hours. The instruments were placed 10 m apart evenly across the natural edge of meadow vegetation at Site 2 (Figure 1.3). The instrument frames also contained RBR Duo instrumentation to simultaneously quantify wave activity and suspended sediment concentrations. Each of the three deployments were characterized by different physical conditions, with summary figures showing fluctuations and comparisons in depth, wind speed, wind direction, and H_s in Appendix II. Deployment 1 from May 13 – May 16 had the lowest seagrass densities and low-medium wave activity, Deployment 2 from May 23 – May 26 had similarly low grass densities but the greatest wave activity, and Deployment 3 from June 10 – June 13 had the highest seagrass densities and lowest wave activity. These combinations of meadow morphology and physical setting allowed analysis of how velocity, turbulence, waves, and sediment resuspension respond to different conditions in bare and vegetated areas immediately surrounding a seagrass edge.

Depth and H_s data for each deployment are shown in Table 2.6. On average, water depths were only 0.1 m greater at the bare sampling locations, an intentional reduction

from depth differences of up to 0.5 m between bare and seagrass locations at Site 1 during summer 2021. Identifying an edge site with limited bathymetric changes allowed for more standardized hydrodynamic data analysis in this sampling season, particularly with respect to turbulence regimes. Average overall wave heights for Deployments 1, 2, and 3 were 0.06 m, 0.15 m, and 0.04 m respectively (Figure 2.10A), with maximum wave heights reaching 0.16 m, 0.32 m, and 0.11 m respectively. There were no significant differences between H_s at the two sampling locations within each deployment, consistent with wave data from summer 2021. However, Deployment 2 had elevated wave heights overall. Examining wind activity during Deployment 2 reveals higher average wind speeds during this period and consistent northerly winds, a contrast to the wide range of directionality in Deployments 1 and 2 (Appendix II). Mean wind speeds per deployment were 2.3, 6.9, and 3.2 m/s respectively, closely aligning with trends in H_s (Figure 2.10B)

Mean velocity magnitudes were quantified at each site per deployment to produce an average flow speed (cm/s) for the duration of sampling (Figure 2.11A). Standard deviations are not portrayed as these mainly encompass cyclical deviations from the mean due to tidal cycle. Mean velocities at the unvegetated site ranged from 8.8 to 11.1 cm/s and from 3.3 to 7.7 cm/s at the vegetated site. Velocities were highest during Deployment 1 and decreased with each subsequent deployment, displaying an inverse relationship with seagrass shoot density as in summer 2021 (Figure 2.5). Velocities were consistently and significantly higher in magnitude at the unvegetated location (Two-sided T test, $p < 0.05$). Percent reduction of flow speed between the two sites ranged from 30% during Deployment 1 to over 65% during Deployment 3, similar to reductions during 2021 and again correlating with increases in seagrass shoot density.

Reynolds stress was quantified to address differences in the turbulent energy fluctuations. Due to variability from flow direction and outliers caused by excessively slow flows and/or seagrass blade interference, the absolute value of measured Reynolds stresses was analyzed when mean velocities were above 3 cm/s. The average magnitudes of Reynolds stress per deployment at each sampling location are shown in Figure 2.11B. Reynolds stresses were similar to values from summer 2021, but were consistently and significantly greater in magnitude at vegetated locations (Two-sided T test, $p < 0.05$), ranging from 1.3 to 1.9 cm^2/s^2 at the bare site and from 2.3 to 2.7 cm^2/s^2 at the seagrass site. Like mean velocities, standard deviations are large due to tidal fluctuations and not pictured, but confidence intervals for means were relatively small.

Reynolds stresses were also quantified after performing wave-turbulence decomposition to separate and remove the turbulent energy generated by wave presence and resulting values are shown in Figure 2.11C. Mean TRS in bare locations ranged from 0.29 to 0.36 cm^2/s^2 and in vegetated locations from 0.49 to 0.75 cm^2/s^2 again consistently and significantly greater in vegetated sampling areas (Two-sided T test, $p < 0.05$). TRS generally scaled in magnitude with non-decomposed Reynolds stresses, but values from Deployment 2 showed the greatest decrease after wave-driven turbulence was removed due to high wave activity during this round of sampling. Turbulent kinetic energy (TKE), another metric to quantify turbulent velocity fluctuations, was also measured and recorded when velocities were greater than 3 cm/s but showed high variability, generally elevated values, and no significant or consistent trends between the two sampling locations (Figure 2.12A).

Wave orbital velocities were quantified at the two sites for each deployment to address differences in horizontal orbital motion. Vertical orbital velocities decay to zero in the water column towards the seafloor, but horizontal orbital motions may persist at depth and change in the presence of canopy vegetation. Average horizontal orbital velocities ranged between 3.1 and 17.3 cm/s (Figure 2.12B). Although there were no significant differences in average magnitude between the two sampling locations, consistent with similar H_s between sampling locations, the range of values emphasize that Deployment 2 had the greatest wave activity as also seen with H_s and likely caused by elevated wind speeds.

Differences between wave activity and tidal dominance in the flow regime and resulting changes in mean velocity and turbulence are also visible through PSDs of both horizontal and vertical velocity fluctuations. PSDs of vertical velocities measured concurrently at bare (Figure 2.13A and 2.13C) and vegetated (2.13B and 2.13D) sites were dominated by tidal current during Deployment 1 (2.13A and 2.13B) and by wave activity during Deployment 2 (2.13C and 2.13D). During tidally dominated flow conditions, a distinct $-5/3$ slope exists in the spectra across frequencies of motion, indicating an expected inertial subrange. Energy magnitude across frequencies was generally similar between the unvegetated and vegetated sampling locations in this example, with slightly higher energy at higher frequencies ($\text{Hz} > 1$) in the vegetated PSD, indicating increased turbulence as reflected in elevated Reynolds stresses. During wave-dominated conditions, the same $-5/3$ trend exists outside of the frequencies encompassing the wave band. In this comparison, the energy magnitude at low frequencies ($\text{Hz} < 0.3$) is distinctly higher in the unvegetated PSD, indicating higher instantaneous flow and a

resulting reduction in seagrass vegetation as reflected by mean velocity calculations. Examining frequencies in the wave band ($0.3 < \text{Hz} < 1$), wave motion efficiently penetrated the eelgrass canopy to a similar degree than seen in the unvegetated PSD, mirrored by similar calculated horizontal wave orbital velocities between the sites.

Other PSDs show horizontal (2.14A and 2.14B) and vertical (2.14C and 2.14D) velocities for frequencies from 0 to 2 Hz from Deployment 1 at the bare (2.14A and 2.14C) and vegetated (2.14B and 2.14D) locations. Figure 2.15 shows the same array for Deployment 2. The black line oscillating across the PSDs portrays Equation 5 (see methods), which is the frequency threshold at or above which wave attenuation may be expected due to natural decay of the waves with depth under linear wave theory. Like previous PSDs, $\text{Hz} < 0.3$ correspond to tidally dominated flow activity and frequencies above this are attributable to wave motion. Gaps in these figures represent a lack of data collection due to vegetation interference or low water levels at low tides leaving the sensors exposed. Figures 14 and 15 show minimal attenuation of wave frequencies in vegetated locations. There is a slight reduction in horizontal velocity PSD at frequencies < 0.3 in vegetated locations, reflecting a reduction in mean flow. At all sites, horizontal velocities in the wave band ($\text{Hz} > 0.3$) exhibit a distinctly higher magnitude in Deployment 2, consistent with elevated wind speeds, H_s , and mean horizontal orbital velocities from this round of sampling (Table 2.6, Figure 2.10, Figure 12B).

2.4 Discussion

Physical meteorological conditions, water depth, wave heights, and seagrass densities were similar in magnitude and fluctuation during both years of sampling. Seagrass densities measured at the adjacent SRE site by Spencer Tassone in 2021 were

comparable to those from Site 2 in 2022 and predictably increased as the summer season of growth progressed leading to greater overall biomass. Shoot densities from Site 2 were slightly lower than from the SRE location and previous research in the central South Bay seagrass meadow, indicating that northern edge sites have somewhat reduced shoot density, but simultaneously greater lengths (Hansen & Reidenbach, 2012). Water depth was also similar at Sites 1 and 2, but Site 2 had a much smaller difference in seafloor elevation between vegetated and bare areas resulting in higher confidence in hydrodynamic measurements and comparison across sampling locations.

Wind speeds and significant wave heights were closely correlated during all periods of sampling, with recorded increases in wind leading to greater H_s and wave orbital velocities, particularly visualized by the two significant storms that affected the study sites in 2021 and 2022 both in late May. This enforces that wave activity and characteristics are driven by surface winds in this system, supporting previous research from South Bay and the VCR LTER (Fagherazzi & Wiberg, 2009). Despite this strong positive relationship between winds and waves across the study sites, there was no evidence of wave attenuation in seagrass vegetation compared to naturally bare seafloor at either the 10 or 25 m distance of sampling separation, in contrast with previous results showing consistent H_s attenuation in vegetated areas compared to bare locations hundreds of meters away (Fonseca & Calahan, 1992; Reidenbach & Thomas, 2018). In fact, H_s and orbital velocities were occasionally elevated in seagrass vegetation compared to bare areas when northerly winds led to wave shoaling along the meadow's northern edge. Likely the proximity of sampling sites in this study are responsible for a lack of

measurable attenuation, and future work could be directed at quantifying the threshold of seagrass presence or distance from meadow's edge that results in wave attenuation.

Mean flow velocities were consistently and significantly reduced in seagrass vegetation during all periods of sampling and regardless of distance from the edge or bare seafloor. Reduction in long term mean flow between sampling locations in Site 1 reached over 60% at canopy height, and seagrass presence here also led to greater velocity reduction at lower elevations in the water column compared to unvegetated areas. Instantaneous velocity profiles along shorter edge transects showed local reductions of over 30% in vegetation, and high-resolution burst sampling along the same transects showed up to 75% reductions. Velocity reduction in seagrass ranged between 30 and 65% across the edge transect at Site 2, and corresponding energy magnitude of flow in these locations was similarly lowered. This significant and replicated decrease of mean flow with seagrass presence across all settings agrees with previous research (Fonseca & Fisher, 1986; Hansen & Reidenbach, 2012; Koch & Gust, 1999; Peterson et al., 2004) but adds discovery of the presence and magnitude of these reductions along various edge configurations and distances of a smaller scale. The magnitude of flow reduction in vegetated areas was inversely correlated with seagrass density, suggesting that canopy presence is responsible for mediating the magnitude of decrease of current flows.

Turbulence regimes measured during summer 2021 at Site 1 showed generally reduced Reynolds stresses in seagrass vegetation, but these measurements were potentially unreliable due to excessively low flows, changes in tide over the sampling period, and notable differences in bathymetry across edges of vegetation. These measurements were also taken at a low sampling elevation of $z = 0.1$ m. Results from

summer 2022 in a more standardized sampling environment with concurrent data collection higher in the seagrass canopy ($z = 0.2$ m) reveal opposite trends with consistently and significantly greater Reynolds stresses across the meadow's edge in seagrass vegetation. This pattern remained consistent after performing wave-turbulence decomposition to address turbulent energies regardless of wave presence. This finding aligns with conclusions from Hansen & Reidenbach (2012) who suggested that turbulent energies may be elevated in vegetated areas of low shoot density, which characterized the vegetated edge sampling locations of Sites 1 and 2. Increased stem-wake interactions in a lower density canopy result in higher Reynolds stresses (Nepf et al., 1997, Widdows et al., 2008).

This increase in turbulence was also reflected in PSDs from Site 2 sampling which showed elevated magnitudes of turbulent energy in seagrass at higher frequencies of the energy spectra. These PSDs and those from Site 1 portrayed the concurrent decrease in energy at lower frequencies reflecting a reduction in mean flow. All PSDs revealed the persistence of wave presence in seagrass vegetation as visualized by peaks of energy magnitude in frequencies encompassing the wave band, regardless of sampling location. In summary, the PSDs from high-resolution velocity and turbulence sampling emphasize the similar wave activity, reduced mean flow, and enhanced Reynolds stress in seagrass vegetation at the two study sites both across the meadow's natural edge of vegetation and in the smaller, manmade patch settings.

2.5 Photos, figures, and tables



Photo 2.1. Instrument frame with Aquadopp (black) and RBRduo³ (white) in vegetation.



Photo 2.2. (Left) Vetrino instrument (black) secured to instrument frame recording instantaneous velocity data over seagrass vegetation. **Photo 2.3.** (Right) Vector instrument (black) secured to weighted instrument frame over seagrass vegetation.

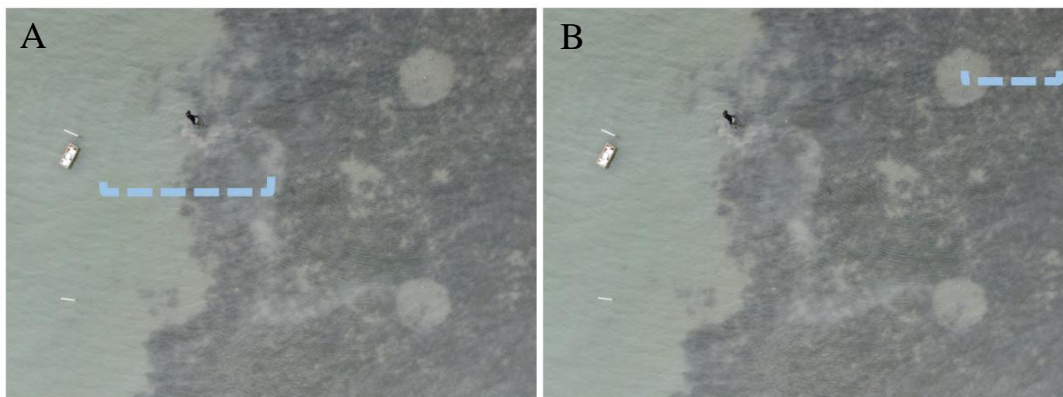


Photo 2.4. Drone photos taken by Spencer Tassone with blue dashed lines showing transects of hydrodynamic sampling at Site 1 in 2021. A) Edge transect spanning the meadow's natural edge of vegetation. B) Patch transect spanning the edge of the manmade bare patch.



Photo 2.5. Drone photo taken by Spencer Tassone showing two Vector instrument frames deployed across the meadow's natural edge of vegetation at Site 2 in summer 2022.

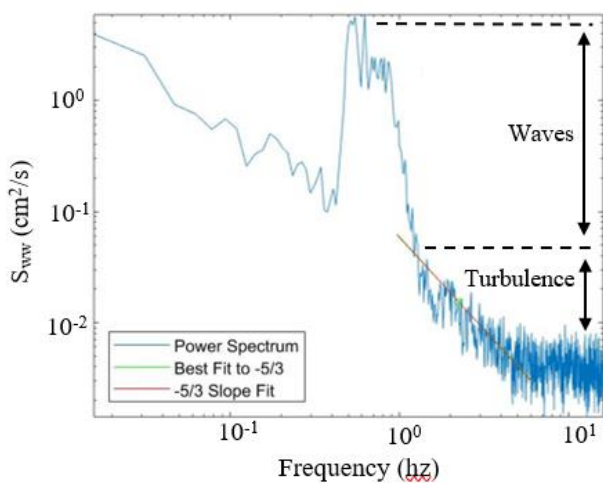


Figure 2.1. Power spectral density (PSD) of the vertical velocity, S_{wv} , for a 10 min representative data series computed at $z = 0.2$ m at an unvegetated site, where z is the vertical distance above the seafloor. Locations in the spectra corresponding to wave and turbulent energies are depicted. Red line shows $-5/3$ slope indicative of inertial subrange and green line shows best fit to the data outside of the wave domain. Adapted from Hansen & Reidenbach (2012).

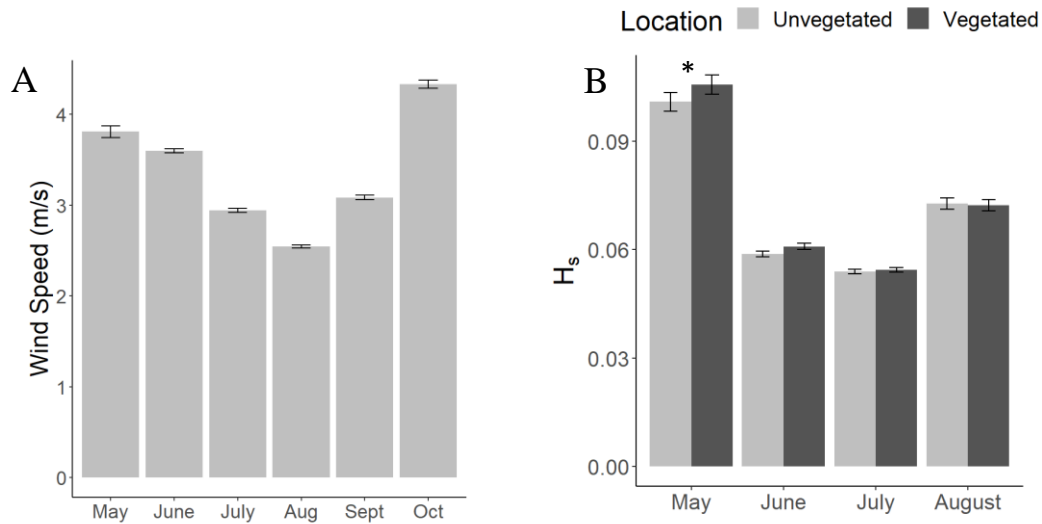


Figure 2.2. A) Monthly average wind speeds (m/s) \pm 1 SE from 2021. B) Monthly average significant wave heights (H_s , m) \pm 1 SE from 2021 at vegetated and unvegetated locations. Asterisk denotes significance (one-way ANOVA, $p < 0.05$) for total May values.

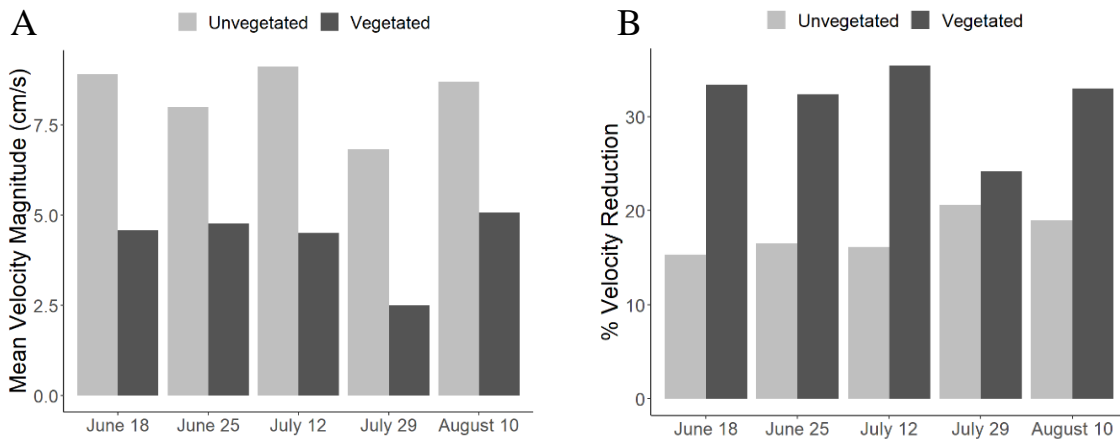


Figure 2.3. A) Mean velocities (cm/s) quantified at a 29 cm elevation above the seafloor for each deployment period of 2021 from unvegetated (light) and vegetated (dark) sampling locations. B) Percent velocity reduction from 59 to 29 cm elevations in the water column at vegetated and unvegetated sampling locations during 2021.

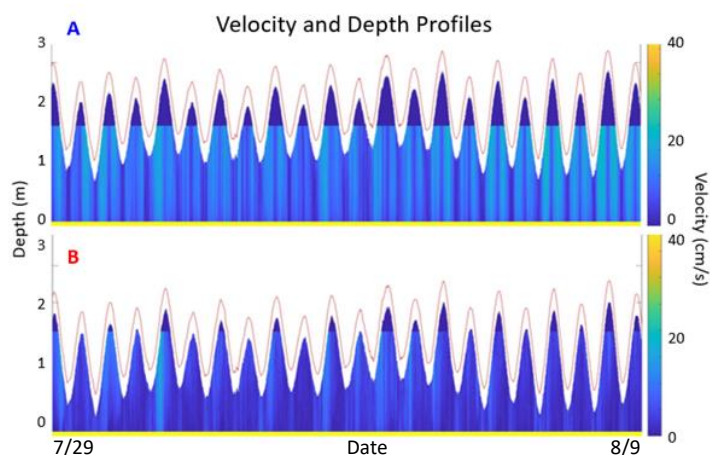


Figure 2.4. Velocity (blue scale, cm/s) and depth (red line, m) fluctuations at the bare (A) and seagrass (B) sites from July 29, 2021 to August 9, 2021. Solid color areas of dark blue and yellow at the top and bottom of each graph reflect locations in the water column where no data was collected due to instrument limitation.

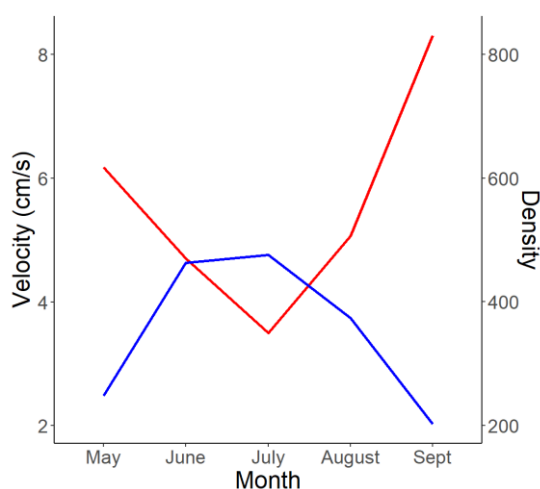


Figure 2.5. Average monthly velocities (red, cm/s) at $z = 29$ cm from Site 1 during 2021 and average monthly seagrass shoot densities (blue, shoots/m²) collected by Spencer Tassone at adjacent northern SRE control sites during 2021.

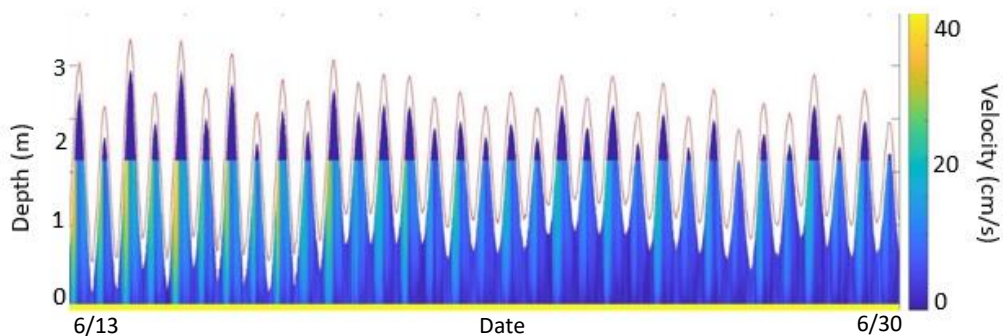


Figure 2.6. Velocity (blue scale, cm/s) and depth (red line, m) fluctuations in vegetation at Site 2 from June 13, 2022 – June 30, 2022. Solid color areas of dark blue and yellow at the top and bottom of the graph reflect locations in the water column where no data was collected due to instrument limitation.

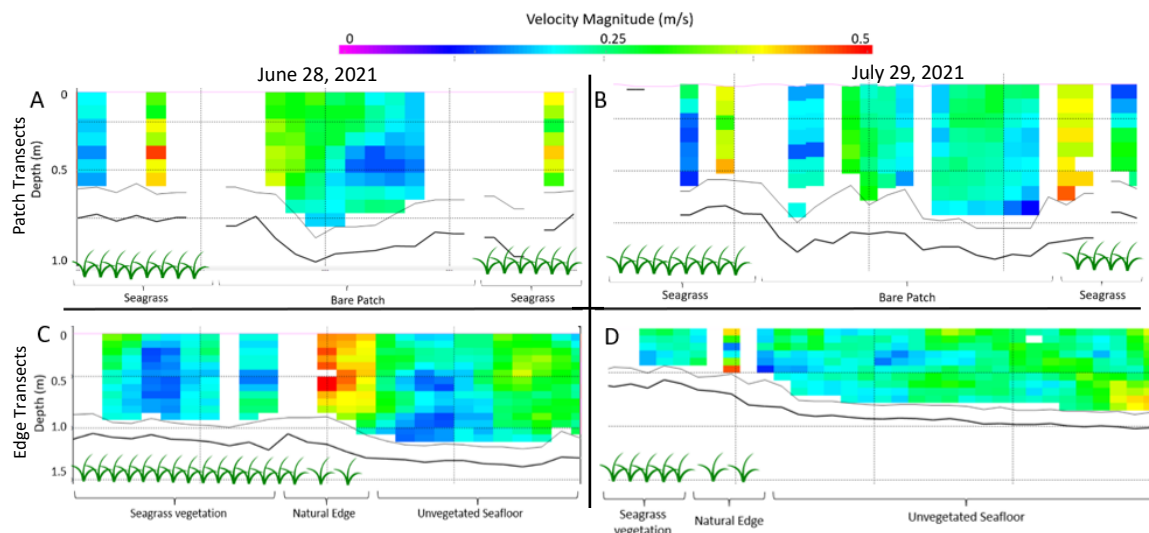


Figure 2.7. Depth (black line, m) and velocity magnitude (color scale, m/s) profiles over transects spanning the meadow's natural edge (C and D) and the manmade bare patch (A and B) at Site 1. Profiles A and C are from June 28, 2021, and B and D are from July 29, 2021.

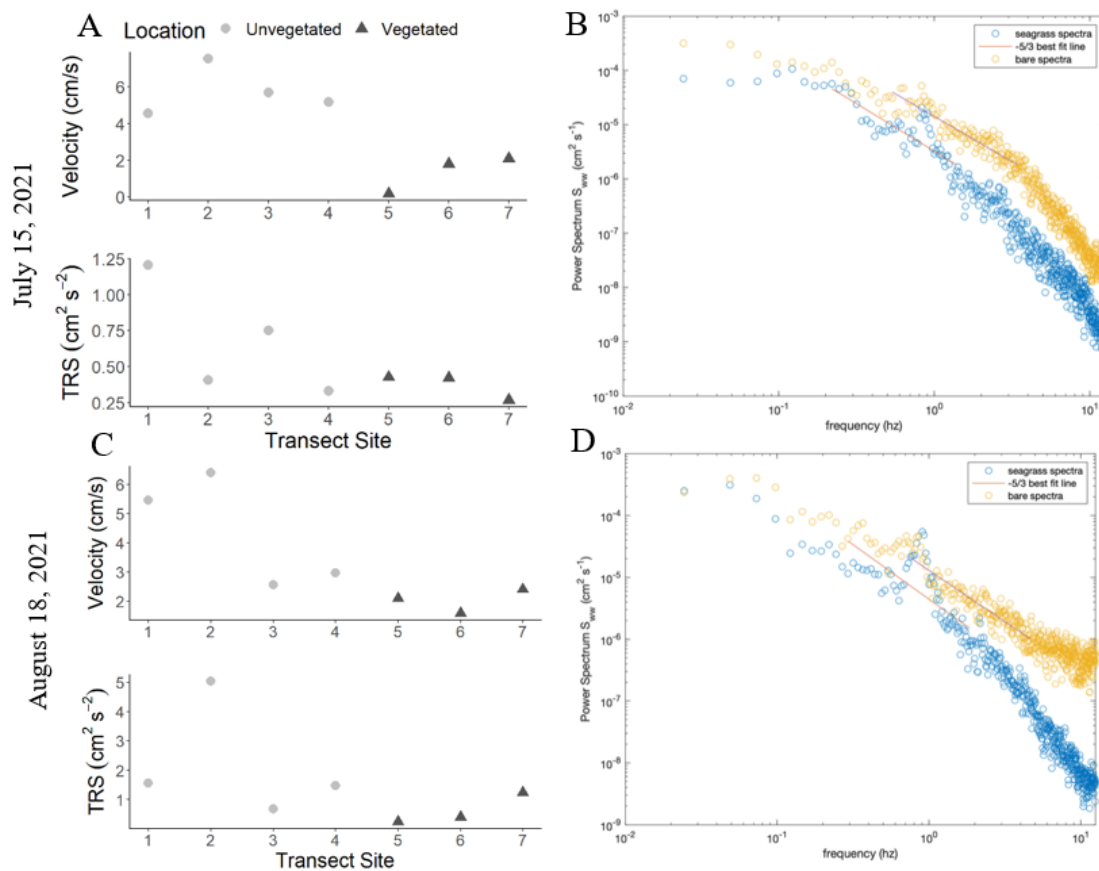


Figure 2.8. Profiles of mean velocity (cm/s) and turbulent Reynolds stress (cm^2/s^2) from transects spanning the edge of manmade bare patch on July 15, 2021 (A) and August 18, 2021 (C) in addition to PSDs from the same dates (B and D, respectively) quantified in unvegetated (yellow) and vegetated (blue) sampling locations.

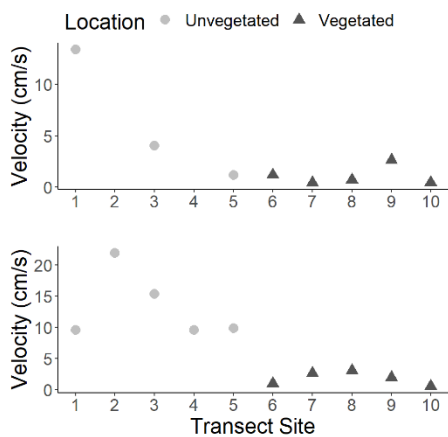


Figure 2.9. Profiles of mean velocity (cm/s) from transects spanning the meadow's natural edge of vegetation on July 26, 2021 (top) and August 10, 2021 (bottom).

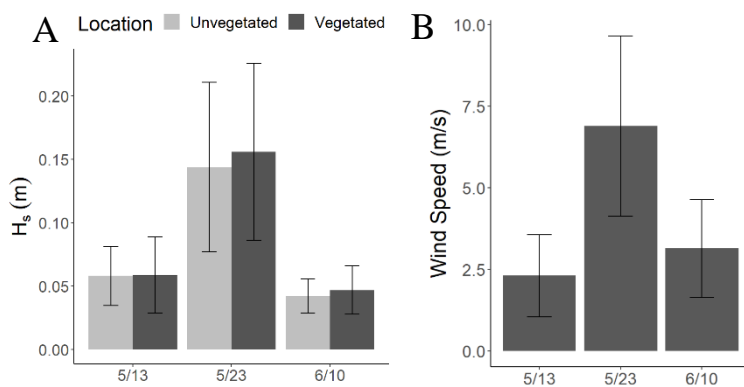


Figure 2.10. A) Average H_s (m) \pm 1 SD from the unvegetated and vegetated sampling locations and B) average wind speed (m/s) \pm 1 SD during Vector deployment in 2022.

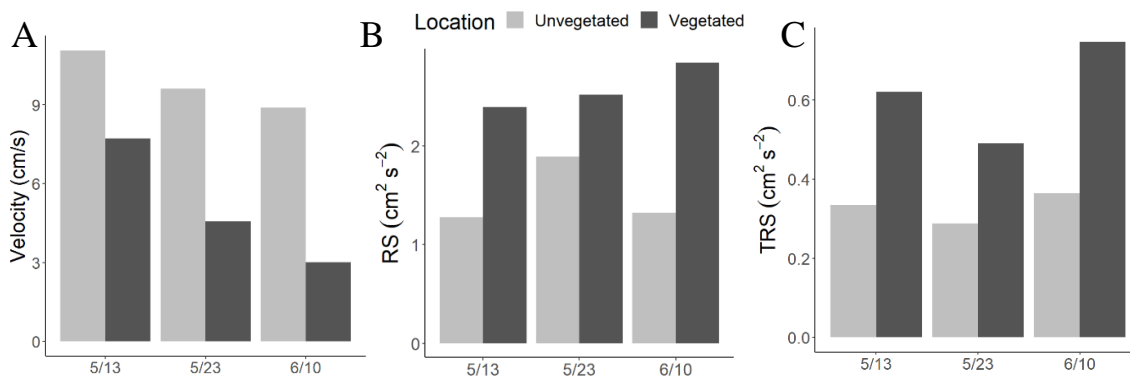


Figure 2.11. A) Velocities (cm/s), B) overall Reynolds stresses (cm^2/s^2), and C) turbulent Reynolds stresses (cm^2/s^2) after removing the influence of wave energy. Mean values shown from unvegetated and vegetated sampling locations during the three Vector deployments in 2022.

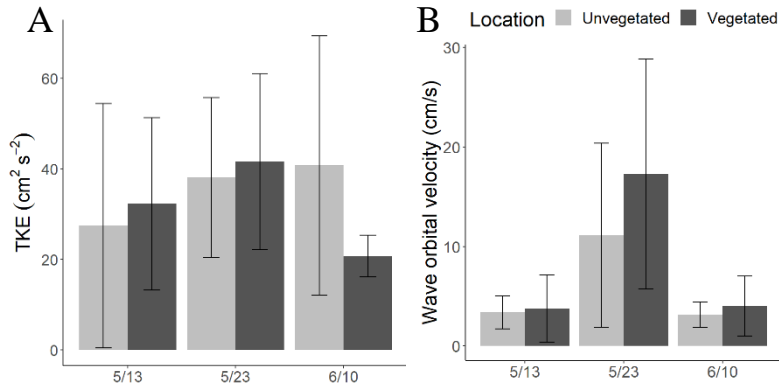


Figure 2.12. Mean values of A) TKE (cm^2/s^2) and B) horizontal wave orbital velocities (cm/s) from unvegetated and vegetated sampling locations during the three Vector deployments in 2022. Error bars reflect ± 1 SD.

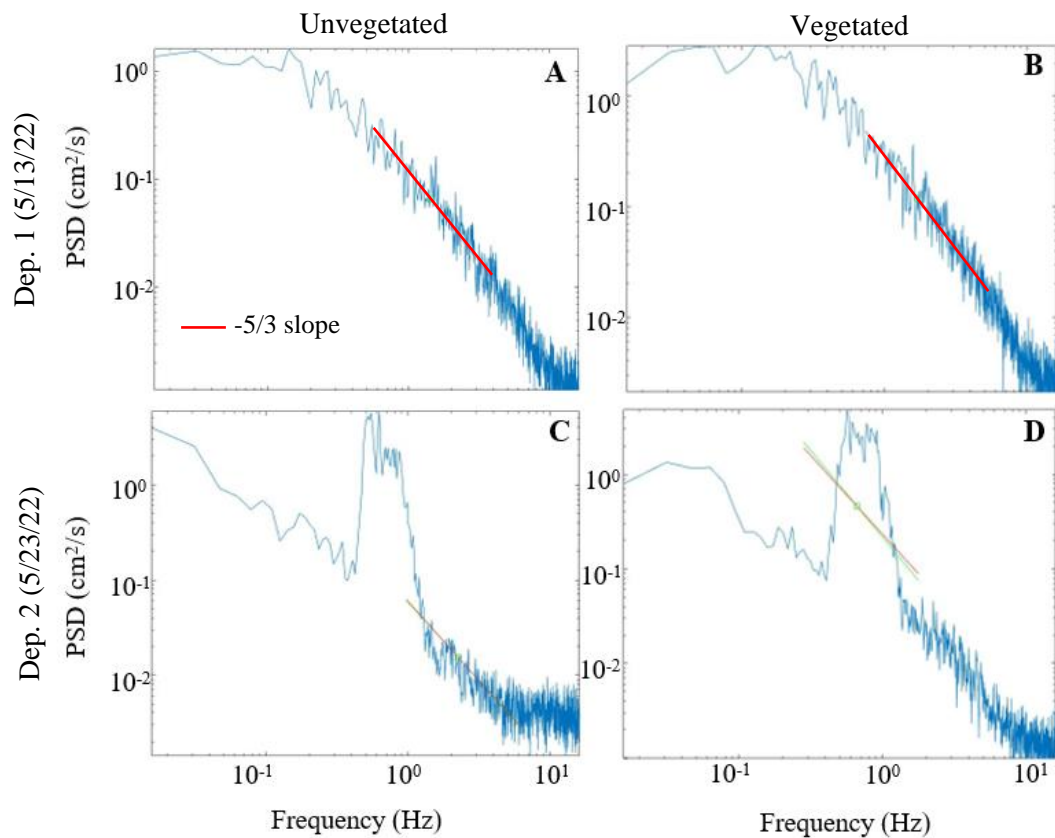


Figure 2.13. PSDs of vertical velocity energy magnitude at various frequencies from unvegetated (A and C) and vegetated (B and D) sampling locations during Deployment 1 (A and B) with tide-dominated conditions and Deployment 2 (C and D) with wave-dominated conditions. The $-5/3$ in A and B indicates the characteristic inertial subrange of tidal flow while the faint lines in C and D are artifacts of data processing.

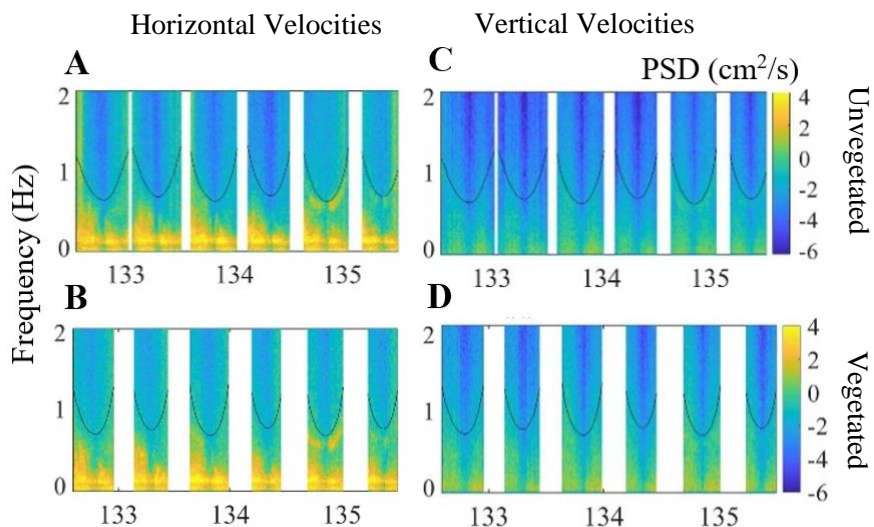


Figure 2.14. PSDs of horizontal (A and B) and vertical (C and D) velocities at frequencies under 2 Hz at unvegetated (A and C) and vegetated (B and D) sampling locations during Vector Deployment 1 from 5/13/22 – 5/16/22, corresponding to Julian days 133-135 on the x-axes. Black lines show the lower threshold of expected wave attenuation. Gaps in the figure represent periods of no data collection due to instrument exposure at low tide.

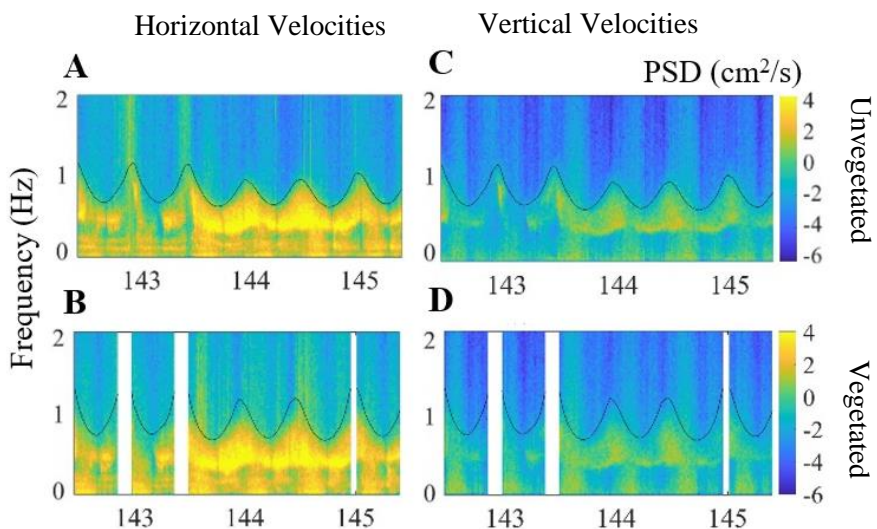


Figure 2.15. Same array as Figure 2.14 but showing Dep. 2 from 5/23/22 – 5/26/22.

Table 2.1. Monthly averages of depth (m) \pm 1 SE at sampling locations during 2021.

| <i>Average Depths (m)</i> | <i>Unvegetated</i> | <i>Vegetated</i> |
|---------------------------|--------------------|------------------|
| <i>May</i> | 1.52 \pm 0.014 | 1.20 \pm 0.014 |
| <i>June</i> | 1.15 \pm 0.007 | 1.11 \pm 0.007 |
| <i>July</i> | 1.47 \pm 0.007 | 1.09 \pm 0.007 |
| <i>August</i> | 1.52 \pm 0.01 | 1.17 \pm 0.01 |

Table 2.2. Monthly averages of depth (m), significant wave height \pm 1 SE (H_s , m), wind speed \pm 1 SE (m/s), and mean flow velocity (cm/s) from seagrass vegetation in 2022 at Site 2. Velocities were recorded at an elevation of $z = 29$ cm.

| | <i>Depth (m)</i> | <i>Wind Speed (m/s)</i> | <i>H_s (m)</i> | <i>Mean Velocity (cm/s)</i> |
|-------------|------------------|-------------------------|-----------------------------|-----------------------------|
| <i>May</i> | 1.20 | 4.67 \pm 0.05 | 0.070 \pm 0.06 | 4.8 |
| <i>June</i> | 1.16 | 3.39 \pm 0.04 | 0.068 \pm 0.06 | 4.5 |

Table 2.3. Blade length, width, and shoot density per square meter from vegetated sampling locations during summer 2022 with number of counts performed per month as n_{density} .

| | <i>Blade Length (cm)</i> | <i>Blade Width (cm)</i> | <i>Density (shoots/m²)</i> | <i>n_{density}</i> |
|-------------|--------------------------|-------------------------|---------------------------------------|--|
| <i>May</i> | NA | NA | 153 \pm 28 | 6 |
| <i>June</i> | 48 \pm 8 | 0.35 \pm 0.05 | 245 \pm 72 | 8 |

Table 2.4. Average wind speeds (m/s) and H_s (m) from the four designated Vectrino deployments spanning the two transects at Site 1 during summer 2021. H_s quantified from bare (unvegetated) and seagrass (vegetated) sampling locations near the transects.

| | <i>Wind speed (m/s)</i> | <i>H_s (bare, m)</i> | <i>H_s (seagrass, m)</i> |
|----------------------|-------------------------|-----------------------------------|---------------------------------------|
| <i>July 15 Patch</i> | 1.29 | 0.044 | 0.037 |
| <i>July 26 Edge</i> | 3.00 | 0.032 | 0.050 |
| <i>Aug 10 Edge</i> | 3.93 | n/a | n/a |
| <i>Aug 18 Patch</i> | 5.04 | n/a | n/a |

Table 2.5. Average velocities (cm/s) from unvegetated and vegetated sampling locations from the four designated Vectrino deployments spanning the two transects at Site 1 during summer 2021.

| <i>Mean Velocities (cm/s)</i> | <i>Unvegetated</i> | <i>Vegetated</i> |
|-------------------------------|--------------------|------------------|
| <i>July 15 Patch</i> | 5.7 | 1.4 |
| <i>July 26 Edge</i> | 6.2 | 1.4 |
| <i>Aug 10 Edge</i> | 13.3 | 1.8 |
| <i>Aug 18 Patch</i> | 4.4 | 2.0 |

Table 2.6. Average and maximum of depth (m) and H_s (m) from the unvegetated and vegetated sampling locations of the three Vector deployments at Site 2 during summer 2022.

| | <i>Deployment 1: 5/13 – 5/16</i> | | <i>Deployment 2: 5/23 – 5/26</i> | | <i>Deployment 3: 6/10 – 6/13</i> | |
|-----------------------------|----------------------------------|------------------|----------------------------------|------------------|----------------------------------|------------------|
| | <i>Unvegetated</i> | <i>Vegetated</i> | <i>Unvegetated</i> | <i>Vegetated</i> | <i>Unvegetated</i> | <i>Vegetated</i> |
| <i>Avg Depth</i> | 1.04 | 0.90 | 1.20 | 1.09 | 0.97 | 0.89 |
| <i>Max Depth</i> | 1.95 | 1.78 | 1.92 | 1.83 | 1.86 | 1.78 |
| <i>Avg H_s</i> | 0.06 | 0.06 | 0.14 | 0.16 | 0.04 | 0.05 |
| <i>Max H_s</i> | 0.14 | 0.16 | 0.32 | 0.32 | 0.09 | 0.11 |

Chapter 3: Effects of flow conditions on sediment transport and bivalve recruitment

3.1 Objectives

Research questions #2 and #3 ask: How do the altered flow conditions of seagrass ecosystems and their various edge settings influence sediment resuspension and transport, and bivalve settlement and recruitment? The objective of question 2 is to examine how the variable hydrodynamic conditions of vegetated areas and their edges lead to differential outcomes for sediment movement in this system. I hypothesize that areas of vegetation and their corresponding lower energy flows will experience less sediment resuspension and transport, contributing to the depositional environments that eelgrass meadows often promote. The objective of question 3 is to understand how these altered flow conditions affect the associated fauna inhabiting seagrass ecosystems, particularly bivalves which have been shown to have a close relationship with their surrounding flow environments. I hypothesize that bivalve settlement and recruitment will be higher in any areas of vegetation, but especially higher along initial edges of vegetation compared to locations farther into the meadow.

3.2 Background

Sediment suspension and transport

Seagrass ecosystems in shallow, coastal bays and in South Bay specifically have been described as depositional environments for suspended sediment where resuspension is limited (Hansen & Reidenbach, 2012; Lawson et al., 2007). A variety of methods have been used at the VCR LTER to quantify suspended sediment concentrations (SSCs) and turbidity in the coastal bays, as well as net erosion, deposition, or accumulation of

sediment in the seagrass meadows and unvegetated areas, often with the goal of quantifying long term bathymetric changes in this system and to understand total sediment budgets and sediment movement in the coupled marsh-seagrass system. Less work has been focused on understanding short term changes in sediment transport and how seagrass presence mediates a response in SSCs through changes in flow regime, particularly in edge settings. A goal of research question #2 was to address this knowledge gap, and a method was needed to measure quantities and movement of suspended sediment in these settings, instead of net deposition or erosion.

Trap structures designed to collect suspended particulate settlement have been used in marine environments since the 1960s and became more intensely utilized in the following decades. Storlazzi et al. (2011) published a comprehensive review of sediment trap history and best use practices drawing on the theories, calculations, and laboratory and field experiments performed by researchers in the 1970s-1990s. Synthesizing the results of these influential studies, Storlazzi et al. (2011) formed guidelines for sediment trap use regarding trap dimension, spacing, and deployment that were incorporated in this work's methodology. They also found significant correlations between magnitude of hydrodynamic energy, near-bed shear stress, turbidity, and amount of particulate material collected by the traps suggesting that flow regime mediated the response in SSCs and the resulting trap collection rates in their study system.

An important distinction lies in defining exactly what these traps measure. Storlazzi et al. (2011) state that sediment traps of this design and deployment are "used to capture a representative sample of the net vertical flux of sediment particles in the water column," meaning they provide information about relative amounts of SSCs that

were in suspension. In coral reef environments where these traps have been frequently used, researchers have incorrectly inferred net sedimentation, deposition, or accumulation rates in areas of trap deployment. However, due to their configuration and design, these traps collect a sample of resuspended particulate matter that moves in the water column, and Storlazzi et al. recommend using the language of “trap collection rate” to describe the result. After particulates enter the trap, the design should prevent their resuspension and removal from it, so they capture the total amount of suspended material that settled into them over a period of deployment. They do not inform net deposition, accretion, erosion, or accumulation, and compared to these metrics over the same time, trap collection rates are much greater since they are capturing a gross total.

The updated definition and purpose of these sediment traps aligns with research question #2 in assessing how sediment resuspension and transport changes across a seagrass edge due to altered flow conditions. Using traps to measure overall levels of sediment transport and compare this to the magnitude of SSCs in the water column across the study area provided a method to assess whether variable levels of energy in the wave-current flow regime based on seagrass presence or absence influenced overall sediment movement. Sediment traps of this design have not been frequently used in shallow coastal bay systems and have no documented use at the VCR LTER, so this methodology represents the first attempt to use sediment traps in this system to assess relative flux in areas with and without vegetation particularly at edges.

Bivalve settlement and recruitment

Sediment cores were used to measure bivalve settlement and recruitment within the study area to address whether the changing flow conditions across a seagrass edge

influence these spatial patterns of abundance. Due to uncertainty regarding total yield and composition, no single species was selected for explicit study, but based on anecdotal evidence that clam species dominate the bivalve community in South Bay, methodological decisions were based on work regarding the hard clam (*Mercenaria mercenaria*) as this has been well-studied in previous literature. Cores have been widely used to measure the settlement and recruitment of clams (Bologna & Heck, 2000; Morse & Hunt, 2013; Peterson et al., 1984; Peterson, 1986) with a range of methodologies depending on the size class of interest. Since larval clams are unable to deeply burrow into the sediment, cores in this study extended through only the top 5 cm of sediment. The size delineations for larvae follow the work of Wilson (1990) and are based on the biology of different juvenile clam stages as outlined by Carriker (1961). The 500 μm size threshold captures larvae through the pediveliger (swimming-creeping) stage into the plantigrade ('crawler', dissoconch) stage. Larvae in this size range will have settled onto the sediment and may crawl on it, but not burrow. Moving into the byssal plantigrade category, hard clams from 500 μm to 1 mm begin byssal attachment to substrata and siphons begin to form allowing superficial burrowing into sediment.

Upon reaching roughly 1 cm in size, juvenile clams lose function of their byssus and retain their position in the sediment (Carriker, 1961), while prior to this point they may still move either purposefully or passively under the influence of prevailing hydrodynamic conditions. While not a direct measure of initial settlement patterns, the use of cores in this work provides insight into the "temporal persistence of the spatial patterns established at the time of settlement" (Wilson, 1990), revealing how juvenile

bivalves are distributed along a seagrass edge system as flow conditions continue to influence their settlement and subsequent recruitment.

3.3 Methods

Instrumentation

To assess differences in SSCs and turbidity across the meadow's edge of seagrass vegetation, two turbidity sensors (Richard Branker Research© RBRduo³) were deployed concurrently and from May through August 2021. These instruments were fastened to weighted metal frames which remained on the seafloor for weeks at a time in their respective locations, one in naturally bare seafloor near transect locations A and one in full vegetation near location D at Site 1 (Figure 1.2). These instruments were programmed to measure Nephelometric Turbidity units (NTUs) every ten minutes at 4 Hz for a one-second burst over which samples were averaged to produce a data point for that time frame. In summer 2022, turbidity data was collected with a RBRvirtuoso³ instrument programmed to quantify NTU every ten minutes at 2 Hz for a one-second burst. This instrument was attached to the weighed metal frame deployed in vegetation at Site 2 (Figure 1.2). NTUs are a scaled unit of water turbidity that are not described with any specific metrics and instead provide information about the relative magnitude of turbidity. These can be converted to SSCs in mg/L using instrument calibrations based on the water and sediment properties of the systems where data was collected.

In summer 2022, SSCs were also concurrently quantified across the meadow's edge of seagrass vegetation. An optical backscatter sensor (OBS; Campbell Scientific OBS3+) was connected to each Vector and housed on the same instrument frame to collect data simultaneously. Values of NTU measured by the OBSs were converted to

SSCs with units of mg/L using previously calculated calibration values (Hansen and Reidenbach, 2012), performed on the same instruments and with sediment from the South Bay seagrass meadow. From Hansen and Reidenbach (2012), “sediment samples were collected, suspended, and known volumes of suspended sediment were mixed into 60 l of filtered seawater. Suspended sediment sample volumes were then dried and weighed, and a linear regression was formed between the backscatter intensity from the OBS and the SSC. Each calibration had an $R^2 > 0.99$.” The OBSs were positioned with sensor tips facing inward at 30 cm heights on the instrument frames.

Sediment traps

A PVC trap design was used to measure movement of suspended sediment across Sites 1 and 2 (Photo 3.1). The trap and sleeve design utilized here was adapted from Wilson (1990) who used them to measure settling mollusk larvae in Bogue Sound, North Carolina, a similarly shallow, low energy system with *Z. marina* vegetation. The “sleeves” held the actual traps in place and provided an easier vehicle for frequent removal and replacement instead of continually redeploying into the sediment. Sleeves were made from PVC Charlotte Pipe of 10.2 cm diameter while the traps themselves were the same material of 7.6 cm diameter. The sleeves were cut to 28 cm lengths while the traps were cut to 30.5 cm lengths providing a slight extension and serving as the highest obstruction to the flow. The final trap dimensions formed a 4:1 aspect ratio which has been deemed appropriate for lower energy systems (Storlazzi et al., 2011).

The sleeves were deployed into the sediment with an extension of 10 ± 2 cm above the seafloor where they remained for the entire study period. Considering the length difference of the trap insert, this resulted in a final total trap height between 10 and

15 cm above the seafloor at deployment. To avoid faunal interference, most deployments included a polypropylene mesh covering (6 mm mesh size) covering the trap's opening. Pipe caps (Charlotte ©) and duct tape were used to seal the bottom ends of the traps preventing sediment from leaking but allowing for water drainage. Considering the spacing guidelines described by Storlazzi et al., (2011), traps were deployed at Sites 1 and 2 (red Xs) where each transect location (A-D) had 3 replicates, yielding a total of 12 samples per deployment at Site 1 and 9 total samples at Site 2.

After the first deployment and depending on total yield, traps were exchanged roughly every two weeks by removing the used one filled with sediment from its sleeve and quickly replacing it with a new empty one. Care was taken either to not disturb the surrounding sediment or allowing it to settle before inserting the new trap. The full, used traps were immediately sealed with another cap and brought back to the laboratory where excess water was left to drain or was manually removed. Trap contents were emptied into pre-weighed aluminum bins and any fauna collected were removed. Remaining sediment contents were dried at 60° C for at least 24 hours depending on volume and measured again for a final dry weight. This weight was divided by days of data collection and trap opening area to produce a total collection rate per area ($\text{g}/\text{cm}^2/\text{day}$) reported here, mirroring the units used in other sediment trap methodologies (Storlazzi et al., 2011).

Bivalve coring

Sediment cores of a 7.6 cm diameter were taken from the top 5 cm of sediment roughly every week from June through August 2021 at Site 1. Samples were taken at each of the 12 total locations at this study site with the exact spot of coring selected haphazardly within a 3 m diameter. An additional set of samples was taken in September

in between previously used transect sampling locations to account for potential disturbance. All contents were immediately put in plastic bags and placed on ice for transport to the laboratory where they were refrigerated and then processed within 48 hours of collection. All samples were wet-sieved through a 500 μm mesh and remaining contents were examined visually and through a dissecting microscope. An identification key was used to distinguish ambiguous specimens and ensure that only bivalves were recorded, but specific species identifications were not performed. A “count” in this methodology represents a bivalve between 500 μm and 1 cm height with its hinge completely maintained and its valves almost entirely in-tact. Shell fragments, partial hinges, or significantly weathered specimens were not counted. The final contents were preserved in 70% ethanol and frozen. Two additional rounds of samples were collected and processed in June 2022 at Site 1 to assess consistency of results after disturbance generated by creating the manmade bare traps and frequent sampling in summer 2021.

3.4 Results

Sediment suspension and transport

Instrumentation and physical sampling techniques were used to quantify sediment suspension and transport in the study areas. In summer 2021, PVC traps were continually deployed from May 21, 2021 to October 12, 2021 at Site 1 during which they were exchanged 7 times for a total of 8 rounds of sampling. One round of collection in mid-July was excluded from analysis due to excessive disturbance of the traps by fish, so 7 rounds are reported. The frequency of trap sampling ranged from weekly to monthly depending on seasonality and expected trap yield, with more frequent measurements occurring in mid-summer and monthly exchanges occurring later in the season.

Rates from all collection over the 2021 sampling period are shown in Table 3.1 and Figure 3.1A, where the replicates from each transect sampling location (A-D) are averaged into one value. To address spatial variation in sediment transport across Site 1, measured rates were grouped by these sampling locations and averaged over the 2021 study period from May through October where mean rates for sites A-D were 0.67, 0.65, 0.74, and 0.56 g/cm²/day respectively (Table 3.1, Figure 3.1B). To address temporal variation or seasonal changes in sediment transport, collection rates from each round of sampling were pooled and averaged regardless of location to produce a mean rate for each deployment (Figure 3.3A). The first round of deployment from May 25 to June 2 had sediment collection rates nearly ten times higher than other time periods. These high rates are likely due to a large storm and are further addressed below, and to limit variability from this outlier, the spatial groupings were analyzed again excluding the first round of collection. These averages for sites A – D were 0.26, 0.28, 0.37, and 0.27 g/cm²/day respectively (Table 3.1, Figure 3.2). Variability between sampling locations over this shorter period remained high despite the exclusion, but in both cases mean trap collection was slightly elevated at C locations corresponding to the manmade bare patches.

To make comparisons with turbidity and physical conditions, trap collection was grouped by month (Figure 3.3B). To meet assumptions of normality and address statistical significance of spatial and temporal differences, a log transformation was applied to trap collection rates. A one-way ANOVA comparing the spatial groupings A-D (Figures 3.1B and 3.2B) yielded non-significant results ($p > 0.05$) even after excluding the outlying first round of data collection. A one-way ANOVA and Tukey's test

performed on the collection rates grouped by month (Figure 3.3B) yielded significant differences between groups ($p < 0.001$) where collection rates during May and September were significantly different from other months and each other. Low sample size and high variability led the decision to analyze the data with these ANOVAs, and temporal fluctuations were analyzed independently from spatial trends to address overall changes in seasonality across the entire study area.

From May through September 2021, sediment sensors (RBRduo3) were concurrently deployed at the opposite ends of Site 1 to quantify NTU over the study period (Figure 1.2). Because NTUs are an unspecified and scaled unit of measurement for water turbidity, the values reported here provide information about relative levels of suspended sediment in the water column and the magnitude of turbidity at each location for comparison. Monthly averages of NTU from the bare and vegetated sampling locations are shown in Figure 3.4A. There were no significant differences between these values based on their location in bare or vegetated seafloor, aligning with results from sediment trap collection. NTU values were then grouped by month regardless of sampling location to address seasonal changes, and the resulting means are shown in Figure 3.4B where, like trap collection rates, NTU was elevated in May with a magnitude of increase compared to other monthly averages similar to that seen in trap collection data.

Higher levels of sediment resuspension and transport in May shown from trap collection rates and NTU measurements initially raised questions regarding the validity of this sampling round following disturbance of the seafloor upon trap deployment. To investigate, comparisons were made to concurrent physical conditions. Figure 3.5 shows

monthly averages of trap collection rate and NTU across the study site next to monthly averaged wave heights (H_s) and wind speeds from the same time periods of data collection. Wind speed and wave heights were also elevated and reached their seasonal maximums in late May due to the largest storm event of the 2021 sampling period on May 30th. During this event, northerly winds were closely aligned with wave heights resulting in elevated NTU and trap collection (Figure 3.6). This close relationship mirrors the entire 2021 study period, where there were significant correlations between monthly averages of NTU, trap collection rate, and H_s . (Pearson correlation tests between NTU and trap collection rate ($r = 0.986$, $p < 0.05$), NTU and H_s ($r = 0.988$, $p < 0.05$), trap collection rate and H_s ($r = 0.958$, $p < 0.05$)).

In summer 2022, sediment traps were deployed at Site 2 following the same methodology as Site 1. Sampling locations at Site 2 also included areas spanning the meadow's natural edge of vegetation (locations A and B, Figure 1.3) but covered distances farther from the edge and included the addition of an interior site deeper into vegetation (C, Figure 1.3) instead of manmade bare patches. The purpose of repeated sampling in this manner was to validate previous results and determine a threshold of distance from the meadow's edge where levels of SSCs and sediment transport may be reduced by vegetation, since sampling during summer 2021 revealed no consistent trends in the effect of seagrass presence on suspended sediment movement. Traps were collected and measured four times during summer 2022 from late April through late June.

Rates from all rounds of collection during 2022 are shown in Table 3.2 and Figure 3.7A, where the replicates from each sampling location (A-C) are averaged into one value. To address spatial variation in sediment transport across Site 2, measured rates

were grouped by these sampling locations and averaged over the 2022 study period from April through June where mean rates for sites A-C were 0.6, 0.74, and 0.62 g/cm²/day respectively, similar to average rates from 2021 (Figure 3.8A). To address temporal variation or seasonal changes in sediment transport, rates from each round of sampling were pooled and averaged regardless of location to produce a mean rate for each period (Figure 3.7B). The first round of collection from April 26 – May 13 had sediment collection rates nearly ten times higher than other rounds. To limit variability from this outlier, the spatial groupings were analyzed again excluding the first round of deployment. These averages for sites A – C were 0.2, 0.29, 0.15 g/cm²/day respectively (Figure 3.8B), again corresponding to 2021 data following the outlying exclusion. Both including and excluding the first round of measurements, location B (vegetated location closest to natural edge) had slightly elevated collection rates and after excluding the first round from analysis, location C (furthest into vegetation away from meadow's edge) had distinctly lower collection rates.

Like summer 2021, trap collection rates from the first round of data collection in 2022 were elevated so comparisons were made to concurrent physical conditions. Average wind speeds from each deployment were 5.17, 4.07, 3.03, 3.12 m/s respectively (Figure 3.9), highest on average during the first deployment. Instrumentation quantifying NTU and wave characteristics were not deployed during the first round of trap collection, but average H_s and NTU from subsequent rounds are shown in Figure 3.9, also scaling with trap collection rate. This instrumentation was deployed in vegetation only so no comparisons of NTU were made to bare sampling locations in summer 2022.

To further address sediment movement across seagrass edges, in 2022 Campbell Scientific OBS 3+® sediment sensors were connected to Vector instruments to simultaneously measure SSCs in the water column during 3-day deployments spanning the meadow's natural edge of vegetation. Figure 3.10A shows the resulting average SSCs per site for each deployment with average values between 54 and 106 mg/L based on calibrations with sediment from South Bay. Consistent with trap collection data, there were no significant differences between SSCs at the bare and vegetated sampling locations, but SSCs were higher overall during Deployment 2. Wave activity and wind speeds were also highest during this time (Figure 3.10B and C). Winds were consistent from the northerly direction (Appendix II) and resulted in elevated H_s and SSCs in seagrass sampling locations compared to bare ones during this deployment. Vector deployment 2 also had elevated wave orbital velocities, total turbulent Reynolds stresses, and energy magnitude of flow in the wave band (see Chapter 2 results).

Bivalve settlement and recruitment

Sediment cores were collected and processed on nine separate occasions from June through September 2021 at Site 1 to quantify bivalve settlement and recruitment across the study site. Although specific identifications were not performed for each specimen due to difficulties with quantity and size, identification keys from the VCR LTER and surrounding areas were used to conclude the species of frequently collected individuals. Common species identified at the VCR LTER and in these samples include hard clams (*Mercenaria mercenaria*), soft clams (*Mya arenaria*), other clam species (*Anadara ovalis*, *Anadara transversa*, *Ensis directus*, *Gemma gemma*, *Macoma tenta*, *Nucula proxima*, *Solen viridis*, *Tagelus plebeius*, *Tagelus divisus*), and other bivalve

species (*Abra aequalis*). The smallest adult of this community is *Macoma tenta* or *Gemma gemma* at roughly 0.5 cm while most adults range from 1 – 15 cm (Appendix III). Based on this information and the size threshold of this methodology, the sample of bivalves represented here may be assumed as predominately recently settled juvenile recruits. Abundances from all rounds of core sampling during 2021 are shown in Table 3.3 and Figure 3.11, where the 3 replicates for each sampling location (A-D) are averaged into one value with a unit of mean abundance of individuals per core.

To address spatial variation in bivalve recruitment across the sampling area, abundances from core samples were grouped by sampling location and averaged over the 2021 study period where mean abundances per core for sites A-D were 1.1, 5.1, 2.8, and 4.9 respectively (Table 3.3, Figure 3.12A). To address temporal variation or seasonal changes in settlement and recruitment, abundances from each round of collection were pooled and averaged regardless of location to produce a mean abundance for each collection date (Figure 3.12B). There was high temporal variability from June – September with a minimum average abundance of 2.17 per core on July 16 and a maximum of 4.75 on September 14. Considering how average abundances at each specific spatial location changed over the study period, there was also high temporal variation and no consistent pattern (Figure 3.11).

A square-root transformation was applied to abundance values in this dataset to meet assumptions of normality and perform statistical analyses. A one-way ANOVA and Tukey's test were performed to address differences between core abundances at the four different sampling locations over the entire study period (Figure 3.12A). This yielded a significant difference between the groups ($p < 0.001$) where all pairwise comparisons

were significant except between groups B and D, indicating that bivalve abundances were lowest in naturally bare areas (A), elevated in the manmade bare patch within the seagrass bed (C), and greatest in areas of full vegetation regardless of edge proximity (B and D). Compared to naturally bare group A, mean abundances were over 2.5 times elevated in group C and over 4 times elevated in groups B and D. A separate one-way ANOVA was performed to address temporal variation, but there were no significant differences ($p > 0.05$). Spatial patterns were analyzed independently from seasonal fluctuations due to high temporal variability and to address more persistent trends in bivalve presence based on location in vegetation.

Considering the disturbance caused by creating the removal sites (C) and to verify consistency of results, core samples were collected and processed in the same way at Site 1 on two separate occasions during summer 2022. The removal sites were not cleared again so 2022 samples from location C reflect a year of re-growth, but these locations were still roughly 80% unvegetated. Due to high temporal variability in 2021 sampling, particularly during the month of June, this was assumed to be a representative time to measure bivalve recruitment and both 2022 samples were collected during June. The resulting spatial averages from sampling locations A-D were 1.5, 5.7, 3.2, and 4.7 individuals per core, respectively (Table 3.4, Figure 3.13), similar to those from 2021.

3.5 Discussion

Sediment suspension and transport

This work presents the first documented use of sediment trap structures at the VCR LTER with the goal of measuring total collection rates of suspended sediment driven by hydrodynamic conditions and weather patterns across edges of seagrass

vegetation. This methodology was chosen to answer research question #2 asking how the altered flow conditions of seagrass ecosystems and various edge settings influence sediment resuspension and transport, with a hypothesis that vegetated areas would experience lower SSCs and trap collection rates due to lower energy flow regimes. Measuring total transport and collection of suspended sediment over shorter timescales instead of net erosion or deposition provides detailed insight into how sediment resuspension is immediately influenced by changes in flow regime. Collection rates reported here have magnitudes and ranges similar to results from previous literature using this trap methodology in coral reef environments with similar magnitudes of flow velocity and near-bed shear stress (Storalzzi et al., 2011) despite different sediment compositions. Collection rates from this study were validated using concurrent instrumentation measuring relative levels of water turbidity and SSCs across the same study areas.

Sediment trap collection rates at Sites 1 and 2 during 2021 and 2022 showed no significant spatial trends across sampling locations. Collection rates were not significantly different at any location in the sampling regime whether in bare or vegetated areas, manmade removal areas, or at locations further into seagrass vegetation over 100 meters away from the meadow's edge. This result was consistent with all data collected across various edges of seagrass vegetation and over different timescales, and quantifying NTU and SSCs (mg/L) in these settings revealed no significant spatial differences in turbidity or suspended sediment based on vegetation. Low sample size and high variability from trap collection data could explain statistical similarities in these results, but high resolution, longer-term data sets with large samples sizes from instrumentation

were used to concurrently quantify relative levels of SSCs and confirmed nonsignificant differences in turbidity in similar locations, validating the resulting rates of trap collection. This demonstrated lack of reduction in SSCs between bare and vegetated areas contrasts results from previous literature showing significantly lower turbidity in vegetated locations (Carr et al., 2010; Granata et al., 2001; Hansen & Reidenbach, 2013; Zhu et al., 2021). This suggests that, as seen with wave attenuation (Verduin & Backhaus, 2000), a threshold of shoot density or distance from the meadow's edge may exist for vegetation to reduce SSCs (Zhu et al., 2022).

Considering temporal changes and seasonality of trap collection rates, SSCs, and physical conditions of winds and waves did yield more consistent trends. In summer 2021, trap collection rates were significantly elevated, nearly ten times, during the first round of collection from May 25 – June 2, when a storm passed through the area resulting in seasonal maximums of wind speeds, wave heights, and NTUs. During summer 2021 in total, trap collection rate and NTU were significantly correlated with each other and with H_s , which had a positive relationship with wind speeds controlling wave activity in this system (Fagherazzi & Wiberg, 2009). Agreeing with previous research from the VCR LTER (Lawson et al., 2007), wave height was a major predictor in sediment resuspension and transport across these edge settings, and similar wave heights in these locations explain similar levels of sediment movement.

All trends and results from summer 2021 were confirmed with 2022 data collection, where average trap collection rates were similar to results from the previous summer and again had no consistent differences between differing areas of vegetation. Instrumentation and analysis of physical conditions during trap deployments again

confirmed positive relationships between wind speeds, wave heights, NTU, and trap collection. These relationships were also apparent from shorter-term deployments of Vector instrumentation to concurrently measure SSCs across the meadow's edge of vegetation. There were no significant differences between the sampling locations, but strong positive relationships between wave activity, turbulent Reynolds stresses, and SSCs during deployments. Interestingly, vegetated locations in these settings experienced simultaneously elevated Reynolds stresses, wave orbital velocities, and SSCs, agreeing with conclusions from previous literature that vegetation at low density or near edges may enhance sediment resuspension and transport (Carr et al., 2016; Chen et al., 2007; Lawson et al., 2012; Nepf et al., 1999).

In both 2021 and 2022, there was nonsignificant evidence of elevated NTU and trap collection in the manmade bare patches or at vegetated locations closest to the seagrass edge, suggesting that enhanced turbulence or wave activity in these locations during periods of northerly winds could elevate SSCs and transport in low-density, edge-adjacent seagrass vegetation under these conditions. This complements the work of Zhu et al. (2021 & 2022) who concluded that vegetation density mediates the response of SSCs and sediment transport to variable hydrodynamic and wave conditions in South Bay. High-density vegetation in the summer significantly attenuated flow, waves, and SSCs, but low-density vegetation (< 160 shoots/m²) in the winter resulted in much smaller reductions (Zhu et al., 2021). Meadow edges were also the most sensitive to changes in erosional or depositional conditions and controlled the amount of suspended sediment advected through the meadow at large (Zhu et al., 2022). While net erosion and deposition were not addressed in this thesis, edge-adjacent and low-density sampling

locations did experience elevated SSCs, sediment transport, and sensitivity to variable conditions of flow and waves.

Based on the analysis of results from two years of physical sampling and instrumentation measurements, seagrass presence near edges has no significant influence on SSCs or sediment transport compared to nearby bare areas. This likely stems from the documented absence of wave attenuation in these edge locations, and the demonstrated correlations between NTU, trap collection, wind speeds, and wave heights. These results confirm that sediment resuspension and transport in shallow coastal bays and South Bay specifically are controlled by wind-driven wave activity, which was similar across the seagrass edges studied here. However, evidence for enhanced trap collection, SSCs, wave activity, and Reynolds stresses near the seagrass edge during periods of high, northerly winds suggests that edge-adjacent, low-density areas of vegetation are more susceptible to sediment resuspension and transport driven by weather events or changes in flow.

Bivalve settlement and recruitment

Core sampling was conducted in summer 2021 and 2022 at Site 1 to answer research question #3 and determine whether the altered flow conditions of seagrass vegetation and its edges mediate a response in bivalve settlement and recruitment. While previous work has confirmed elevated density of bivalves in vegetated environments (Orth, 1992), this result has not been documented at the VCR LTER. Further, edge effects on bivalve communities in heterogeneous landscapes remain ambiguous (Bologna & Heck, 2000; Carroll et al., 2012, Moore & Hovel, 2010), and a goal of this research was to supplement the existing literature with robust, concurrent hydrodynamic analysis of edge settings in elucidating these influences.

Abundances of juvenile bivalves were consistently and significantly elevated in all vegetated sampling locations regardless of proximity to edges. Abundances were lower in manmade bare patches and lowest in naturally unvegetated seafloor. These results are consistent with work showing greater bivalve presence and density in seagrass ecosystems (Glaspie & Seitz, 2017; Orth et al., 1984), but do not explicitly confirm the frequently reported presence of a settlement shadow with greatest abundances near edges of vegetation (Bologna & Heck, 2002; Carroll et al., 2012). However, locations with elevated bivalve abundances corresponded to sampling locations with significant and similar reductions in mean flow, despite the persistence of wave activity and sediment transport similar to unvegetated areas. This suggests that mean current flow may still mediate bivalve settlement across all vegetated locations (Bologna & Heck, 2000; Orth, 1992), and that lower energy flow conditions encourage greater recruitment. This could stem from decreased mortality and predation in these locations (Orth et al., 1984), or from the previously-documented benefits of a reduction in energy of flow regime on bivalve growth and survival (Irlandi, 1996; Peterson et al., 1984; Peterson, 1986).

A broad range of specimens were included in this analysis, spanning a large size class and including a multitude of species. Specific size measurements and identifications were not performed on samples from this study and although several frequently recurring species were confirmed to represent a recently recruited, juvenile community, the variability of sizes and species pose difficulties in forming generalized results about the explicit effect of hydrodynamic conditions on initial settlement. Explicitly attributing results to concurrent hydrodynamic conditions also poses difficulties as differences in mortality across the study site were not directly addressed. Ongoing collaborative work

by researchers at the VCR LTER (Cornish et al., in prep) will expand on hard clam mortality in various seagrass settings and could provide further insight into results presented here. However, a reasonable conclusion is that seagrass presence enhances the subsequent recruitment and survival of juvenile bivalves, and that flow conditions may control the spatial distributions formed at initial settlement (Morse & Hunt, 2013).

3.6 Photos, figures, and tables

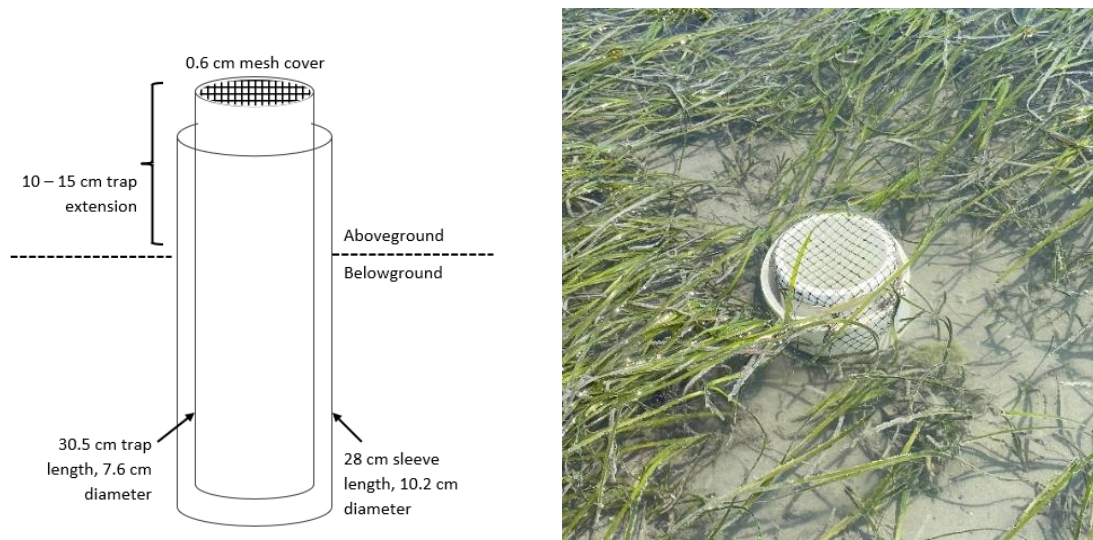


Photo 3.1. (Left) Schematic diagram of PVC sleeve and trap design adapted from Wilson (1990), not to scale. (Right) Photo of sleeve and trap system deployed *in situ*.

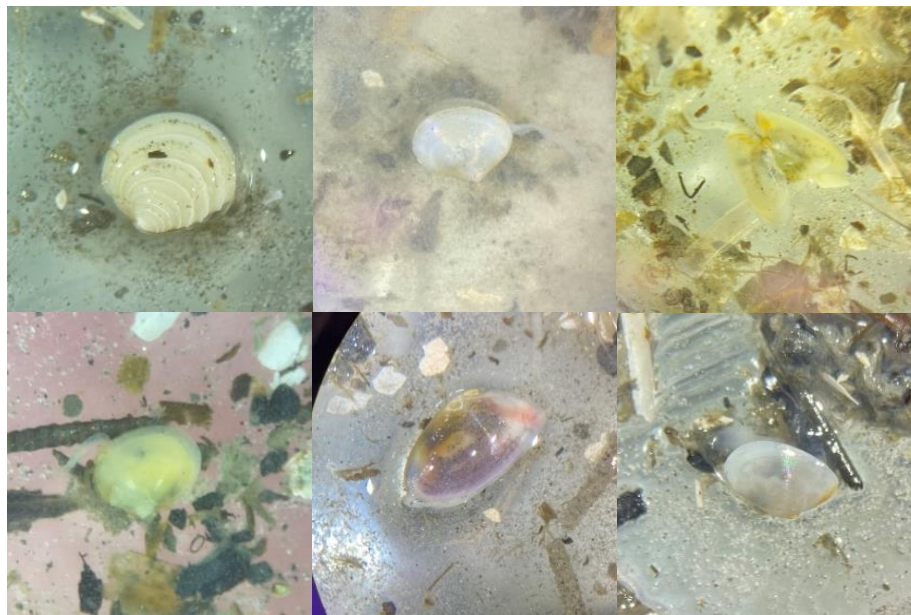


Photo 3.2. Assortment of juvenile clam specimens collected from bivalve core samples viewed under a dissecting microscope. Top left photo: *Mercenaria mercenaria*. See Appendix III.

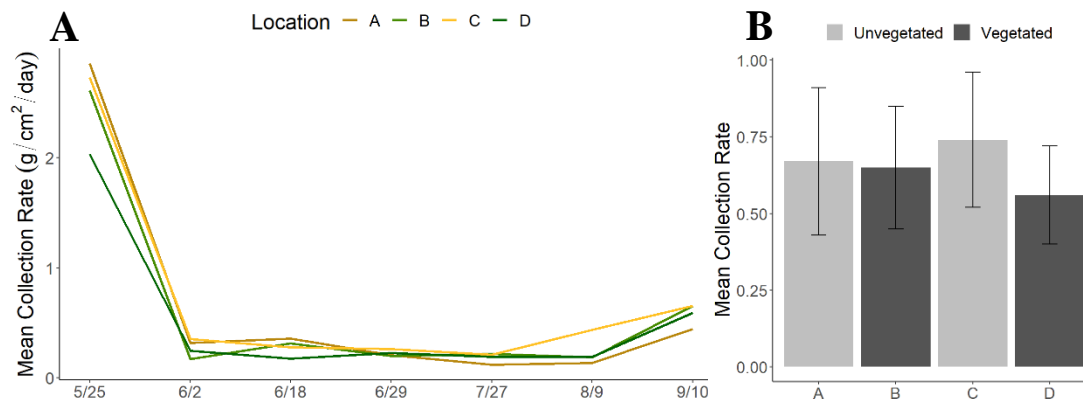


Figure 3.1. A) Mean collection rate ($\text{g}/\text{cm}^2/\text{day}$) of sediment traps per sampling location (A-D) from each round of viable deployment during 2021. B) Mean collection rate ($\text{g}/\text{cm}^2/\text{day}$) \pm 1 SE of sediment traps per sampling location (A-D) averaged over the entire study period of 2021. Location A in naturally bare seafloor, C in the manmade bare patch, B and D in vegetation 5 and 25 m past the meadow's natural edge, respectively.

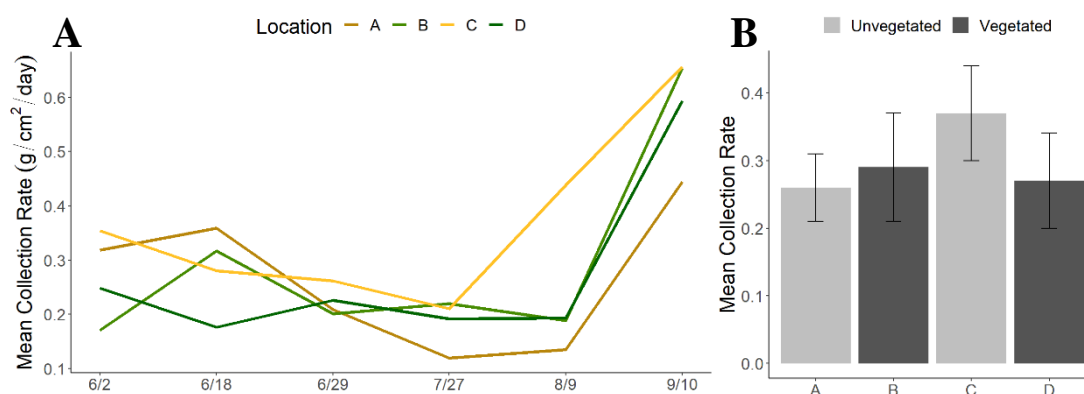


Figure 3.2. A) Mean collection rate ($\text{g}/\text{cm}^2/\text{day}$) of sediment traps per sampling location (A-D) from each round of viable deployment during 2021 excluding Round 1 from 5/25 – 6/2. B) Mean collection rate ($\text{g}/\text{cm}^2/\text{day}$) \pm 1 SE of sediment traps per sampling location (A-D) averaged over the entire study period of 2021 excluding Round 1 from 5/25 – 6/2. Location A in naturally bare seafloor, C in the manmade bare patch, B and D in vegetation 5 and 25 m past the meadow's natural edge, respectively.

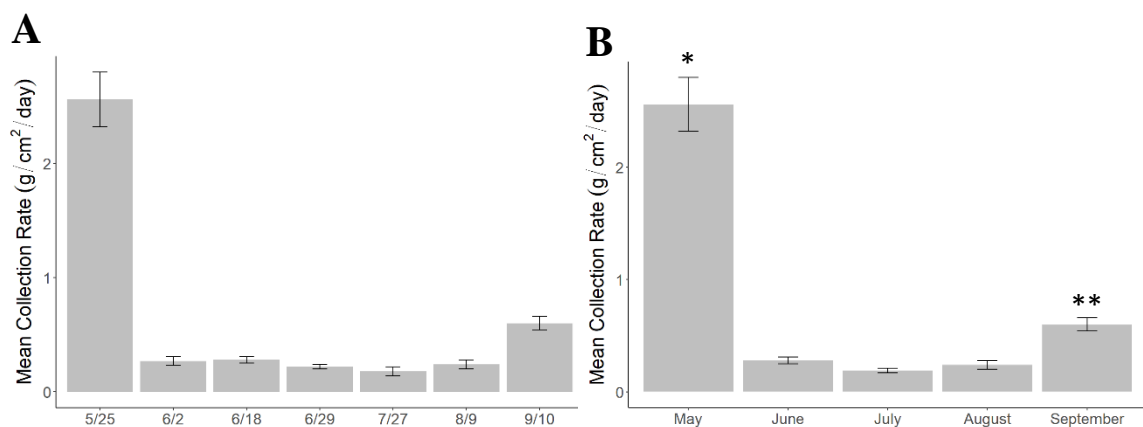


Figure 3.3. A) Mean collection rate ($\text{g}/\text{cm}^2/\text{day}$) \pm 1 SE of sediment traps at all sampling locations from each round of viable deployment during 2021. B) Mean collection rate ($\text{g}/\text{cm}^2/\text{day}$) \pm 1 SE of sediment traps at all sampling locations grouped by month during 2021. Significant differences denoted with asterisks (one-way ANOVA, $p < 0.001$).

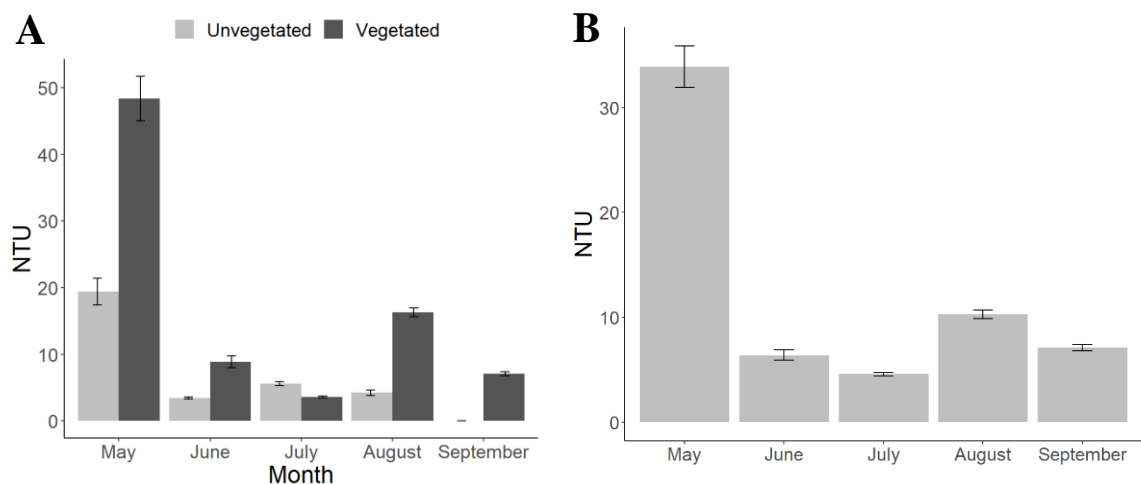


Figure 3.4. A) Mean NTU \pm 1 SE from each month of sampling during 2021 from unvegetated and vegetated sampling locations at Site 1 (no data collected at unvegetated site in September). B) Mean NTU \pm 1 SE from each month of sampling during 2021 averaged over both sampling locations at Site 1.

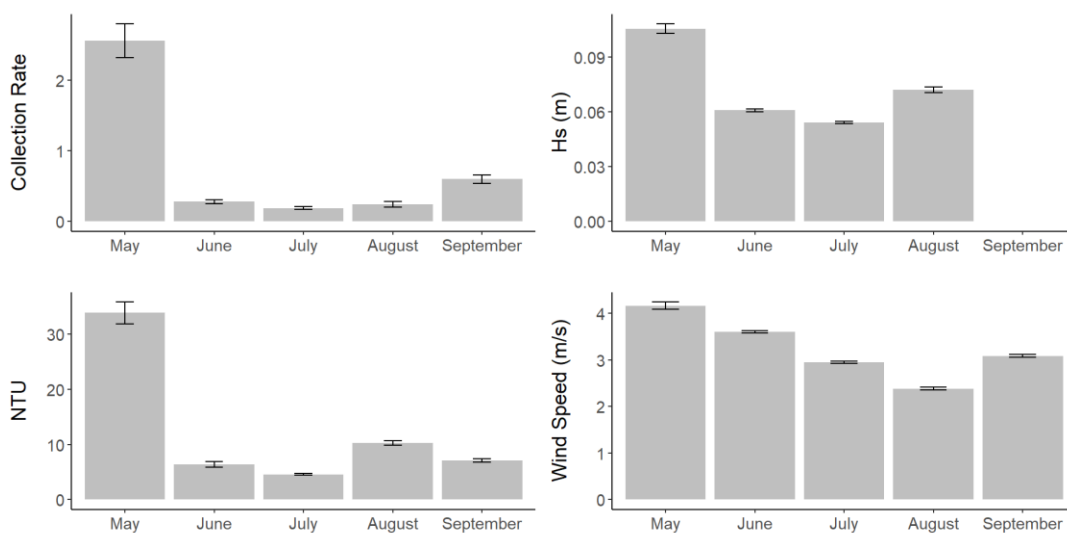


Figure 3.5. Monthly averages \pm 1 SE of trap collection rate (g/cm²/day), NTU, H_s (m), and wind speed (m/s) from Site 1 during 2021.

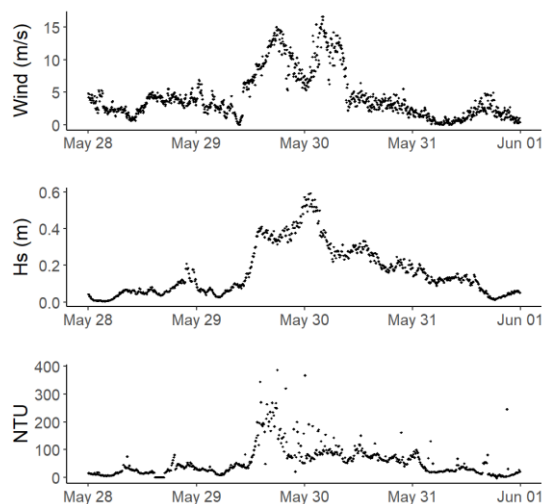


Figure 3.6. Aligned time series data of wind speed (m/s), H_s (m), and NTU from the vegetated sampling location at Site 1 during the storm from May 28 – June 1, 2021.

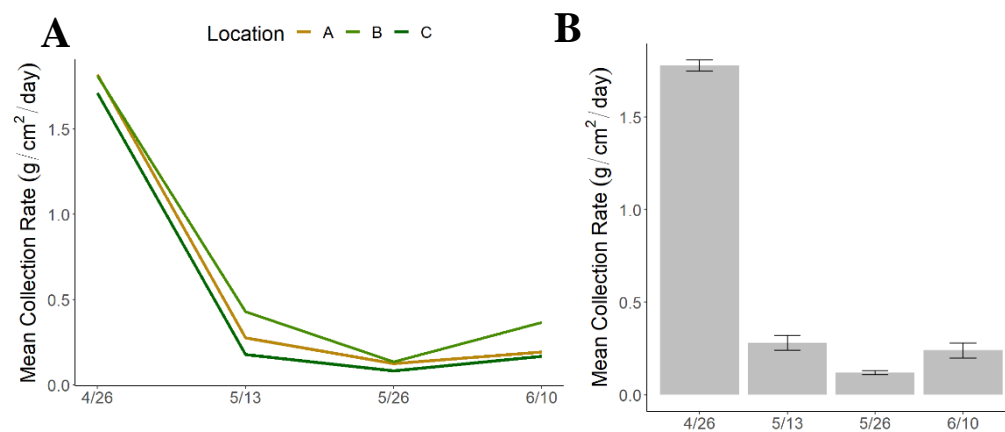


Figure 3.7. A) Mean collection rate ($\text{g}/\text{cm}^2/\text{day}$) of sediment traps per sampling location at Site 2 (A-C) from each round of 2022 deployment. Location A in naturally bare seafloor, B and C in vegetation 10 and 110 m past the meadow's natural edge, respectively. B) Mean collection rate ($\text{g}/\text{cm}^2/\text{day}$) \pm 1 SE of traps at all sampling locations from each round of 2022 deployment.

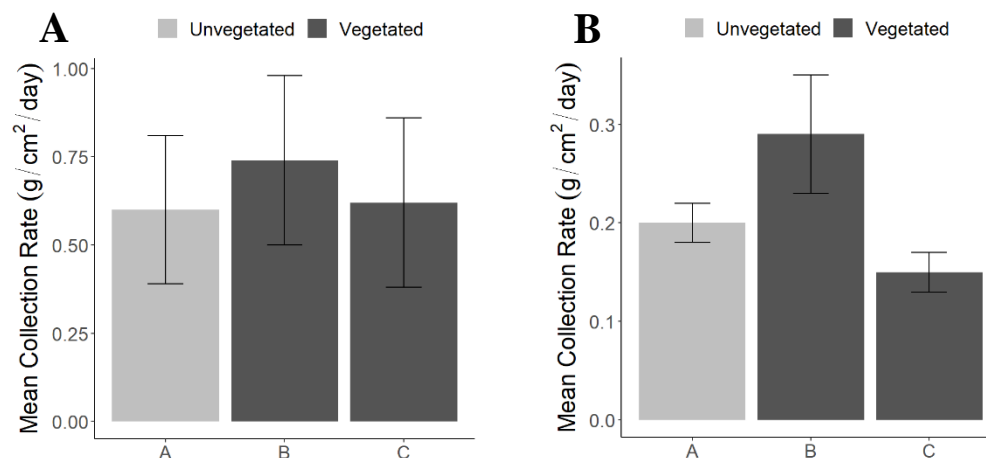


Figure 3.8. Mean collection rate ($\text{g}/\text{cm}^2/\text{day}$) ± 1 SE of sediment traps per sampling location (A-C) A) averaged over the entire study period of 2022 and B) averaged over the entire study period of 2022 excluding Round 1 from 4/26 – 5/13. Location A in naturally bare seafloor, B and C in vegetation 10 and 110 m past the meadow's natural edge, respectively.

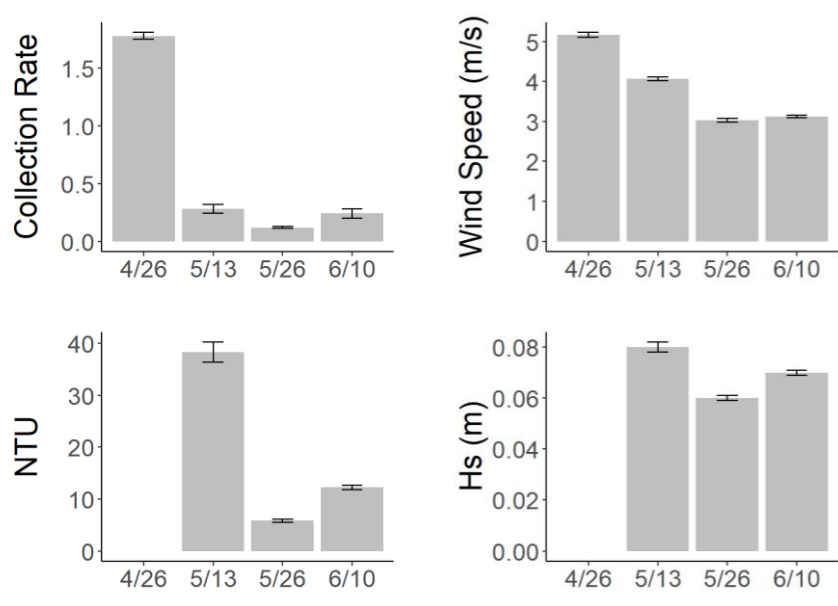


Figure 3.9. Averages ± 1 SE of trap collection rate ($\text{g}/\text{cm}^2/\text{day}$), NTU, H_s (m), and wind speed (m/s) from each period of trap deployment at Site 2 during 2022. Instrumentation measuring H_s and NTU was not deployed during Round 1 from 4/26 – 5/13.

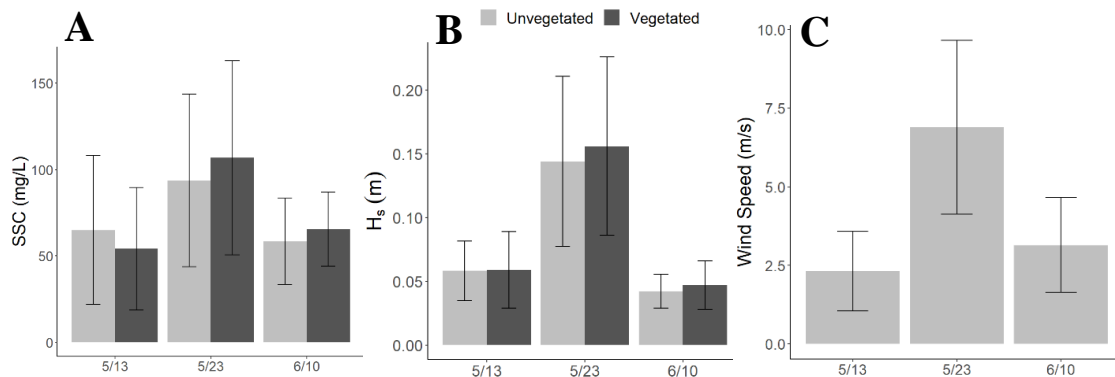


Figure 3.10. Averages ± 1 SD of A) suspended sediment concentration (SSC, mg/L), B) H_s (m), and C) wind speed (m/s) from periods of Vector deployment at Site 2 during summer 2022. SSC and H_s were quantified in vegetated and unvegetated locations.

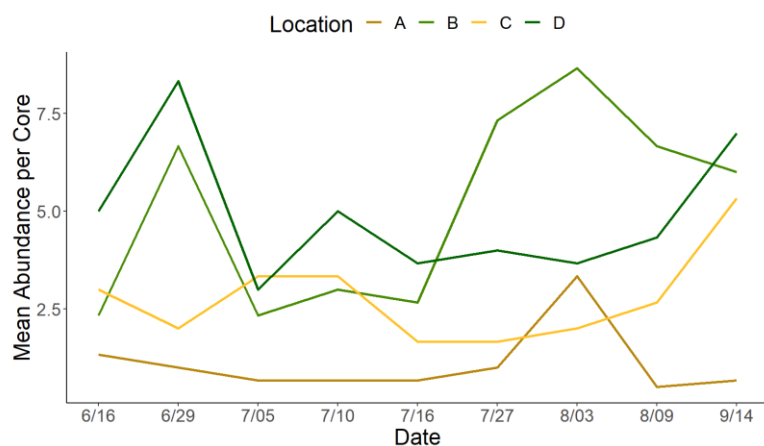


Figure 3.11. Mean abundances of bivalves per core from each sampling location at Site 1 (A-D) during each round of sampling in 2021. Location A (brown) in naturally bare seafloor, C (yellow) in the manmade bare patch, B (light green) and D (dark green) in vegetation 5 and 25 m past the meadow's natural edge, respectively.

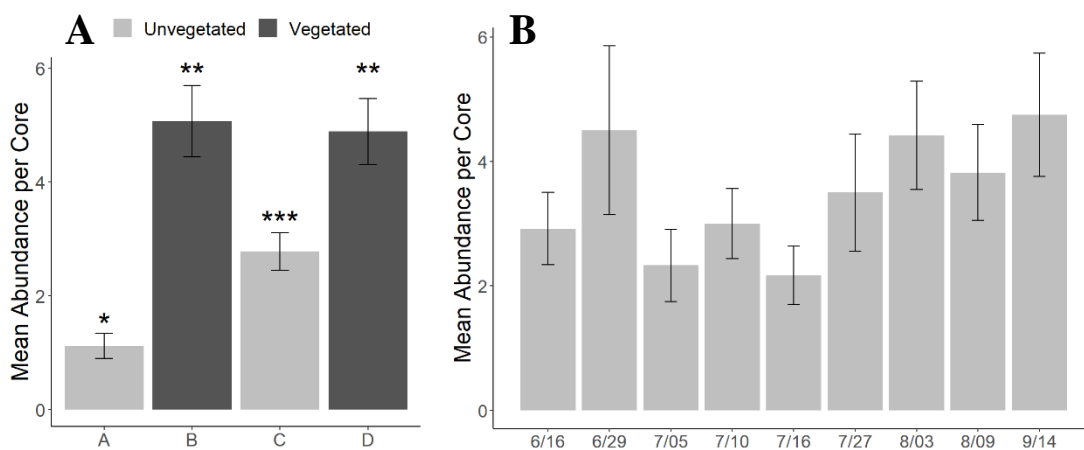


Figure 3.12. A) Mean abundances \pm 1 SE of bivalves per core from each sampling location (A-D) averaged over the entire study period of 2021. Location A in naturally bare seafloor, C in the manmade bare patch, B and D in vegetation 5 and 25 m past the meadow's natural edge, respectively. Significance denoted with asterisks (one-way ANOVA, $p < 0.001$). B) Mean abundances \pm 1 SE of bivalves per core at all sampling locations from each round of collection during summer 2021.

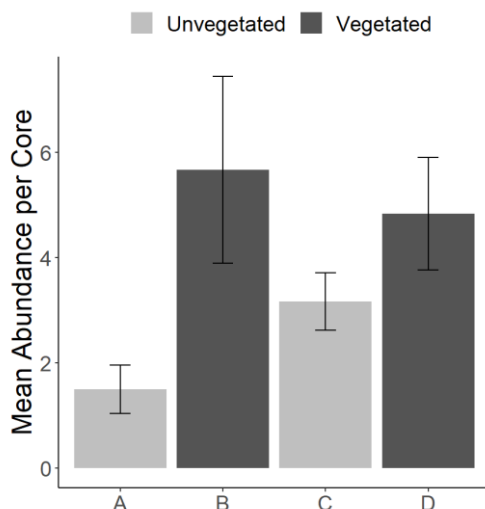


Figure 3.13. Mean abundances ± 1 SE of bivalves per core from each sampling location (A-D) averaged over the entire study period of 2022. Location A in naturally bare seafloor, C in the manmade bare patch, B and D in vegetation 5 and 25 m past the meadow's natural edge, respectively.

Table 3.1. Sediment trap accumulation rates ($\text{g}/\text{cm}^2/\text{day}$) from 2021 at Site 1 where the three replicates from each sampling location (A-D) are averaged into one value for that round of data collection. Bottom two rows show the total mean of that sampling location over the study period ± 1 SE both including and excluding the elevated first round of trap collection (Rd1) in late May.

| ($\text{g}/\text{cm}^2/\text{day}$) | A | B | C | D |
|---------------------------------------|-----------------|-----------------|-----------------|-----------------|
| 5/25 – 6/2 | 2.86 | 2.61 | 2.73 | 2.03 |
| 6/2 – 6/16 | 0.32 | 0.17 | 0.35 | 0.25 |
| 6/18 – 6/29 | 0.36 | 0.32 | 0.28 | 0.18 |
| 6/29 – 7/10 | 0.21 | 0.20 | 0.26 | 0.23 |
| 7/27 – 8/9 | 0.12 | 0.22 | 0.21 | 0.19 |
| 8/9 – 9/10 | 0.13 | 0.19 | 0.44 | 0.19 |
| 9/10 – 10/12 | 0.44 | 0.65 | 0.66 | 0.59 |
| <i>Mean incl. Rd1</i> | 0.67 ± 0.24 | 0.65 ± 0.2 | 0.74 ± 0.22 | 0.56 ± 0.16 |
| <i>Mean excl. Rd1</i> | 0.26 ± 0.05 | 0.28 ± 0.08 | 0.37 ± 0.07 | 0.27 ± 0.07 |

Table 3.2. Sediment trap accumulation rates ($\text{g}/\text{cm}^2/\text{day}$) from 2022 at Site 2 where the three replicates from each sampling location (A-C) are averaged into one value for that round of data collection. Bottom two rows show the total mean of that sampling location over the study period ± 1 SE both including and excluding the elevated first round of trap collection (Rd1) in late April.

| (g/cm ² /day) | A | B | C |
|--------------------------|-------------|-------------|-------------|
| 4/26 – 5/13 | 1.82 | 1.81 | 1.71 |
| 5/13 – 5/26 | 0.28 | 0.43 | 0.18 |
| 5/26 – 6/10 | 0.13 | 0.14 | 0.08 |
| 6/10 – 6/30 | 0.19 | 0.37 | 0.17 |
| <i>Mean incl. Rdl</i> | 0.60 ± 0.21 | 0.74 ± 0.24 | 0.62 ± 0.24 |
| <i>Mean excl. Rdl</i> | 0.20 ± 0.02 | 0.29 ± 0.06 | 0.15 ± 0.02 |

Table 3.3. Mean abundances of bivalves per core from 2021 at Site 1 where the three replicates from each sampling location (A-D) are averaged into one value for that round of data collection. Bottom row shows the total mean ± 1 SE of that sampling location over the study period.

| | A | B | C | D |
|-------------------|-------------|-------------|-------------|-------------|
| <i>June 16</i> | 1.3 | 2.3 | 3 | 5 |
| <i>June 29</i> | 1 | 6.7 | 2 | 8.3 |
| <i>July 5</i> | 0.7 | 2.3 | 3.3 | 3 |
| <i>July 10</i> | 0.7 | 3 | 3.3 | 5 |
| <i>July 16</i> | 0.7 | 2.7 | 1.7 | 3.7 |
| <i>July 27</i> | 1 | 7.3 | 1.7 | 4 |
| <i>Aug 3</i> | 3.3 | 8.7 | 2 | 3.7 |
| <i>Aug 9</i> | 0.5 | 6.7 | 2.7 | 4.3 |
| <i>Sept 14</i> | 0.7 | 6 | 5.3 | 7 |
| <i>Total Mean</i> | 1.12 ± 0.22 | 5.07 ± 0.63 | 2.78 ± 0.33 | 4.89 ± 0.58 |

Table 3.4. Mean abundances of bivalves per core from 2022 at Site 1 where the three replicates from each sampling location (A-D) are averaged into one value for that round of data collection. Bottom row shows the total mean ± 1 SE of that sampling location over the study period.

| | A | B | C | D |
|-------------------|-------------|-------------|-------------|-------------|
| <i>June 10</i> | 2.3 | 3.7 | 2.7 | 5 |
| <i>June 30</i> | 0.7 | 7.7 | 3.7 | 4.7 |
| <i>Total Mean</i> | 1.50 ± 0.46 | 5.67 ± 1.77 | 3.17 ± 0.55 | 4.83 ± 1.07 |

Chapter 4: Conclusions

Conclusions

Driven by a warming climate and anthropogenic coastal development (Dunic et al., 2021), there is ongoing loss and decline of seagrass habitats worldwide. As concurrent restoration projects and fragmentation continue to influence the heterogeneity of seagrass landscapes, considerations of spatial ecology have resulted in new questions regarding changes in the effects of variable vegetation on hydrodynamic conditions, sediment transport, and faunal (specifically bivalve) presence (Orth & McGlathery, 2012). While an array of previous research has explored aspects of these relationships considering landscape ecology (Allaoui et al., 2016; Hovel et al., 2002; Murphy et al., 2010), results have been ambiguous across many scales of time and distance, and no work has attempted to elucidate these relationships concurrently.

The work of this thesis addressed how the edges of seagrass vegetation that characterize a meadow in entirety or heterogenous areas influence conditions of flow, sediment movement, and bivalve distribution to inform how both persistent fragmentation and expanded restoration efforts lead to consequences for ecosystem services. The results presented here indicate that over various edges of heterogenous vegetation in different spatial configurations, mean flow and bivalve presence respond immediately and significantly, while effects of vegetation on wave activity and sediment transport in the same locations are delayed or not present, suggesting that certain gradients or thresholds of vegetation may exist to generate these effects.

Chapter 2 aimed to address how these different edge settings influence hydrodynamic conditions over varied spatial and temporal scales. Meteorological data and a suite of instrumentation was used at two study sites over two years to quantify physical conditions, wave activity, mean velocities, and turbulence regimes. Mean flow velocities were consistently and significantly reduced in seagrass vegetation regardless of proximity to vegetation edges, with reductions compared to unvegetated areas ranging from 30% to over 75% and scaling with changes in shoot density. These results were observed tens of meters apart across the meadow's natural edge, as well as between locations only a few meters apart within a constructed bare patch within the meadow. These results confirm previous research reporting a reduction of mean flow in seagrass vegetation in general and at the VCR LTER (Hansen & Reidenbach, 2012; Peterson et al., 2004), but present new evidence that reductions occur over small spatial scales and in patchy areas.

Results from Chapter 2 also confirmed the direct relationship between wind speed, direction, and wave activity in this system (Fagherazzi & Wiberg, 2009), but there was no evidence of wave attenuation in any of the vegetated locations addressed here. This was likely due to the short spatial distances studied, with little attenuation directly along the seagrass edge over the scales of meters. H_s and wave orbital velocities were even somewhat elevated in seagrass during storms or northerly winds. This suggests that consistent wave attenuation in seagrass vegetation (Fonseca & Calahan, 1992; Koch et al., 2006) occurs due to the integrated drag of the vegetation as waves propagate across the meadow (Reidenbach & Thomas, 2018) and indicates there may be a distance from

the meadow's edge necessary to generate significant wave attenuation (Verduin & Backhaus, 2000).

However, over these short spatial scales both the mean flow and turbulence were significantly altered between the unvegetated and vegetated seafloor. Interestingly, along edges of vegetation, Reynolds stresses were significantly elevated in seagrass vegetation indicating a higher level of turbulent energy. Previous research has concluded that turbulent energy may increase in areas of low shoot density due to increased stem-wake interactions, including in South Bay, (Hansen & Reidenbach, 2013; Nepf et al., 1997; Widdows et al., 2008), and the density counts measured during summer 2022 along with elevated Reynolds stresses confirm this inference. These elevated levels of turbulence may also occur due to sharp transitions between an unvegetated and vegetated seafloor.

Chapter 3 addressed how sediment transport changes in response to varied flow conditions over different edge settings. While laboratory work has addressed this relationship over the distance scale of centimeters (Zhang et al., 2020), and modeling work has explored it across kilometers of meadow vegetation (Zhu et al., 2021 & 2022), no work has studied these dynamics at an intermediate scale of meters with field-based research. Like wave height, there were no significant changes in turbidity or trap collection rate at locations in the study sites either within or outside the meadow, in contrast to previous literature demonstrating reduced SSCs in vegetation (Carr et al., 2010; Hansen & Reidenbach, 2013). However, significant correlations between NTU, trap collection rate, and H_s across seasonal changes and weather events suggest that sediment resuspension and turbidity in South Bay are controlled by wind-driven waves

(Lawson et al., 2007), demonstrated by a near ten-times increase in trap collection rate during a 2021 storm with similarly elevated NTU and H_s .

Additionally, there was evidence for elevated sediment transport in sampling locations closest to edges of vegetation, agreeing with previous research suggesting that edge-adjacent or low-density vegetation may enhance sediment suspension and transport (Carr et al., 2016; Chen et al., 2007; Lawson et al., 2012). Recent work from South Bay reports that SSCs fluctuate non-linearly as a function of seagrass density and that meadow edges experience the greatest sensitivity to seasonal erosion or deposition while mediating overall advection of SSCs at the meadow scale (Zhu et al., 2022). Recent flume experiments showed a similar density-dependent relationship between flow regime and distance of sediment deposition past a seagrass edge (Zhang et al., 2020). While net accumulation was not addressed in this thesis, these recent findings align with the elevated SSCs, sediment transport, and sensitivity to variable flow and wave conditions along low-density edges of vegetation documented here. This emphasizes that a threshold of density or distance from a meadow's edge may exist to reduce SSCs and total transport (Zhang et al., 2020, Zhu et al., 2021). Further, the significant correlation between NTU and trap collection rates and their similar magnitudes of elevation due to weather and seasonal changes also confirm the validity of the new trap methodology presented here.

Chapter 3 also addressed how bivalve settlement and recruitment changes in these edge settings based on variable flow (research question #3). Abundances of juvenile bivalves were significantly elevated in seagrass vegetation regardless of proximity to edges, with highest densities in full vegetation, lower densities in the manmade bare patches, and lowest densities overall in naturally bare seafloor. These results confirm

elevated bivalve presence in vegetated environments (Orth et al., 1984), but do not provide evidence for a settlement shadow with greater abundances directly along edges (Bologna & Heck, 2002; Carroll et al., 2012). However, these results inversely mirror the response of mean velocities and suggest that overall current flow may mediate the recruitment of bivalves in this system (Bologna & Heck, 2000; Orth, 1992) reinforcing spatial distributions formed at initial settlement (Morse & Hunt, 2013). While the relationship between initial settlement and hydrodynamic conditions could not be explicitly addressed and mortality may influence subsequent recruitment, these results do confirm previous research attributing elevated bivalve presence in seagrass to changes in flow regime (Irlandi, 1996; Peterson et al., 1984), and this phenomenon was not previously documented for the VCR LTER.

Future work and implications for restoration

Future work driven by this research could widely expand the use of validated sediment trap methodology as a valuable, efficient tool to measure sediment transport rates in different areas of variable vegetation density, during extreme weather events, over seasonal changes, or in new restoration efforts to track progress and consequences for sediment movement. Studies addressing differential bivalve mortality or the settlement of specific species could augment the abundance analysis presented here in addition to the quantification of flow regime. All hydrodynamic results could be directly related to the current Seagrass Resilience Experiment in understanding how changes in flow scale with seagrass growth following disturbance and regrowth.

The results presented in this thesis indicate that over various edges of heterogeneous vegetation in different spatial configurations, mean flow and bivalve

presence respond immediately and significantly, while effects on wave activity and sediment transport in the same locations are delayed or not present, suggesting that certain gradients or thresholds of vegetation may exist to generate these effects.

Therefore, restoration settings of a smaller scale, in edge environments, or in patchy areas may not generate wave attenuation and have a limited ability to alter sediment transport, and fragmented landscapes may show similar magnitudes of these consequences.

However, seagrass presence in edge settings or heterogenous landscapes still results in significant mean flow reductions and enhances the recruitment of bivalves. While ecosystem fragmentation or seagrass loss may subsequently reduce these effects, any restoration efforts that protect or produce more seagrass may conversely and quickly restore these ecosystem services providing a valuable and direct benefit to the areas they occupy. To produce sustained wave attenuation and ultimately reduce turbidity in enhancing a positive feedback loop of light availability and seagrass growth, restoration efforts should aim to reduce heterogeneity and patchiness while targeting the protection of expansive, high-density vegetated seagrass ecosystems.

Appendices

Appendix I

Monthly figures from summer 2021 (AI.1-4) show aligned time-series data of water depth (m), wind direction (degrees), wind speed (m/s), and significant wave height (H_s , m). Depth and H_s were quantified concurrently in two sampling locations, with data from the unvegetated location shown in orange and data from the vegetated location shown in green. Wind direction and speed data are trimmed to match periods of other data collection for direct comparison, and their summarized data are portrayed in wind rose plots. The blue line on H_s plots shows the difference in wave heights between the two locations where positive differences indicate higher H_s at the bare location and negative differences reflect higher H_s in seagrass. Gaps in the figures represent times of no data collection.

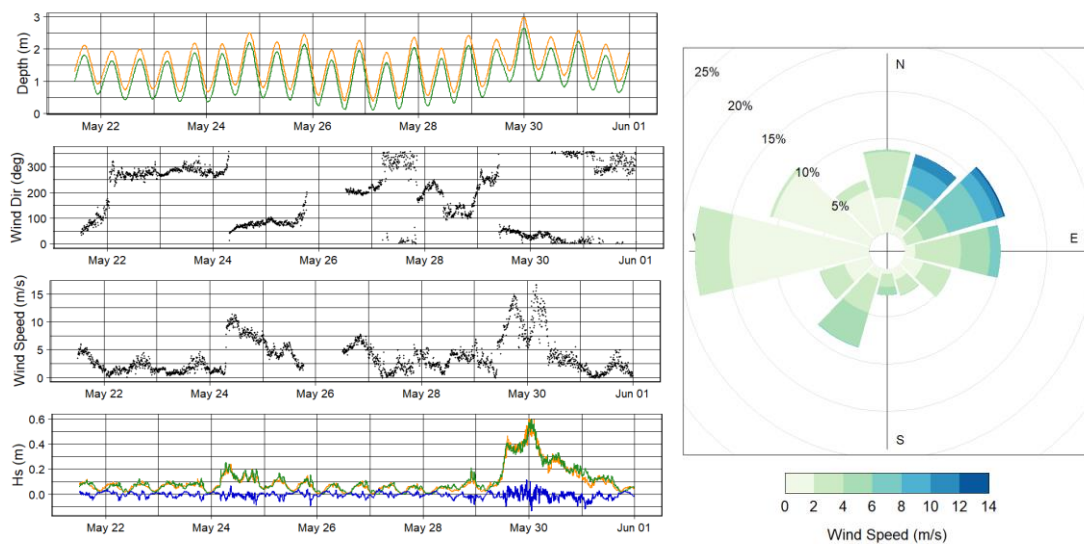


Figure AI.1. (Right) Depth (m), wind direction (degrees), wind speed (m/s), and H_s (m) from periods of data collection during May 2021 at Site 1 in unvegetated (orange) and vegetated (green) sampling locations. (Left) Summarized wind data from May '21.

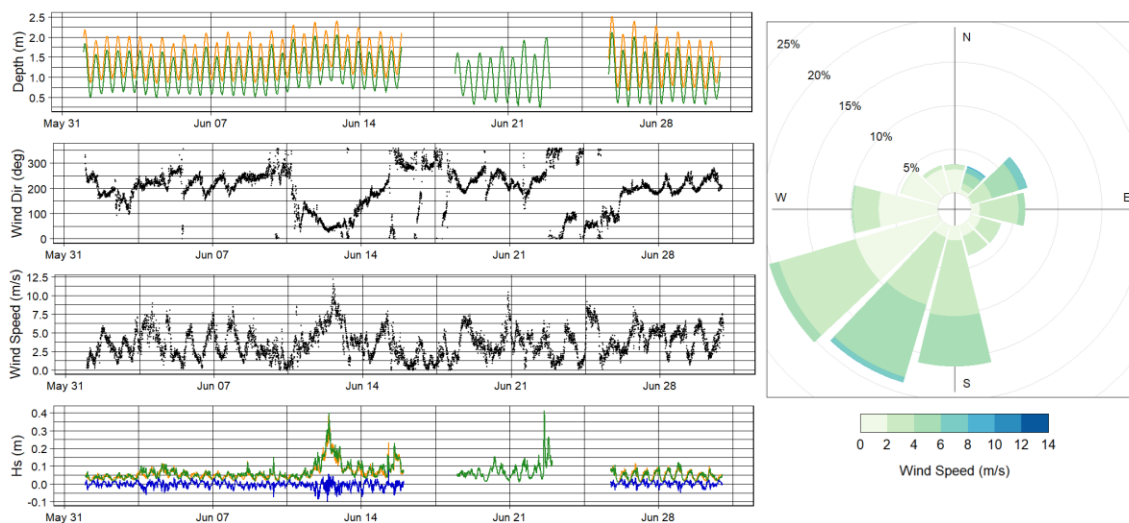


Figure AI.2. (Right) Depth (m), wind direction (degrees), wind speed (m/s), and H_s (m) from periods of data collection during June 2021 at Site 1 in unvegetated (orange) and vegetated (green) sampling locations. Gaps in the figure represent times of no data collection. (Left) Summarized wind data from June '21.

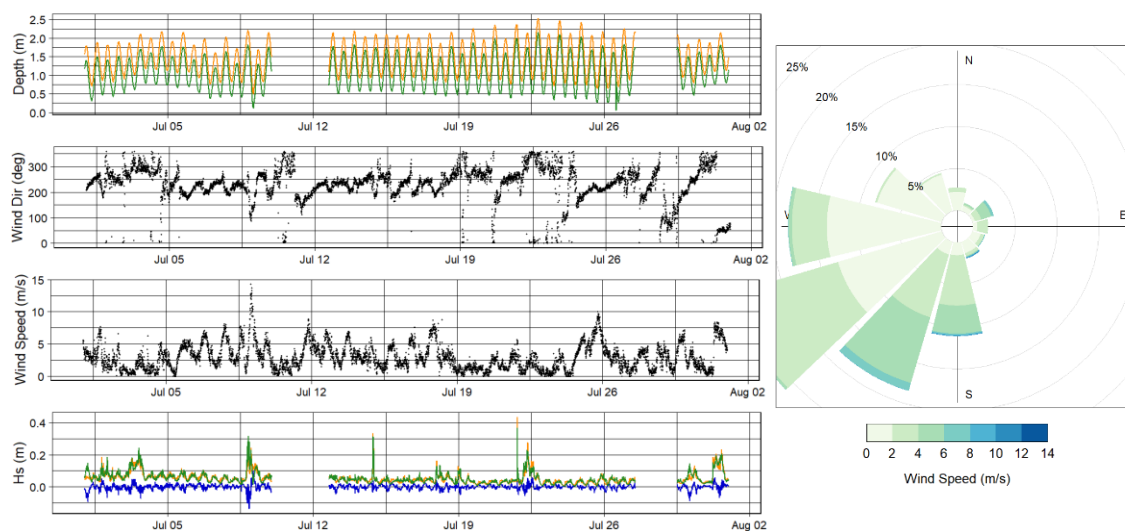


Figure AI.3. (Right) Depth (m), wind direction (degrees), wind speed (m/s), and H_s (m) from periods of data collection during July 2021 at Site 1 in unvegetated (orange) and vegetated (green) sampling locations. Gaps in the figure represent times of no data collection. (Left) Summarized wind data from July '21.

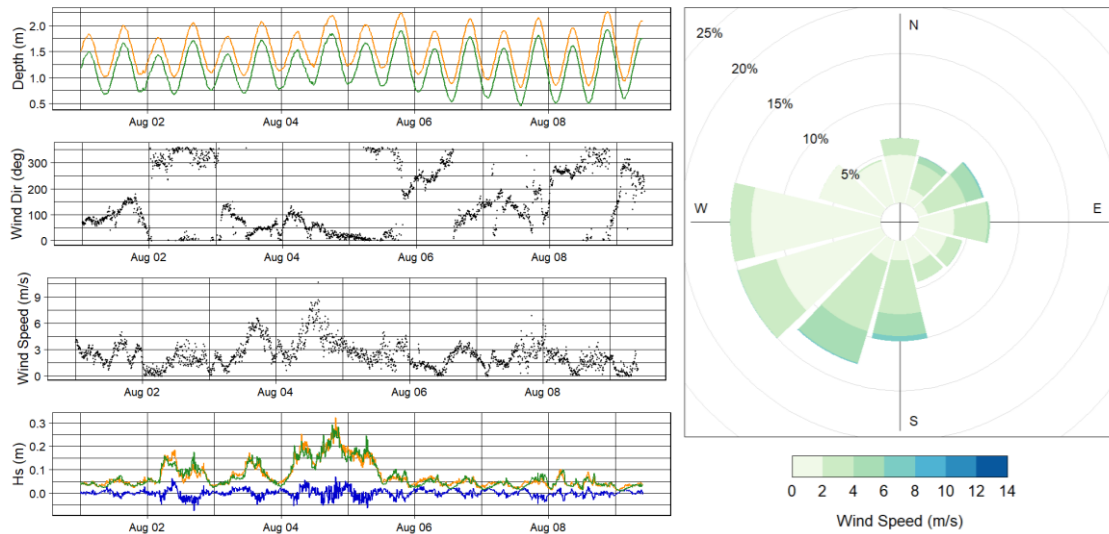


Figure AI.4. (Right) Depth (m), wind direction (degrees), wind speed (m/s), and H_s (m) from periods of data collection during August 2021 at Site 1 in unvegetated (orange) and vegetated (green) sampling locations. Gaps in the figure represent times of no data collection. (Left) Summarized wind data from August '21.

Monthly figures from summer 2022 (AI.5 and 6) show aligned time-series data of water depth (m), wind direction (degrees), wind speed (m/s), and significant wave height (H_s , m). Depth and H_s were quantified in one vegetated sampling location roughly 50 m past the meadow's natural edge of vegetation (blue x, Figure 1.3). Gaps in the figures represent times of no data collection and since concurrent data was not collected in an unvegetated location, no comparison of H_s or depth are portrayed here.

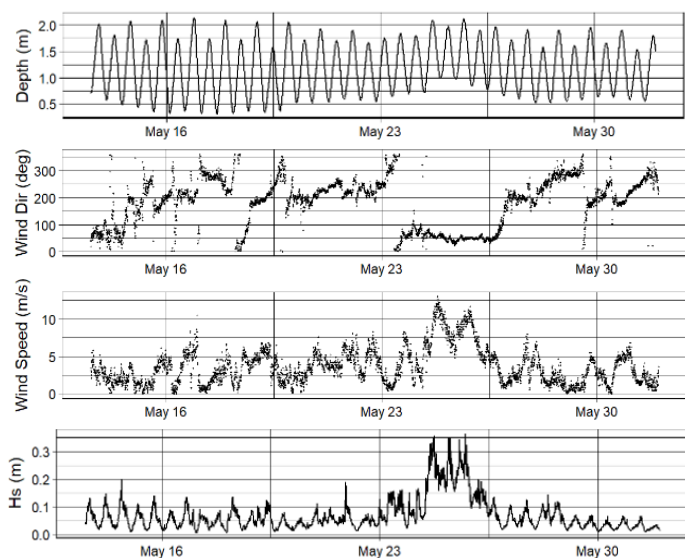


Figure AI.5. Depth (m), wind direction (degrees), wind speed (m/s), and H_s (m) from periods of data collection during May 2022 at Site 2 in the vegetated sampling location.

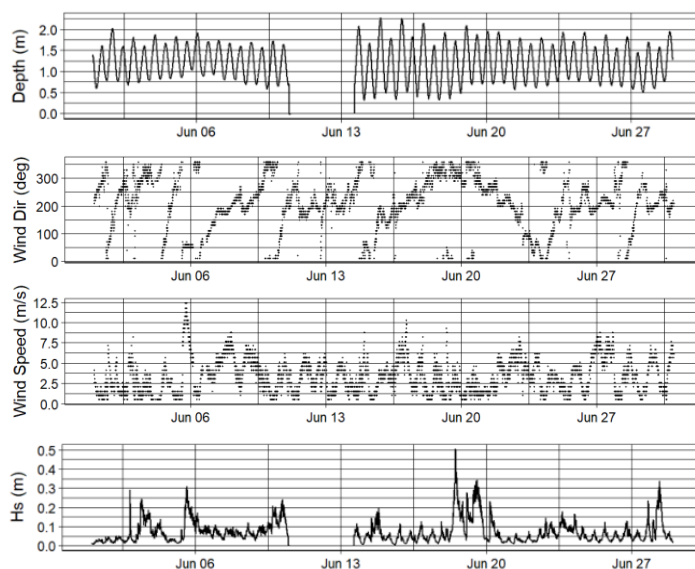


Figure AI.6. Depth (m), wind direction (degrees), wind speed (m/s), and H_s (m) from periods of data collection during June 2022 at Site 2 in the vegetated sampling location.

Appendix II

Physical characteristic data from periods of Vector instrument deployment during summer 2022 at Site 2 are shown in Figures AII.1-3. These include the same information as Appendix I except for wind rose plots and a calculated difference in H_s , but there were no significant differences in H_s between unvegetated (orange) and vegetated (green) sampling locations.

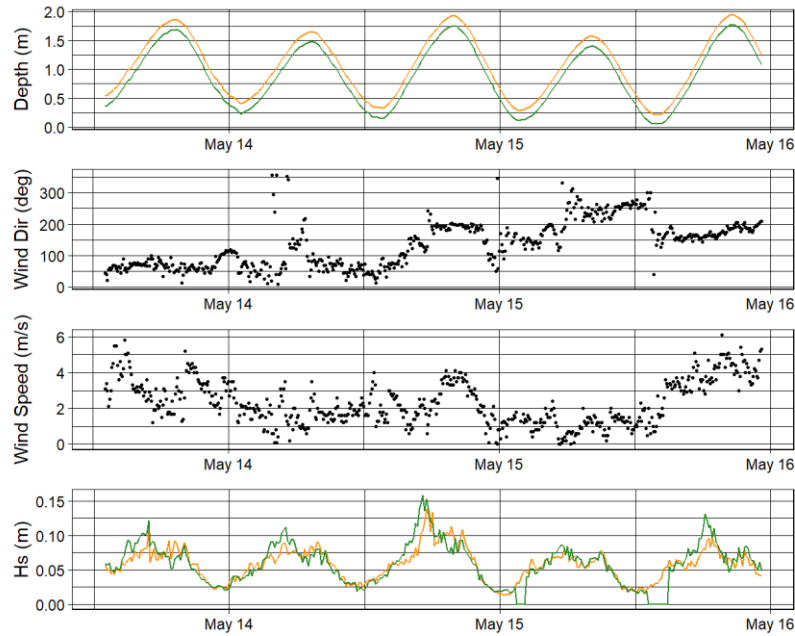


Figure AII.1. Depth (m), wind direction (degrees), wind speed (m/s), and H_s (m) during Vector Deployment 1 from May 13 – May 16, 2022 at Site 2 in unvegetated (orange) and vegetated (green) sampling locations.

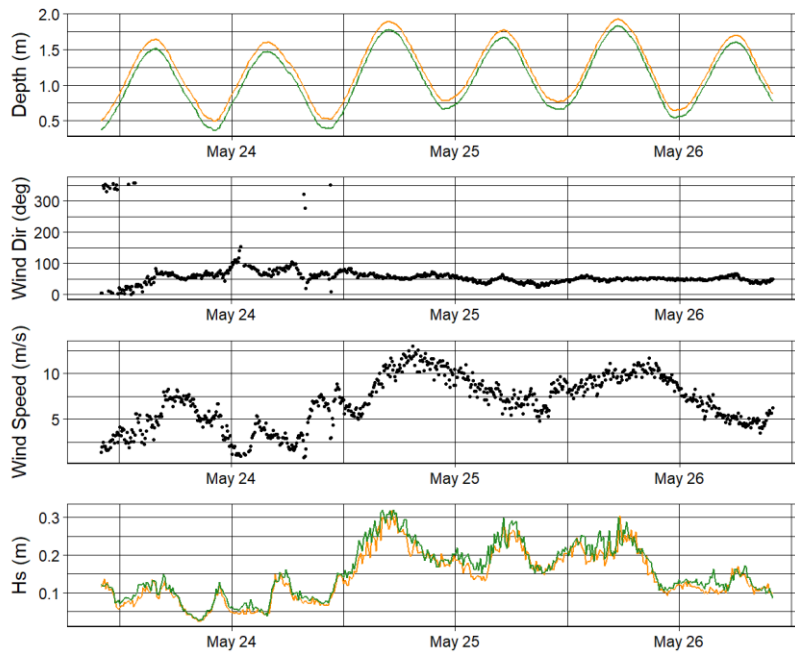


Figure AII.2. Depth (m), wind direction (degrees), wind speed (m/s), and H_s (m) during Vector Deployment 1 from May 23 – May 26, 2022 at Site 2 in unvegetated (orange) and vegetated (green) sampling locations.

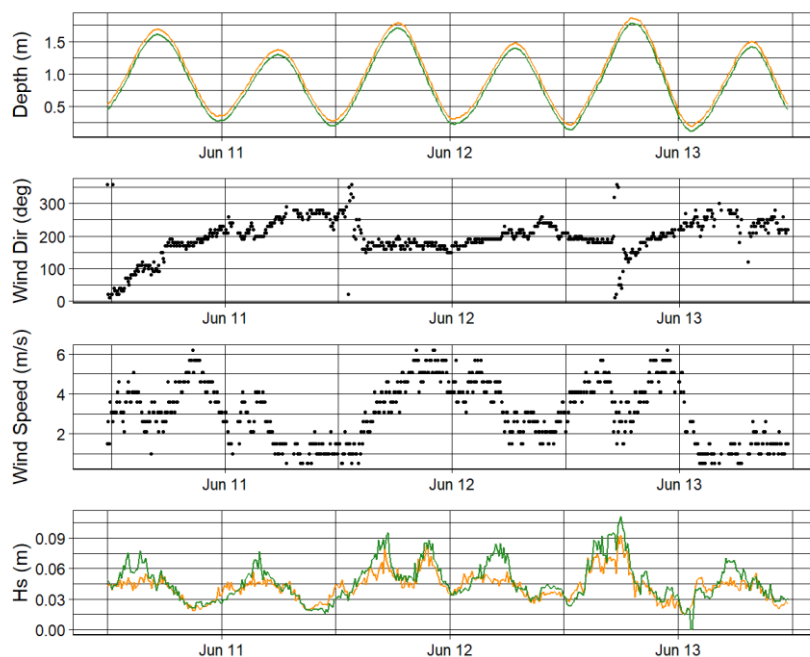


Figure AII.3. Depth (m), wind direction (degrees), wind speed (m/s), and H_s (m) during Vector Deployment 1 from June 10 – June 13, 2022 at Site 2 in unvegetated (orange) and vegetated (green) sampling locations.

Appendix III

Although specific identifications were not performed in the bivalve sampling methodology, identification keys from the VCR LTER and surrounding areas were used to conclude the species of frequently collected individuals. Common species identified at the VCR LTER and in these samples included hard clams (*Mercenaria mercenaria*), soft clams (*Mya arenia*), other clam species (*Anadara ovalis*, *Anadara transversa*, *Ensis directus*, *Gemma gemma*, *Macoma tenta*, *Nucula proxima*, *Solen viridis*, *Tagelus plebeius*, *Tagelus divisus*), and other various bivalve species (*Abra aequalis*). Table AIII.1 lists these species and their size information used to conclude that the bivalves

sampled in this work were predominately recently recruited juveniles. (Abbott & Morris, 1995; Mikkelsen & Bieler, 2008).

Table AIII.1. Common bivalve species at the VCR LTER and their size information.

| <i>Species</i> | <i>Size Information</i> |
|---------------------------------|--------------------------------------|
| <i>Abra aequalis</i> | Adult 0.7 - 1.3 cm |
| <i>Anadara ovalis</i> | Adult 2.5 cm |
| <i>Anadara transversa</i> | Adult 0.2 cm – 2.5 cm |
| <i>Ensis directus</i> | Adult up to 23 cm |
| <i>Gemma gemma</i> | Adult 0.4 cm |
| <i>Macoma tenta</i> | Adult 0.3 cm |
| <i>Mercenaria mercenaria</i> | Juvenile up to 1 cm, adult 7 – 15 cm |
| <i>Mercenaria campechiensis</i> | Adult 10 – 11 cm |
| <i>Mya arenaria</i> | Adult up to 18 cm |
| <i>Nucula proxima</i> | Adult 0.3 – 1 cm |
| <i>Solen viridis</i> | Adult 0.5 cm |
| <i>Tagelus divisus</i> | Adult 0.5 – 1 cm |
| <i>Tagelus plebeius</i> | Adult 0.5 – 1 cm |

References

- Abbott, R. T. & Morris, P. A. (1995). *Shells of the Atlantic and Gulf Coasts of the West Indies*. Houghton Mifflin.
- Ackerman, J. D. & Okubo, A. (1993). Reduced mixing in a marine macrophyte canopy. *Functional Ecology*, 7(3), 305-309.
- Allaoui, N. E., Serra, T., Colomer, J., Soler, M., Casamitjana, X., & Oldham, C. (2016). Interactions between fragmented seagrass canopies and the local hydrodynamics. *PLoS ONE*, 11(5), 1-19. doi:10.1371/journal.pone.0156264
- Ambrose, W. G., Peterson, C. H., Summerson, H. C., & Lin, J. (1992). Experimental tests of factors affecting recruitment of bay scallops (*Argopecten irradians*) to spat collectors. *Aquaculture*, 108, 67-86. doi: 10.1016/0044-8486(92)90319-G
- Bell, S. S., Brooks, R. A., Robbins, B. D., Fonseca, M. S., & Hall, M. O. (2001). Faunal response to fragmentation in seagrass habitats: implications for seagrass conservation. *Biological Conservation*, 100, 115-123. doi: 10.1016/S0006-3207(00)00212-3
- Berger, A. C., Berg, P., McGlathery, K. J., & Delgrad, M. L. (2020). Long-term trends and resilience of seagrass metabolism: A decadal aquatic eddy covariance study. *Limnology and Oceanography*, 65, 1423 – 1438. doi: 10.1002/lno.11397
- Bologna, P. A. X. & Heck, K. L. (1999). Differential predation and growth rates of bay scallops within a seagrass habitat. *Journal of Experimental Marine Biology and Ecology*, 239, 299-314. doi: 10.1016/S0022-0981(99)00039-8
- Bologna, P. A. X. & Heck, K. L. (2000). Impacts of seagrass habitat architecture on bivalve settlement. *Estuaries*, 23(4), 449-457. doi: 10.2307/1353138
- Bologna, P. A. X. & Heck, K. L. (2002). Impact of habitat edges on density and secondary production of seagrass-associated fauna. *Estuaries*, 25(5), 1033-1044. doi: 10.1007/BF02691350
- Bostrom, C., Jackson, E. L., & Simenstad, C. A. (2006). Seagrass landscapes and their effects on associated fauna: A review. *Estuarine, Coastal and Shelf Science*, 68, 383-403. doi: 10.1016/j.ecss.2006.01.026
- Bowen, R. A., St. Onge, J. M., Colton, J. B., & Price, C. A. (1972). Density-gradient centrifugation as an aid to sorting planktonic organisms. I. Gradient materials. *Marine Biology*, 14, 242-247.
- Bricker, J. D. & Monismith, S. G. (2007). Spectral wave-turbulence decomposition. *Journal of Atmospheric and Oceanic Technology*, 24(8), 1479 – 1487. <https://doi.org/10.1175/JTECH2066.1>

- Bradley, K. & Houser, C. (2009). Relative velocity of seagrass blades: Implications for wave attenuation in low-energy environments. *Journal of Geophysical Research*, *114*, 1-13. doi:10.1029/2007JF000951
- Butman, C. A. (1986). Sediment trap biases in turbulent flows: Results from a laboratory flume study. *Journal of Marine Research*, *44*, 645-693. doi: 10.1357/002224086788403051
- Butman, C. A. (1989). Sediment-trap experiments on the importance of hydrodynamical processes in distributing settling invertebrate larvae in near-bottom waters. *Journal of Experimental Marine Biology and Ecology*, *134*, 37-88. doi: 10.1016/0022-0981(90)90055-H
- Caley, M. J., Carr, M. H., Hixon, M. A., Hughes, T. P., Jones, G. P., & Menge, B. A. (1996). Recruitment and the local dynamics of open marine populations. *Annual Review of Ecology and Systematics*, *27*, 477-500. doi: 10.1146/annurev.ecolsys.27.1.477
- Carr, J. A., D'Odorico, P., McGlathery, K., & Wiberg, P. (2010). Stability and bistability of seagrass ecosystems in shallow coastal lagoons: Role of feedbacks with sediment resuspension and light attenuation. *Journal of Geophysical Research*, *115*(3), 1-14. <http://dx.doi.org/10.1029/2009JG001103>; doi:10.1029/2009JG001103
- Carr, J. A., D'Odorico, P., McGlathery, K. J., & Wiberg, P. L. (2012). Stability and resilience of seagrass meadows to seasonal and interannual dynamics and environmental stress. *Journal of Geophysical Research*, *117*, G01007. <http://dx.doi.org/10.1029/2011JG001744>
- Carr, J. A., D'Odorico, P., McGlathery, K. J., & Wiberg, P. L. (2016). Spatially explicit feedbacks between seagrass meadow structure, sediment and light: Habitat suitability for seagrass growth. *Advances in Water Resources*, *93*(B), 315 – 325. <https://doi.org/10.1016/j.advwatres.2015.09.001>
- Carriker, M. R. (1961). Interrelation of functional morphology, behavior, and autecology in early stages of the bivalve *Mercenaria mercenaria*. *Journal of the Elisha Mitchell Scientific Society*, *77*(2), 168-241.
- Carroll, J. M., Furman, B. T., Tettelbach, S. T., & Peterson, B. J. (2012). Balancing the edge effects budget: bay scallop settlement and loss along a seagrass edge. *Ecology*, *93*(7), 1637-1647. doi: 10.1890/11-1904.1
- Chen, S., Sanford, L. P., Koch, E. W., Shi, F., & North, E. W. (2007). A nearshore model to investigate the effects of seagrass bed geometry on wave attenuation and suspended sediment transport. *Estuaries and Coasts*, *30*(2), 296-310. doi: 10.1007/BF02700172

- Colomer, J. & Serra, T. (2021). The world of edges in submerged vegetated marine canopies: from patch to canopy scale. *Water*, 13, 2430. <https://doi.org/10.3390/w13172430>
- Dean, R.G. and Dalrymple, R.A. (1991) *Water Wave Mechanics for Engineers and Scientists*. Advanced Series on Ocean Engineering, 2. <http://dx.doi.org/10.1142/1232>
- Denny, M. W. (1988). *Biology and the Mechanics of the Wave-Swept Environment*. Princeton University Press.
- Dunic, J. C., Brown, C. J., Turschwell, M. P., & Cote, I. M. (2021). Long-term declines and recovery of meadow area across the world's seagrass bioregions. *Global Change Biology*, 27, 4096 – 4109. DOI: 10.1111/gcb.15684
- Eckman, J. E. (1983). Hydrodynamic processes affecting benthic recruitment. *Limnology and Oceanography*, 28(2), 241-257. doi: 10.4319/lo.1983.28.2.0241
- Eckman, J. E. (1987). The role of hydrodynamics in recruitment, growth, and survival of *Agropecten irradians* (L.) and *Anomia simplex* (D'Orbigny) within eelgrass meadows. *Journal of Experimental Marine Biology and Ecology*, 106, 165-191. doi: 10.1016/0022-0981(87)90154-7
- Eckman, J. E. (1990). A model of passive settlement by planktonic larvae onto bottoms of differing roughness. *Limnology and Oceanography*, 35(4), 887-901. doi: 10.4319/lo.1990.35.4.0887
- Eckman, J. E. & Duggins, D. O. (1998). Larval settlement in turbulent pipe flows. *Journal of Marine Research*, 56, 1285-1312. doi: 10.1357/002224098765093643
- Emerson, C. W. & Grant, J. (1991). The control of soft-shell clam (*Mya arenaria*) recruitment on intertidal sandflats by bedload sediment transport. *Limnology and Oceanography*, 36(7), 1288-1300.
- Fagherazzi, S. & Wiberg, P. J. (2009). Importance of wind conditions, fetch, and water levels on wave-generated shear stresses in shallow intertidal basins. *Journal of Geophysical Research*, 114, 1-12. doi: 10.1029/2008JF001139
- Fonseca, M. S. & Cahalan, J. A. (1992). A preliminary evaluation of wave attenuation by four species of seagrass. *Estuarine, Coastal and Shelf Science*, 35, 565-576.
- Fonseca, M. S. & Fisher, J. S. (1986). A comparison of canopy friction and sediment movement between four species of seagrass with reference to their ecology and restoration. *Marine Ecology Progress Series*, 29, 15-22.
- Fonseca, M. S. & Koehl, M. A. R. (2006). Flow in seagrass canopies: The influence of patch width. *Estuarine, Coastal and Shelf Science*, 67, 1-9. doi: 10.1016/j.ecss.2005.09.018

- Gacia, E., Granata, T. C., & Duarte, C. M. (1999). An approach to measurement of particle flux and sediment retention within seagrass (*Posidonia oceanica*) meadows. *Aquatic Botany*, *65*, 255-268.
- Gambi, M. C., Nowell A. R. M., & Jumars, P. A. (1990). Flume observations on flow dynamics in *Zostera marina* (eelgrass) beds. *Marine Ecology Progress Series*, *61*, 159-169. doi: 10.3354/meps061159
- Ghisalberti, M. & Nepf, H. M. (2002). Mixing layers and coherent structures in vegetated aquatic flows. *Journal of Geophysical Research*, *107*(C2), 3-1 – 3-11. <http://dx.doi.org/10.1029/2001JC000871>; doi:10.102
- Glaspie, C. N. & Seitz, R. D. (2017). Role of habitat and predators in maintaining functional diversity of estuarine bivalves. *Marine Ecology Progress Series*, *570*, 113-125. doi: 10.3354/meps12103
- Grizzle, R. E. & Morin, P. J. (1989). Effect of tidal currents, seston, and bottom sediments on growth of *Mercenaria mercenaria*: results of a field experiment. *Marine Biology*, *102*, 85-93.
- Granata, T. C., Serra, T., Colomer, J., Casamitjana, X., Duarte, C. M., & Gacia, E. (2001). Flow and particle distributions in a nearshore seagrass meadow before and after a storm. *Marine Ecology Progress Series*, *218*, 95-206. doi: 10.3354/meps218095
- Grant, W. D. & Madsen, O. S. (1979). Combined wave and current interaction with a rough bottom. *Journal of Geophysical Research*, *84*(C4), 1797 – 1808.
- Hansen, J. C. R. & Reidenbach, M. A. (2012). Wave and tidally driven flows in eelgrass beds and their effect on sediment suspension. *Marine Ecology Progress Series*, *448*, 271-287. doi: 10.3354/meps09225
- Hansen, J. C. R. & Reidenbach, M. A. (2013). Seasonal growth and senescence of a *Zostera marina* seagrass meadow alters wave-dominated flow and sediment suspension within a coastal bay. *Estuaries and Coasts*, *36*(6), 1099-1114. DOI 10.1007/s12237-013-9620-5
- Harvey, M. & Bourget, E. (1995). Experimental evidence of passive accumulation of marine bivalve larvae on filamentous epibenthic structures. *Limnology and Oceanography*, *40*(1), 94-104. doi: 10.4319/lo.1995.40.1.0094
- Homziak, J., Fonseca, M. S., Kenworthy, W. J. (1982). Macrobenthic community structure in a transplanted eelgrass (*Zostera marina*) meadow. *Marine Ecology Progress Series*, *9*, 211-221. doi: 10.3354/meps009211
- Hovel, K. A., Fonseca, M. S., Myer, D. L., Kenworthy, W. J., & Whitfield, P. E. (2002). Effects of seagrass landscape structure, structural complexity and hydrodynamic

- regime on macrofaunal densities in North Carolina seagrass beds. *Marine Ecology Progress Series*, 243, 11 – 24. doi:10.3354/meps243011
- Irlandi, E. A. (1996). The effects of seagrass patch size and energy regime on growth of a suspension-feeding bivalve. *Journal of Marine Research*, 54, 161-185. doi: 10.1357/0022240963213439
- Irlandi, E. A., Ambrose, W. G., & Orlando, B. A. (1995). Landscape ecology and the marine environment: How spatial configuration of seagrass habitat influences growth and survival of the bay scallop. *Oikos*, 72(3), 307-313.
- Irlandi, E. A., Orlando, B. A., & Ambrose, W. G. (1999). Influence of seagrass habitat patch size on growth and survival of juvenile bay scallops, *Agropecten irradians concentricus* (Say). *Journal of Experimental Marine Biology and Ecology*, 235, 21-43. doi: 10.1016/S0022-0981(98)00185-3
- Irlandi, E. A. & Peterson, C. H. (1991). Modification of animal habitat by large plants: Mechanisms by which seagrasses influence clam growth. *Oecologia*, 87, 307-318. doi: 10.1007/BF00634584
- Jing, L. & Ridd, P. V. (1996). Wave-current bottom shear stresses and sediment resuspension in Cleveland Bay, Australia. *Coastal Engineering*, 29, 169-186. doi: 10.1016/S0378-3839(96)00023-3
- de Jonge, V. N. & Bouwman, L. A. (1977). A simple density separation technique for quantitative isolation of meiobenthos using the colloidal silica Ludox-TM. *Marine Biology*, 42, 143-148.
- Jonsson, P. R., Andre, C., & Lindegarth, M. (1991). Swimming behaviour of marine bivalve larvae in a flume boundary-layer flow: evidence for near-bottom confinement. *Marine Ecology Progress Series*, 79, 67-76.
- Koch, E. W. & Gust, G. (1999). Water flow in tide- and wave-dominated beds of the seagrass *Thalassia testudinum*. *Marine Ecology Progress Series*, 184, 63-72. doi: 10.3354/meps184063
- Koch, E. W., Sanford, L. P., Chen, S., Shafer, D. J., & Smith, J. M. (2006). Waves in seagrass systems: Review and technical recommendations. *US Army Corps of Engineers Engineer Research and Development Center*.
- Kraeuter, J. N. & Castagna, M. (2001). *Biology of the Hard Clam*. Elsevier.
- Lawson, S. E., Wiberg, P. L., McGlathery, K. J., & Fugate, D. C. (2007). Wind-driven sediment suspension controls light availability in a shallow coastal lagoon. *Estuaries and Coasts*, 30(1), 102-112. doi: 10.1007/BF02782971
- Lawson, S. E., McGlathery, K. J., & Wiberg, P. L. (2012). Enhancement of sediment suspension and nutrient flux by benthic macrophytes at low biomass. *Marine Ecology Progress Series*, 448, 259 – 270. doi: 10.3354/meps09579

- McGlathery, K. J., Anderson, I. C., & Tyler, A. C. (2001). Magnitude and variability of benthic and pelagic metabolism in a temperate coastal lagoon. *Marine Ecology Progress Series*, 216, 1 – 15. doi:10.3354/meps216001
- Mikkelsen, P. M. & Bieler, R. (2008). *Seashells of Southern Florida: Living marine mollusks of the Florida Keys and adjacent regions: Bivalves*. Princeton University Press.
- Moore, E. C. & Hovel, K. A. (2010). Relative influence of habitat complexity and proximity to patch edges on seagrass epifaunal communities. *Oikos*, 119, 1299-1311. doi: 10.1111/j.1600-0706.2009.17909.x
- Morse, B. L. & Hunt, H. L. (2013). Impact of settlement and early post-settlement events on the spatial distribution of juvenile *Mya arenaria* on an intertidal shore. *Journal of Experimental Marine Biology and Ecology*, 448, 57-65. <http://dx.doi.org/10.1016/j.jembe.2013.06.016>
- Murphy, H. M., Jenkins, G. P., Hindell, J. S., & Connolly, R. M. (2010). Response of fauna in seagrass to habitat edges, patch attributes and hydrodynamics. *Austral Ecology*, 35, 535 – 543. doi:10.1111/j.1442-9993.2009.02062.x
- Neph, H. M., Sullivan, J. A., & Zavistoski, R. A. (1997). A model for diffusion within emergent vegetation. *Limnology and Oceanography*, 42(8), 1735 – 1745. <https://doi.org/10.4319/lo.1997.42.8.1735>
- Nepf, H. M. (1999). Drag, turbulence, and diffusion in flow through emergent vegetation. *Water Resources Research*, 35(2), 479-489. <http://dx.doi.org/10.1029/1998WR900069>; doi:10.1029
- National Oceanic and Atmospheric Administration. (2021, 2022). *Historical data for station WAHV2*. [Data sets]. https://www.ndbc.noaa.gov/station_history.php?station=wahv2
- Oreska, M. P. J., McGlathery, K. J., Aoki, L. R., Berger, A. C., Berg, P., & Mullins, L. (2020). The greenhouse gas offset potential from seagrass restoration. *Scientific Reports*, 10(7325), 1-15. doi: 10.1038/s41598-020-64094-1
- Oreska, M. P. J., Truitt, B., Orth, R. J., & Luckenbach, M. W. (2016). The bay scallop (*Argopecten irradians*) industry collapse in Virginia and its implications for the successful management of scallop-seagrass habitats. *Marine Policy*, 75, 116 – 124. <http://dx.doi.org/10.1016/j.marpol.2016.10.021>
- Orth, R. J. (1973). Benthic infauna of eelgrass, *Zostera marina*, beds. *Chesapeake Science*, 14(4), 258-269.
- Orth, R. J. (1992). A perspective on plant-animal interactions in seagrasses: physical and biological determinants influencing plant and animal abundance. *Plant-Animal Interactions in the Marine Benthos*, 46, 147-164.

- Orth, R. J., Carruthers, T. J. B., Dennison, W. C., Duarte, C. M., Fourqurean, J. W., Heck, K. L., Hughes, A. R., Kendrick, G. A., Kenworthy, W. J., Olyarnik, S., Short, F. T., Waycott, M., & Williams, S. (2006). A global crisis for seagrass ecosystems. *BioScience*, 56(12), 987 – 996. [https://doi.org/10.1641/0006-3568\(2006\)56\[987:AGCFSE\]2.0.CO;2](https://doi.org/10.1641/0006-3568(2006)56[987:AGCFSE]2.0.CO;2)
- Orth, R. J. & Heck, K. L. (1980). Structural components of eelgrass (*Zostera marina*) meadows in the lower Chesapeake Bay: Fishes. *Estuaries*, 3(4), 278-288. doi: 10.2307/1352083
- Orth, R. J., Heck, K. L., & Montfrans, J. V. (1984). Faunal communities in seagrass beds: A review of the influence of plant structure and prey characteristics on predator: prey relationships. *Estuaries*, 7(4A), 339-350.
- Orth, R. J., Luckenbach, M. L., Marion, S. R., Moore, K. A., & Wilcox, D. J. (2006). Seagrass recovery in the Delmarva coastal bays, USA. *Aquatic Botany*, 84, 26-36. doi: 10.1016/j.aquabot.2005.07.007
- Orth, R. J. & McGlathery, K. J. (2012). Eelgrass recovery induces state changes in a coastal bay system. *Marine Ecology Progress Series*, 448, 173-176. doi: 10.3354/meps09596
- Peterson, C. H. (1986). Enhancement of *Mercenaria mercenaria* densities in seagrass beds: Is pattern fixed during settlement season or altered by subsequent differential survival? *Limnology and Oceanography*, 31(1), 200-205.
- Peterson, C. H., Luettich, R. A., Micheli, F., & Skilleter, G. A. (2004). Attenuation of water flow inside seagrass canopies of differing structure. *Marine Ecology Progress Series*, 268, 81-92. doi: 10.3354/meps268081
- Peterson, C. H., Summerson, H. C., & Duncan, P. B. (1984). The influence of seagrass cover on population structure and individual growth rate of a suspension-feeding bivalve, *Mercenaria mercenaria*. *Journal of Marine Research*, 42, 123-138. doi: 10.1357/002224084788506194
- Reidenbach, M. A. & Timmerman, R. (2019). Interactive Effects of Seagrass and the Microphytobenthos on Sediment Suspension Within Shallow Coastal Bays. *Estuaries and Coasts*, 42, 2038–2053. <https://doi.org/10.1007/s12237-019-00627-w>
- Reidenbach, M. A. & Thomas, E. L. (2018). Influence of the seagrass, *Zostera marina*, on wave attenuation and bed shear stress within a shallow coastal bay. *Frontiers in Marine Science*, 5, 1-16. doi: 10.3389/fmars.2018.00397
- Robbins, B. D. & Bell, S. S. (1994). Seagrass landscapes: a terrestrial approach to the marine subtidal environment. *Trends in Ecology & Evolution*, 9(8), 301 – 304. [https://doi.org/10.1016/0169-5347\(94\)90041-8](https://doi.org/10.1016/0169-5347(94)90041-8)

- Roughgarden, J., Gaines, S., & Possingham, J. (1988). Recruitment dynamics in complex life cycles. *Science*, *241*(4872), 1460-1466.
- Smith, T. M., Hindell, J. S., Jenkins, G. P., Connolly, R. M., Keough, M. J. (2011). Edge effects in patchy seagrass landscapes: The role of predation in determining fish distribution. *Journal of Experimental Marine Biology and Ecology*, *399*, 8-16. doi: 10.1016/j.jembe.2011.01.010
- Storzzi, C. D., Field, M. E., & Bothner, M. H. (2011). The use (and misuse) of sediment traps in coral reef environments: theory, observations, and suggested protocols. *Coral Reefs*, *30*, 23 – 38. DOI 10.1007/s00338-010-0705-3
- Thayer, G. W. & Stuart, H. H. (1974). The bay scallop makes its bed of seagrass. *Marine Fisheries Review*, *36*(7), 27-30.
- Verduin, J. J. & Backhaus, J. O. (2000). Dynamics of plant-flow interactions for the seagrass *Amphibolis antarctica*: Field observations and model simulations. *Estuarine, Coastal and Shelf Science*, *50*, 185 – 204. doi:10.1006/ecss.1999.0567
- Ward, L. G., Kemp, W. M., & Boynton, W. R. (1984). The influence of waves and seagrass communities on suspended particulates in an estuarine embayment. *Marine Geology*, *59*, 85-103. doi: 10.1016/0025-3227(84)90089-6
- Waycott, M., Duarte, C. M., Carruthers, T. J. B., Orth, R. J., Dennison, W. C., Olyarnik, S., Calladine, A., Fourqurean, J. W., Heck Jr., K. L., Hughes, A. R., Kendrick, G. A., Kenworthy, W. J., Short, F. T., & Williams, S. L. (2009). Accelerating loss of seagrasses across the globe threatens coastal ecosystems. *PNAS*, *106*(30), 12377-12381. <https://doi.org/10.1073/pnas.0905620106>
- Wiberg, P. L. & Sherwood, C. R. (2008). Calculating wave-generated bottom orbital velocities from surface-wave parameters. *Computers & Geosciences*, *34*(10), 1244 – 1263. <https://doi.org/10.1016/j.cageo.2008.02.010>
- Widdows, J., Pope, N. D., Brinsley, M. D., Asmus, H., & Asmus, R. M. (2008). Effects of seagrass beds (*Zostera noltii* and *Z. marina*) on near-bed hydrodynamics and sediment resuspension. *Marine Ecology Progress Series*, *358*, 125-136. doi: 10.3354/meps07338
- Wilson, F. S. (1989). Temporal and spatial patterns of settlement: a field study of molluscs in Bogue Sound, North Carolina. MS Thesis. University of North Carolina, Chapel Hill.
- Wilson, F. W. (1990). Temporal and spatial patterns of settlement: a field study of molluscs in Bogue Sound, North Carolina. *Journal of Experimental Marine Biology and Ecology*, *139*, 201-220. doi: 10.1016/0022-0981(90)90147-5

- Worcester, S. E. (1995). Effects of eelgrass beds on advection and turbulent mixing in low current and low shoot density environments. *Marine Ecology Progress Series*, 126, 223-232. doi: 10.3354/meps126223
- Yarnall, A. H., Byers, J. E., Yeager, L. A., Fodrie, F. J. (2021). Comparing edge and fragmentation effects within seagrass communities: a meta-analysis. *Ecology*, 103(3). <https://doi.org/10.1002/ecy.3603>
- Zhang, J., Lei, J., Huai, W., & Nepf, H. (2020). Turbulence and particle deposition under steady flow along a submerged seagrass meadow. *Journal of Geophysical Research: Oceans*, 125. <https://doi.org/10.1029/2019JC015985>
- Zhu, Q., Wiberg, P. L., & Reidenbach, M. A. (2021). Quantifying seasonal seagrass effects on flow and sediment dynamics in a back-barrier bay. *Journal of Geophysical Research: Oceans*, 126. <https://doi.org/10.1029/2020JC016547>
- Zhu, Q., Wiberg, P. L., & McGlathery, K. J. (2022). Seasonal growth and senescence of seagrass alters sediment accumulation rates and carbon burial in a coastal lagoon. *Limnology and Oceanography*, 9999, 1 – 12. doi: 10.1002/lno.12178

Acknowledgements

The completion of this thesis is an accomplishment that deserves to be shared by the many people who helped it come to fruition, and who helped me immeasurably along the way. I would first like to thank my advisor Matt Reidenbach for his complete support at every step of my graduate education. He provided room for my intellectual curiosity and independence to grow, patience through my many questions and mistakes, guidance on scientific and technical matters, and professional leadership that I will strive to emulate in the future.

Thank you to committee members Max Castorani and Mike Pace for sharing their time and ecological expertise on this project as I attempted to incorporate multiple interests and topics in my work. Thank you to Karen McGlathery, Dave Carr, and Pat Wiberg for consulting on conceptual, statistical, and coding concerns. Thank you to the entire staff of the Anheuser Busch Coastal Research Center whose accommodation of heightened field-based demands during a pandemic made this research possible. Cora, David, Buck, Jonah, and Donna exemplified the importance of integrity, hard work, community, and fun to operating a field station.

A special thank you goes to the many graduate students who turned from colleagues into helping hands, voices of reason, roommates, and friends. Thanks to the shore house girls, Ieva, Kayleigh, and Kinsey, for making summer 2021 possible and joyful. Thank you to Hayley, Lauren, Michael, and Spencer for their generosity with time and resources in the field. Thank you to lab and office mates Libby and Kelsey for bringing light into Clark 355, and to Marion for making Charlottesville a home. A

heartfelt thank you to Kylor who became my very best friend and who enriches my life exponentially.

Lastly, I save my greatest thanks for my family and loved ones, without whom I would not have met this goal. Thank you to my partner Grant for shining a light of support daily. Words cannot express my gratitude for my sister Anna, grandmothers Karen and Cece, and parents Kristen and Derek whose unwavering love brought me to this point while reminding me that family comes before everything.

This research was funded by the Virginia Coast Reserve Long Term Ecological Research project funded through the National Science Foundation Grants Division of Environmental Biology (DEB) 123772.